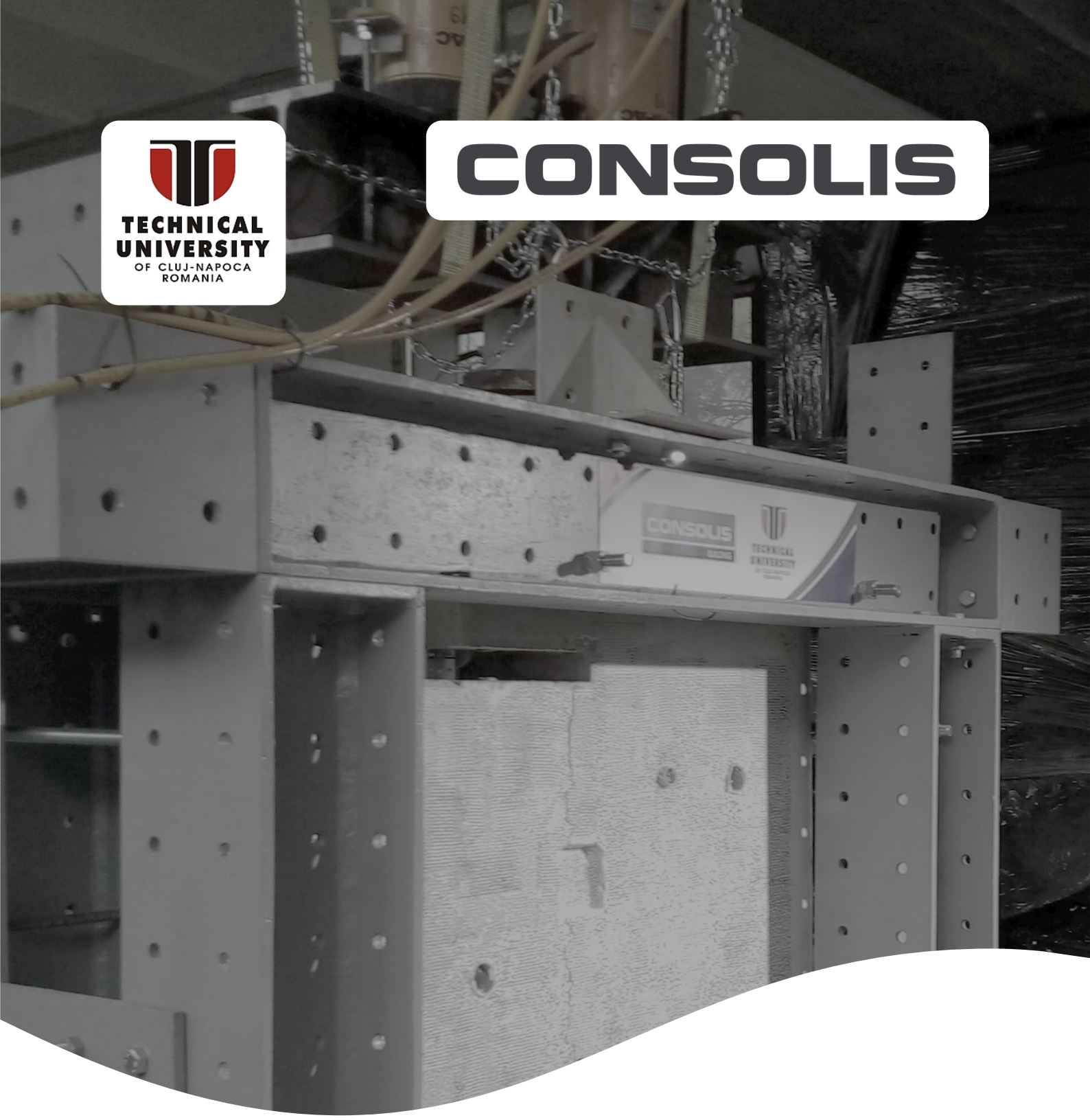

Experimental analysis of vertical connections for precast shear walls

EXPERIMENTAL REPORT

Dan Andrei MICLĂUȘOIU

UTPRESS
Cluj-Napoca, 2023
ISBN 978-606-737-634-0

Dan Andrei MICLĂUȘOIU

Experimental analysis of vertical connections for precast shear walls

UTPRESS
Cluj-Napoca, 2023
ISBN 978-606-737-634-0

Editura UTPRESS
Str. Observatorului nr. 34
400775 Cluj-Napoca
Tel.: 0264-401.999
e-mail: utpress@biblio.utcluj.ro
http://biblioteca.utcluj.ro/editura

Director: Ing. Dan Colțea

Recenzia: Șl.dr.ing. Marius Buru
Conf.dr.ing. Zsolt Nagy

Pregătire format electronic on-line: Gabriela Groza

ISBN 978-606-737-634-0

Bun de tipar: 18.05.2023

FOREWORD

This research report presents the experimental campaign conducted during the PhD programme

"Numerical and experimental studies of precast reinforced concrete walls"

"Analize numerice și experimentale a pereților prefabricați din beton armat"

at Technical University of Cluj-Napoca, Faculty of Civil Engineering, Romania,

by PhD student: Dan Andrei MICLĂUȘOIU, MscEng

PhD advisor: Assoc. Prof. Mihai Nedelcu

ACKNOWLEDGEMENTS

The author is grateful for the financial support offered by **CONSOLIS** who founded this experimental program, the support from **ASA-CONS Turda** for casting the test specimens and **CES Romania** for providing a great working environment. Special thanks to Assoc. Prof. Mihai Nedelcu and Dr. Gabriel Tarța, Dr. Sandor Gabor-Almos, PhD Wim Jansze, PhD Alar Kaes, Eng. Manhal Said, Dr. Horia Constantinescu, Dr. Bogdan Heghes, and Dr. Ovidiu Prodan for the deep involvement during this experimental campaign and for the guidance offered during the entire PhD Program. Furthermore, a number of BSc students have assisted in the experimental campaign, Edina Bardocz, Radu-Cristian Man, and Erhard Szabo, their effort is acknowledged.

SUMMARY

This paper reports the output of eighteen shear tests performed on six different joint layouts currently used to achieve vertical connection between wall panels in structural shear wall assemblies. The 1st chapter starts with a general introduction of the structural shear wall system, the research motivation and a summary of the tested connection layouts. The 2nd chapter presents the test set-up and the measurement technique. The 3rd chapter presents the testing results of the connections with steel assemblies, while the 4th chapter, of the connections with high strength wire ropes. Six additional tests on two wire loops connections layouts are attached to chapter 4. The 3rd and the 4th chapters contain subchapters discussing general descriptions and considerations regarding the connections, followed by the detailed presentation of each connection layout, geometry, casting and test results. Finally, the results are summarized and compared with existing resistance models. The last chapter concludes the test observations and discuss further research directions of this project.

Contents

1 GENERAL INTRODUCTION 1

2 TEST SET-UP 4

3 CONNECTION WITH GROUTED SHEAR KEYS AND STEEL ASSEMBLIES 7

3.1 Introduction 7

3.2 Welded plates and shear keys (SA1) 8

3.2.1 Specimens' presentation 8

3.2.2 Experimental results 11

3.3 Welded plates and shear keys (SA2) 13

3.3.1 Specimens' presentation 13

3.3.2 Experimental results 16

3.4 Grouted connection with shear keys and bolts - CLock connection (SA3) 19

3.4.1 Specimens' presentation 19

3.4.2 Experimental results 23

3.5 Summary of the results. Comparisons with calculations 27

4 CONNECTION WITH HIGH STRENGTH WIRE LOOPS 31

4.1 Introduction 31

4.2 Wire loops series 1: Peikko PVL 80 (WL1) 32

4.2.1 Specimens' presentation 32

4.2.2 Experimental results 35

4.3 Wire loops series 2: Pintos Okaria WI 80 (WL2) 38

4.3.1 Specimens' presentation 38

4.3.2 Experimental results 41

4.4 Wire loops series 3: Phillip constructive rails (WL3) 43

4.4.1 Specimens' presentation 43

4.4.2 Experimental results 46

4.5 Wire loops series 4: RSteel R3L-WIDE 100 (WL4) 48

4.5.1 Specimens' presentation 48

4.5.2 Experimental results 51

4.6 Wire loops series 4: Philipp Power Duo Rails (WL5) 52

4.6.1 Specimens' presentation 52

4.6.2 Experimental results 55

4.7 Summarized wire loops test results (with the supplementary test series) 57

5 CONCLUSIONS 64

5.1 Discussions and conclusion 64

5.2 Further research 65

1 GENERAL INTRODUCTION

Precast concrete shear walls are widely used to secure the stability of multistory precast buildings. To achieve a robust wall structure and structural interaction between the wall elements, it is important that the forces can be transferred from one wall panel to another and, finally, to the foundation. This requires a good design of the wall panels and good wall connections. However, most importantly, this requires a very good understanding of the stiffness of the precast wall panel connections that are assumed in the global calculation model. The structural response of the building structure is heavily influenced by this choice. This relates to the vertical and horizontal connections between the precast wall panels.

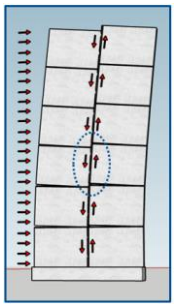

Figure 1-1 Precast concrete shear wall with vertical connections

To achieve structural interaction between the wall panels, adequate capacity must be provided for the structural connections. The shear capacity of the vertical connections (Figure 1-1) has been the subject of many experimental research projects starting from the 60s [1] [2] [3] up to present [4] [5] [6]. The current design practice in Europe relies upon EN 1992-1-1, chapter 6.2.5, "Shear at the interface of concrete cast at different times" [7]. The multitude of novel connection layouts, more and more economical from the casting and labor time perspective, rises debates whether such a general approach is universally applicable or not.

Besides the shear capacity of the connections, the main motivation for the present work is to assess the force – shear slip behavior of vertical connections. The design based on linear-elastic Finite Elements Method provides the possibility to model the stiffness of the connection (e.g., with linear springs). The use of stiffness values ranging between 0 to 10^7 kN/m/m (stiffness value associated to monolithic concrete) drastically influence the building response to lateral loads and the distribution of internal forces. Current design practice assumes a value of $5 \cdot 10^4$ kN/m/m. Moreover, if the stiffness of the connections is damaged (plastic behavior due to cracking), then the internal forces redistribution takes place. A linear-elastic finite element global analysis model cannot estimate this redistribution. Therefore, it is very important to assess the force – shear slip behavior, to determine if a linear behavior occurs up to the ULS of the connections.

The goal of this project is to better understand the behavior of connected precast concrete shear walls. To achieve this, testing and Non-Linear Finite Element Analyses of different types of vertical wall-to-wall connections are proposed. This report will present the experimental part of this project.

The structural connection type divides the experimental program in two sections: connections using grouted shear keys with steel assemblies (SA series) and connections with high strength wire loops (WL series). First two series are inspired by one of the Strängbetong preferred solution (SA1 and SA2). The 3rd, is a prototype proposed within Consolis' R&D department (SA3). Wire loops series investigates three different wire loops connections layouts (provided by different producers). A test series comprises three specimens designed to be identical. The aim of repeating the tests is to assess the consistency of the results. There is also the possibility of statistic interpretation if at least three results are available. The experimental program overview is presented in Figure 1-2. The

connections layouts are briefly described in Table 1.1. A detailed presentation of the test specimens will be presented for each test series separately in the following sections (chapter 3 and 4).

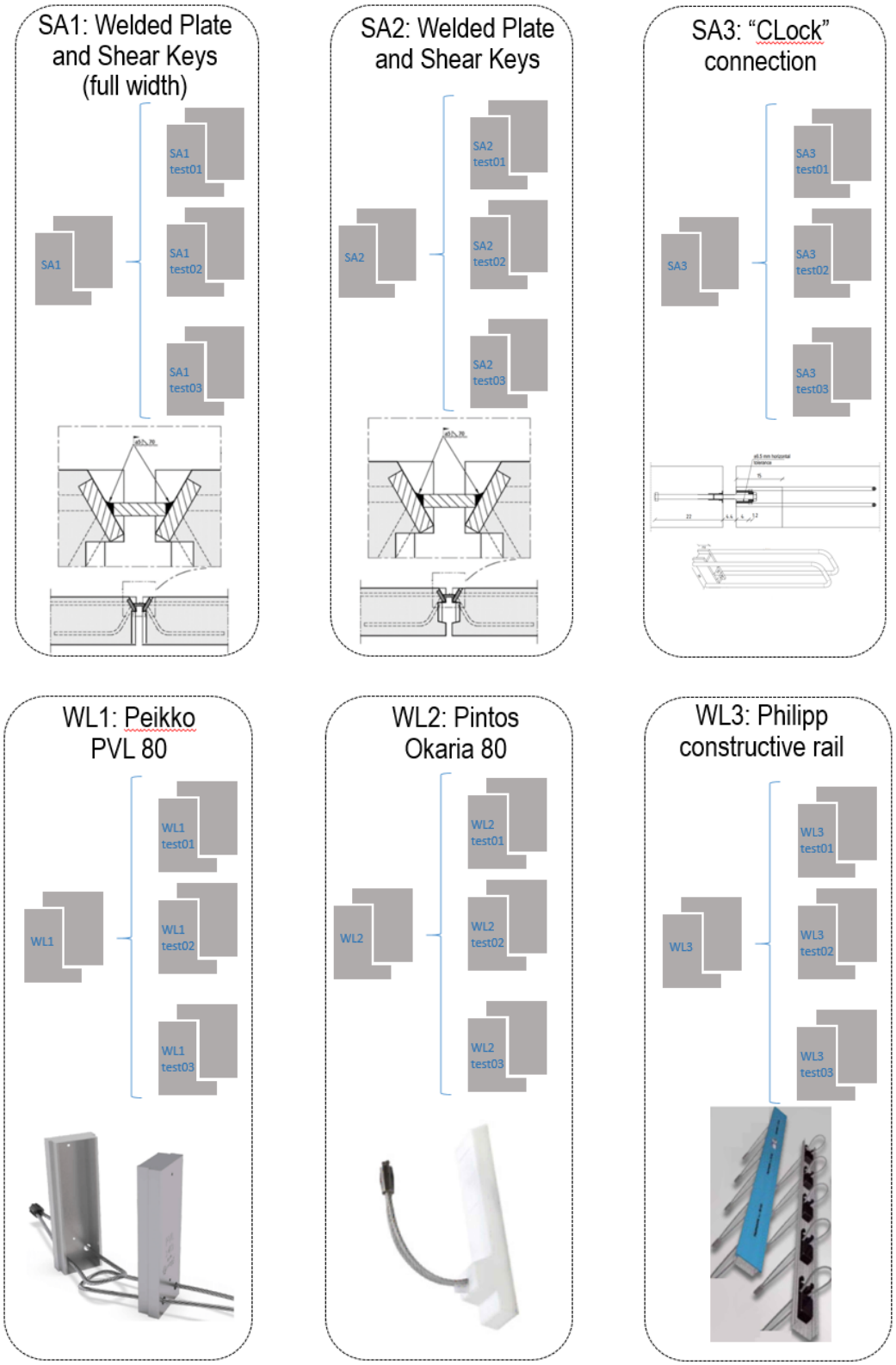

Figure 1-2 Experimental program overview

The wire loops test series outcome caused the experimental campaign to extend with two additional series for wire (WL4 and WL5 showed in Figure 1-3).

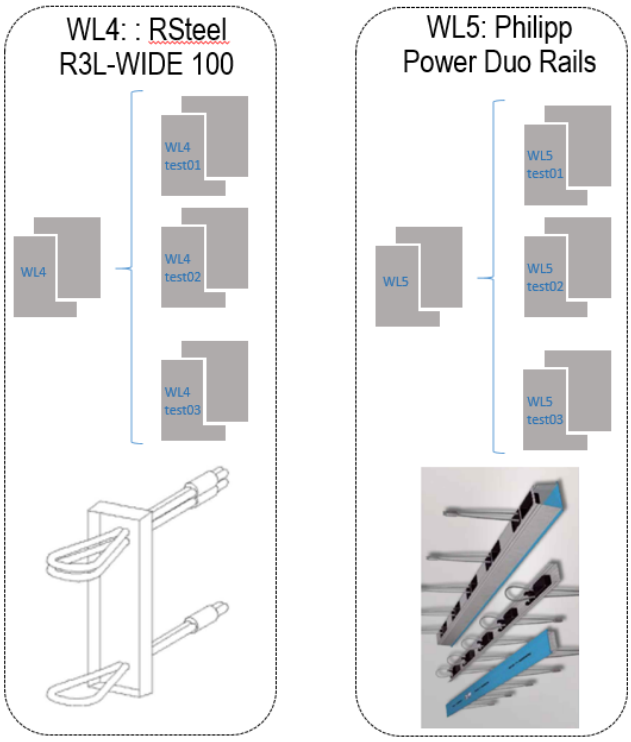

Figure 1-3 Experimental program extension

Table 1.1 Geometry description summary

Connection	Test index		Wall Panels Concrete Grade	Joint Filling Material Type	Joint Filling Material Grade	Connection Geometry: L_{joint} / B_{joint}	Shear keys dimensions: h_{key} / b_{key} / d_{key}	Shear keys number: n^{key}	Tying system
Steel assemblies	SA1	SA1T1 SA1T2 SA1T3	C30/37	Fluid Mapei Mapegrout SV	55MPa (according EN 12190)	1,20m / 20cm	60mm / 200mm / 12mm	7	4 pairs of embedded inserts
	SA2	SA2T1 SA2T2 SA2T3	C30/37	Thixotropic Weber ESL C30/37	50MPa (according EN 12190)		60mm / 65mm / 12mm	10	4 pairs of embedded inserts
	SA3	SA3T1 SA3T2 SA3T3	C30/37				60mm / 65mm / 12mm	9	2 CLock assemblies with M16 bolts
Wire loops	WL1	WL1T1 WL1T2 WL1T3	C30/37	Thixotropic Weber ESL C30/37	50MPa (according EN 12190)	1,25m / 20cm	Wire-box: 160mm / 50mm / 22mm	3	3 pairs of 6mm wire loops
	WL2	WL2T1 WL2T2 WL2T3	C30/37				Wire-box: 232mm / 65mm / 20mm	3	3 pairs of 5mm wire loops
	WL3	WL3T1 WL3T2 WL3T3	C30/37				Wire-rail: 1250mm / 50mm / 20mm	1	5 pairs of 6mm wire loops

2 TEST SET-UP

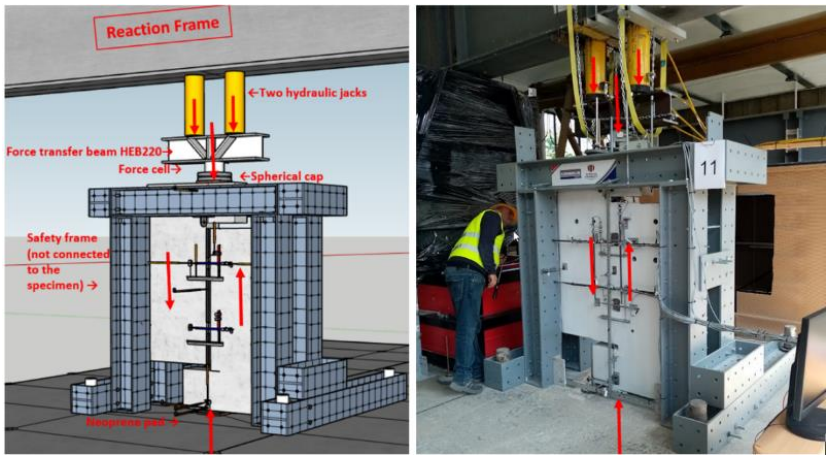

Figure 2-1 Laboratory test set-up (theory and practice)

The tests were performed at one of the testing facilities of the Technical University of Cluj-Napoca using an existing reaction frame and two interconnected hydraulic jacks (900kN capacity each). The forces from the two jacks are transferred to the specimen by a steel transfer beam (HEB 220 S355, with strengthened web and stiffening plates), under which a load cell and a spherical cap are placed. Between the spherical cap and the specimen, a steel plate (200x250x10mm) is placed. A neoprene pad (250x250x20mm) is positioned under the specimen to assure uniform support pressure and to offer a minimal rotational capacity. Around the specimen, a safety frame has been assembled using multi-purpose, adjustable and reusable steel beams. The role of the safety frame is to secure the specimen position and provide support for the ground fixed transducers. The safety frame is not connected to the specimen during testing (around 2.5cm of clearance allowed).

The loading was applied in incremental load steps. The maximum load step size is chosen so at least 10 loads steps are applied up to the failure of connection ($F_{LoadStep} = F_{Peak}/10$). For the first test specimens of each test series, the ultimate load was determined by calculations. In some cases, the specimens test resistance was underestimated, and the load step size was doubled after 10 load steps. To ensure deformation and internal stress stabilization, the load level was kept constant between the load steps for 100-200 seconds. This waiting period is considered adequate by assessing the real time readings of the force, deformations and displacements. In few cases, when the specimens test resistance was overestimated, the waiting periods were increased at the first signs of damage. Time spans of 10-15 minutes were taken, after the occurrence of cracking for manual marking of crack lengths and crack-width readings.

Displacement measurements were performed on both faces of the specimen, with Linear Variable Differential Transducers (LVDT) on the front face, and with a Digital Image Correlation (DIC) system on the rear face (Figure 2-2). Both faces were monitored to assess if there are other significant force components in the connection (e.g., out-of-plane shear, bending over the vertical axis, caused by force eccentricity or casting imperfections).

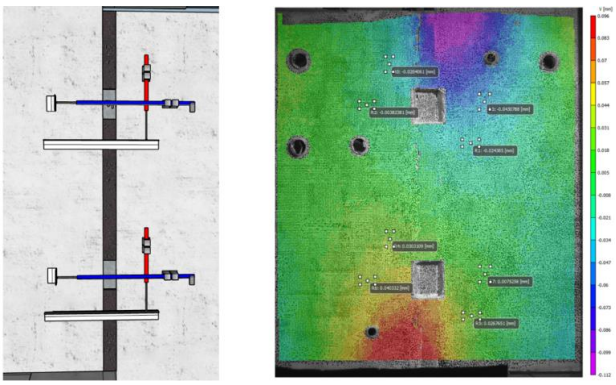

Figure 2-2 LVDT (left) and DIC measurement points + vertical displacements field before cracking load for SA1T2 specimen (right)

Due to the very high stiffness of the joint, relatively high rigid body motions obscure the relevant displacements. The LVDTs presented in Figure 2-2 are fixed relatively on the two walls and the rigid body movements caused by the boundary conditions do not affect their measurements. The software used for DIC has an option of removing the rigid body motion (VIC 3D 8 Testing Guide [8]). LVDTs and DIC measurements were compared and the largest deviation in terms of displacements was around 20%. This verification was performed for each test of the program.

Further on, it was noticed by observing the displacement fields captured with DIC, that the number and position of the LVDTs (presented in Figure 2-2) are not able to capture the entire shear-slip behavior of the joint accurately. Therefore, a new analysis method was proposed. Several measurement points were added at an incremental distance of 10 cm along the joint height and displacement values were extracted (Figure 2-3 and Figure 2-4: the left images show the measurement points positions). To obtain the relative displacement of two points (placed on each precast panel), the displacement (vertical or horizontal) of one point is subtracted from the other. Plots from Figure 2-3 and Figure 2-4 (right hand side) show that the shear slip is almost two times bigger at the joint extremities than in the middle and the other way around for the joint dilation. Further, the challenge is to find the most relevant measurement points for estimating the stiffness of this connection. More research is needed to assess the stress state taking place in a push-off configuration and compare it with a vertical connection of a shear wall. For the current stage of the research, an average of 10 measurement points along the height of the joint was plotted along with the force. The stiffness was calculated as a secant slope for each behavior stage specific for each connection type (e.g. pre-cracking stage, post-cracking stage etc.). The stiffness values will be presented for each test and it can be described as an average secant shear stiffness of the joints.

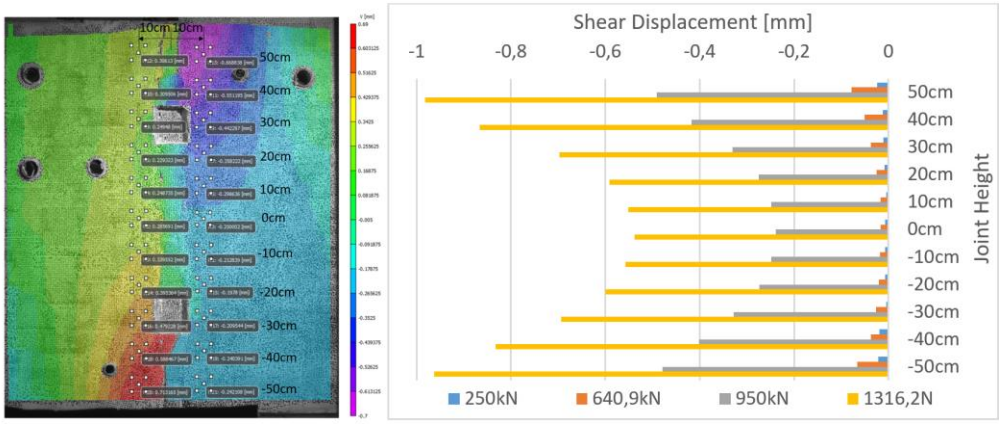

Figure 2-3 Vertical displacements field at peak load for SA1T2 (left); Shear slip over the joint height (right)

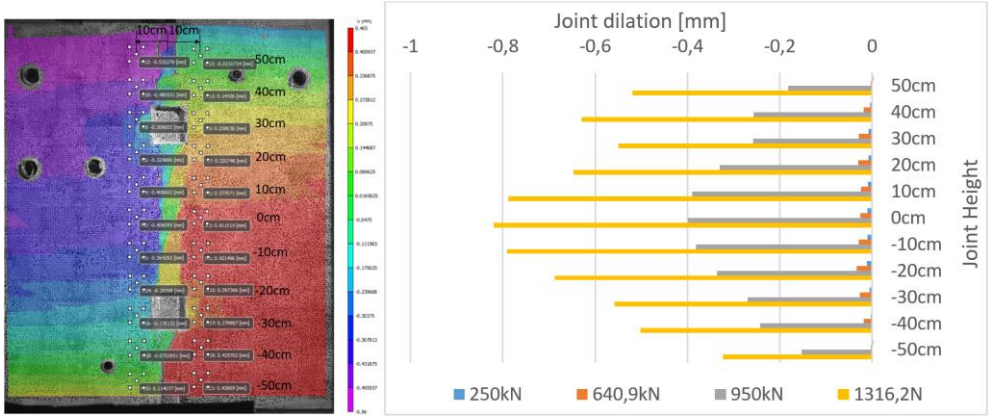

Figure 2-4 Horizontal displacements field at peak load for SA1T2 (left); Joint dilation over the joint height (right)

Figure 2-5 Strain gauges on the welded plates (left image: SA1; right image: SA2)

The strain gauges presented in Figure 2-5 were used to better understand when and how the welded plates are loaded. In simplified code calculations it is assumed that the welded plates are loaded only in axial tensile horizontal stresses. Any bending and shear stresses are neglected. To accurately determine the stress state in the steel assembling tying system, a dedicated local study would be required. The strain gauges results will be used in the future for Nonlinear Finite Element model – experimental results comparison.

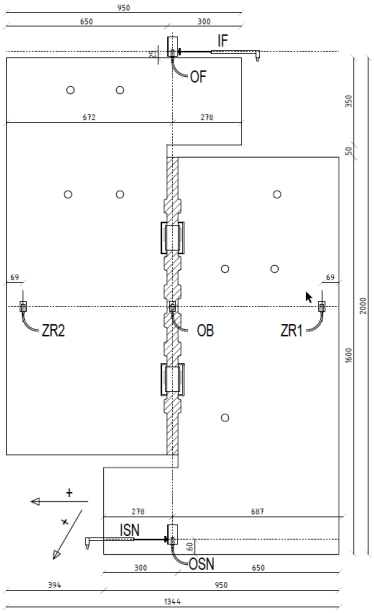

Figure 2-6 Test safety monitoring instrumentation

Additional measurements were carried out for real time monitoring the behavior of the test set-up. The LVDTs layout shown in Figure 2-6 is able to assess the specimen rotations over the three axis: IF and ISN used for in-plane rotation; OF and OSN for out-of-plane rotation; ZR1 and ZR2 for rotation over the vertical axis. Eventual sliding in the boundary conditions would also be pointed out. These measurements are important on one hand, for the safety during testing and on the other hand, to ensure that the specimen is properly centered into the test set-up and no significant force components are induced to the connection, altering the shear test results. ISN and OSN sensors reported little base sliding (around 3 mm for some specimens). Alongside the rotations of around two degrees, it was considered that pure shear loading is a good assumption.

3 CONNECTION WITH GROUTED SHEAR KEYS AND STEEL ASSEMBLIES

3.1 Introduction

This chapter will discuss vertical shear connections that are using steel assemblies (SA series). These connections can be classified as “dry” or “wet”. Dry connections use steel assemblies to provide stiffness and capacity. The steel assemblies mostly consist of two embedded inserts anchored in the precast panels and a third part, welded or bolted in the assembly stage. Wet connections can use several types of reinforcement configurations and the force transfer is achieved through the structural grout poured in joints in the assembly stage. The most common solution is the overlapped U-bars connection. Structural integrity regulations contain minimum requirements for horizontal ties between the components of the vertical structural stability system. These ties can be designed in a way to provide also the necessary clamping forces needed for the vertical shear connections. Present studies propose methods for estimating the capacity [5], [6] and stiffness [5], [9] of overlapped U-bar connections. Sørensen [6] proposes a shear capacity calculation method, considering the biaxial compressive stress state in the grout, the geometry of the shear keys, the overlapped reinforcement and the lacer bar contribution. The current design practice in Europe is dictated by the EN 1992-1-1, chapter 6.2.5, “Shear at the interface of concrete cast at different times” [7], [10]. This calculation method considers the tensile strength of concrete or grout, the reinforcement area and it provides coefficients depending on the interface roughness.

This chapter studies the in-plane shear behavior, capacity and stiffness, of a special type of connection consisting of welded plates and grouted shear keys. This connection can be described as a “dry” connection detail, having welded steel plate on site between two embedded adjacent inserts. Yet, the joint is grouted, and the interface is provided with shear keys, geometrically complying with chapter 6.2.5 from EN 1992-1-1. The welded steel plate combined with casted joint is not a fully dry solution. It starts to operate directly after welding but it gets full capacity and fire safety after casting. This connection type is a combination of two typical connections with different force transfer mechanisms. If a dry connection detail is used in combination with a grouted joint, then the forces from the steel connectors are associated with clamping forces, rather than shear forces [11]. If clamping forces are predominant, these connections capacity should be calculated according to chapter 6.2.5 from EN 1992-1-1. This implies assessing all possible tensile failure mechanisms of the welded plates assembly: yielding of the anchorage bars, welding rupture, or yielding of the welded plate. To the best of the authors knowledge, no similar connection has been studied through experimental testing in the past. Two test series were casted with a slight parameter variation based on the connection layout presented in Figure 3-1: SA1 and SA2. In the last series (SA3) the welded plates assemblies are replaced with a more construction friendly steel assembly that is using bolts instead of welds. A detailed presentation of the test specimens geometry, properties, casting and test results is shown in the following subchapters.

The topic was debated at the 6th fib International Congress in Oslo from 2022 [12].

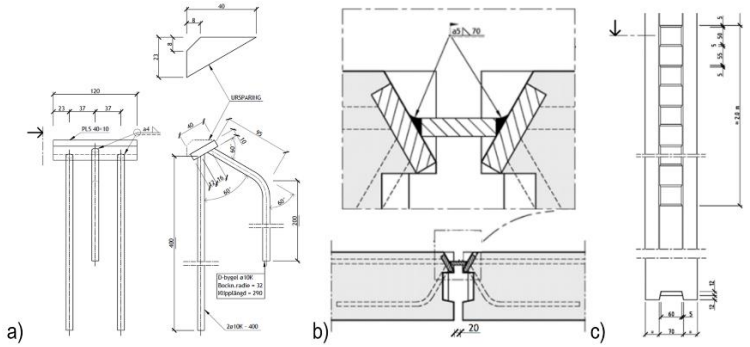

Figure 3-1 Preferred vertical connection layout in Strängbetong: a) embedded insert; b) typical connection layout; c) shear keys detail

3.2 Welded plates and shear keys (SA1)

3.2.1 Specimens' presentation

This connection detail (Figure 3-2) was inspired by a typical connection detail used to joint together walls in Sweden (Figure 3-1). However, some adaptations have been carried out:

- the reinforcement of the precast panels was designed to ensure the failure of the connections in a push-off configuration (avoiding any type of wall failure, e.g. corbel failure or panels excessive cracking) without following any specific reinforcement configurations used in normal buildings (Figure 3-3);
- the inserts were placed on both sides of the wall in order to create a symmetrical connection. A non-symmetric connection will cause losing the planarity of the specimen bringing safety concerns for the push-off test configuration. Moreover, it is considered that a symmetric configuration has more similar conditions to the real structure, where out of plane movement is blocked by other structures (e.g. perpendicular adjacent walls, horizontal connections);
- usually, shear keys are placed into a recess in order to obtain a higher capacity for out-of-plane actions. Since the out-of-plane behavior was not part of our study and the edges of the recess obstruct the view on the cracking patterns of the joint, the width of the shear keys was equal to the wall thickness;
- the joint interface did not receive any special treatment (e.g., cleaning, or the opposite, greasing) emulating normal on-site casting conditions;
- the welding was performed in site conditions with a AS B-248 Coated Electrode Φ 3.25 x 350 mm, available on the local Romanian market;
- joint grouting was done with a dry mix grout available on Romanian market, Mapei Mapegrout SV [13], that seemed to have similar mechanical properties to those used for this connection type. The joint was cast in a vertical position, molded on both sides and grouted from above;
- mean material properties are presented in Table 3.2.1 and 3.2.2 and their coefficient of variation with normal distribution (CoV).

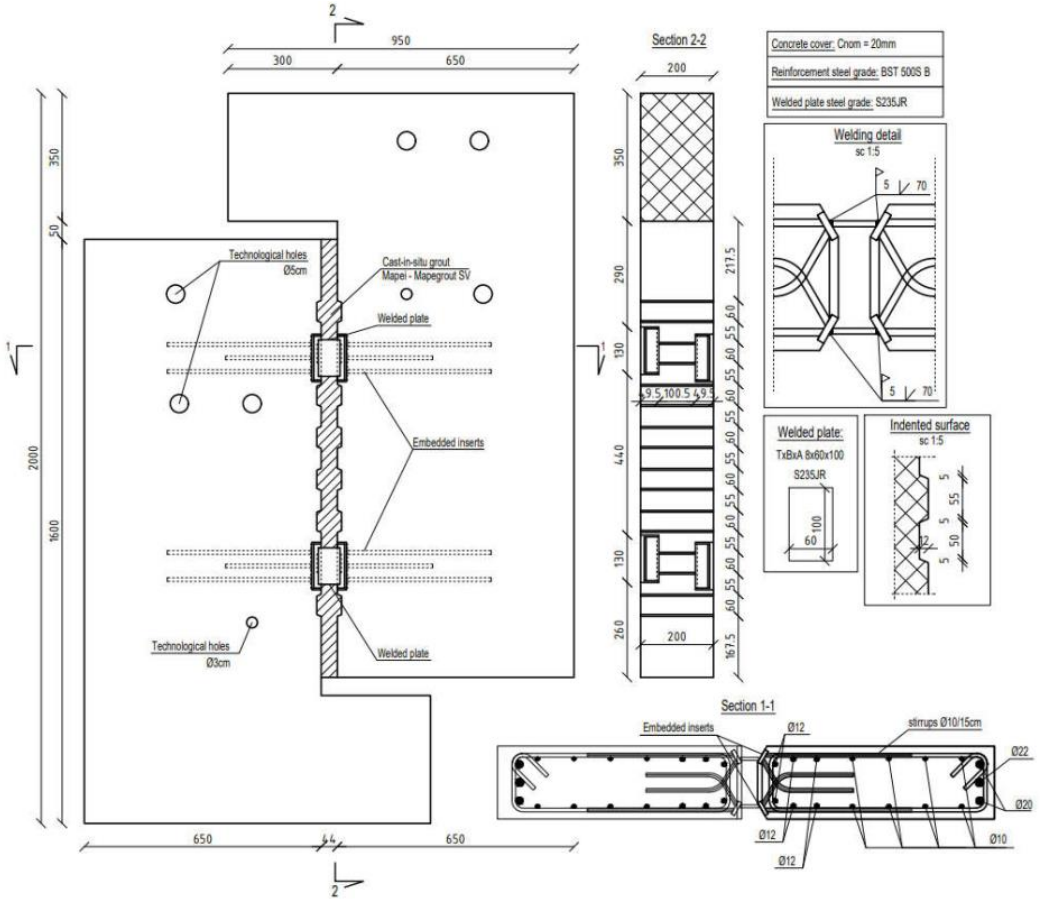

Figure 3-2 Configuration of SA1 specimens (dimensions in mm)

Figure 3-3 Specimens from SA1 (from left to right test 1, test 2 and test 3)

The three test specimens are designed to be identical, and the test results show a good agreement in terms of capacity and displacements, yet there were few casting imperfections. The joints were designed with half width keys between the embedded inserts, but not all of them were completed (Figure 3-4). The theoretical welding dimensions are 5mm in thickness and 70mm in length, yet after the failure was observed that proper welding thickness was not achieved for the 3rd test specimen (Figure 3-5).

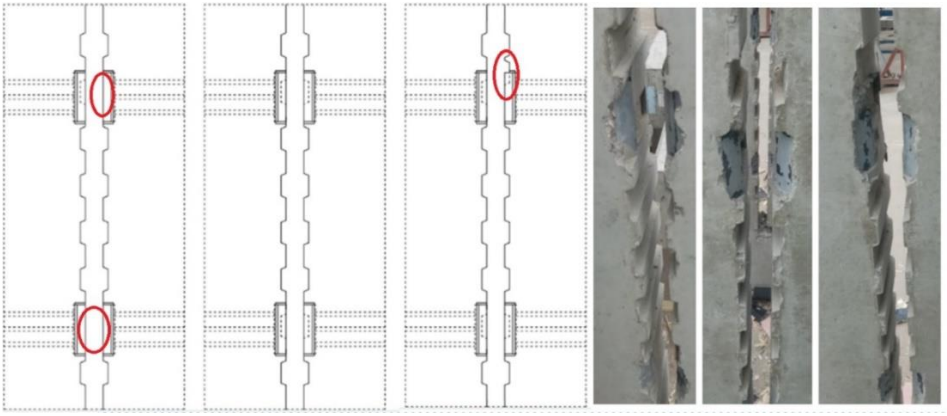

Figure 3-4 Real position of the half shear keys (specimen 1, specimen 2 and specimen 3)

Figure 3-5 Welded plates after failure (1st test vs 3rd test)

The results presented in chapter 3.2.2, are showing a progression that might be caused by the imperfections presented in Figure 3-4. SA1T2 has the higher capacity (no keys missing), followed by SA1T3 (with only half-key missing) and SA1T1 (with two half-keys missing). Yet, we cannot assess the influence of the welding imperfections presented in Figure 3-5, since the welding was not the only variable. That would require a parametric experimental investigation with a very high number of test specimens for only one connection layout. It can also be observed that the cracking loads had a very small variation.

Table 3.2.1 - Concrete mechanical properties

$f_{cm.cube}$[1] [MPa]	f_{ctm}[2] [MPa]	E_{cm}[3] [GPa]	$f_{cm.prism}$[4] [MPa]
73,15	3,69	33,56	55,28
CoV: 0,01	CoV: 0,15		CoV: 0,07

1 - average of 3 compressive tests according to SR EN 12390-3 on 150mm cubes; specimens age 218 days

2 - average of 4 tensile splitting tests using SR EN 12390-6 multiplied with a factor of 0,9 [7]; specimens age 218 days

3 - average of 2 elasticity modulus tests using SR EN 12390-13 on 100x100x300mm prisms; specimens age 427 days

4 - average of 3 prisms compressive tests according to SR EN 12390-13; specimens age 427 days

The concrete strength class requested was C30/37

Table 3.2.2 - Joint mortar mechanical properties

$f_{cm.cube}$[1] [MPa]	$f_{cm.cube.40mm}$[2] [MPa]	f_{ctm}[3] [MPa]	$f_{ctm.40mm}$[4] [MPa]	E_{cm}[5] [GPa]	$f_{cm.prism}$[6] [MPa]
65,55	81,21		10,63	32,07	59,91
CoV: 0,08	CoV: 0,06		CoV: 0,09	CoV: 0,03	

1 - average of 3 compressive tests according to SR EN 12390-3 on 150mm cubes; specimens age 194 days

2 - average of 6 compressive tests on 40mm cubes according to SR EN 196-1 ; specimens age 194 days

3 - tests not performed

4 - average of 3 flexural tensile tests on 40x40x160mm prisms according to SR EN 196-1 and converted according to 3.23 relationship from EN 1992-1-1; specimens age 194 days

5 - average of 3 elasticity modulus tests using SR EN 12390-13 on 100x100x300mm prisms; specimens age 340 days

6 - average of 2 prisms compressive tests according to SR EN 12390-13; specimens age 340 days

Mapei Mapegrout SV is declared as repairment mortar according to EN 1504-3. It does not have a strength class declared according to EN1992-1-1 and EN206-1. The declared compressive strength according to EN 12190 is 55MPa.

Table 3.2.3 - Steel mechanical properties

	f_y[1] [MPa]	f_u[2] [MPa]	E_s[3] [MPa]	ε_u[4] [%]
Insert anchors BST 500S	560,3	669,0	202.141	11,5
Steel insert S355	362,9	505,0	225.305	15,1
Welded plate S235	326,0	463,5		

1 - Lower yielding strength

2 - Stress at the maximum force

3 - Young modulus (determined using digital extensometer and/or DIC)

4 - Strain at the maximum force (determined using digital extensometer and/or DIC)

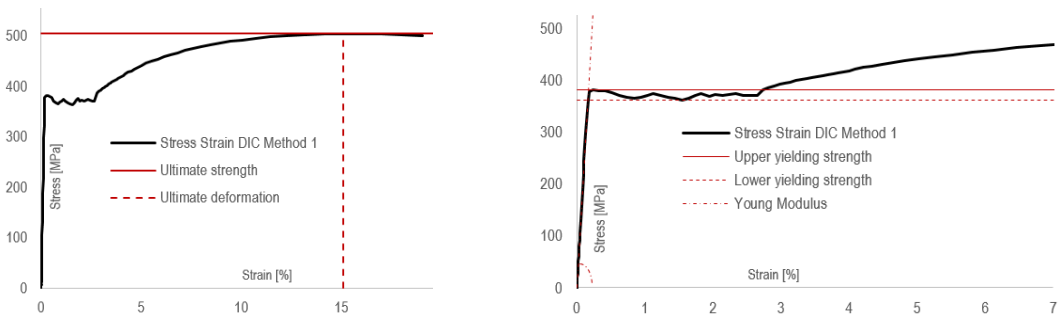

Figure 3-6 Experimental stress strain curve for steel insert material test specimen

3.2.2 Experimental results

The tests were carried out after the grouting material reached 180 days of maturity (advanced age caused by Covid restrictions). During all three tests, a similar behavior has been observed: very high initial stiffness, without noticeable cracks up to the cracking load of 646kN (mean value of the three tests). The moment of cracking is marked by a powerful sound, a severe increase of strains in the welded steel plates (before cracking, almost null values were measured), radical increase in shear displacement, joint dilation, and visual appearance of the crack (0.25-0.3 mm crack width, Figure 3-7). Cracking sounds were heard, occasionally, between the cracking load and the failure load. The results are considered consistent. Figure 3-7 in the middle shows an interface de-bonding crack, while the other two showed inclined cracks. The crack changed its orientation before the peak load, becoming similar with the other two.

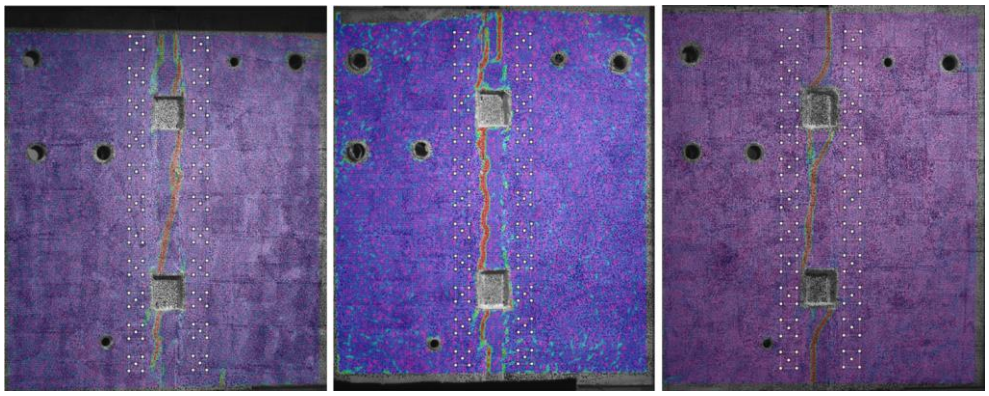

Figure 3-7 Crack pattern visualization after cracking load (from left to right) SA1T1: 646kN, SA1T2: 641kN, SA1T3: 650kN, (using DIC, major strains)

At the ultimate load, the failure was marked by severe decrease in force and a very wide opening of the main crack. The failure crack went through the grout shear keys. The inclined cracks across the joint are showing the possibility of a strut and tie failure type. The crack pattern occurring in the grout is typical for keyed joints. The concrete around the embedded inserts bursted, the anchor bars developed plastic hinges (in the expulsion zone) and the welds presented partial/complete ruptures (the events were very brittle appearing to take place simultaneously, see Figure 3-8). After attempting to further increase the load, the welding continued to rupture under a seemingly constant load, indicating that the welded plates cannot provide a significant secondary force transfer mechanism associated with dry connections (Figure 3-9). One can assume that the tensile yielding occurred at first in the anchor bars (associated with the shear-lock/shear-friction mechanisms). If the welding would have failed before the tensile yielding of the anchor bars, then bursting of concrete and plastic hinge formation in the anchor bar should not have occurred. That should be the reason why the weaker welding (shown in Figure 3-5) did not had a major influence. However, to ensure a favorable failure mechanism, we have to emphasize that welding of the plates should be the strongest component of the connection and the last one to fail.

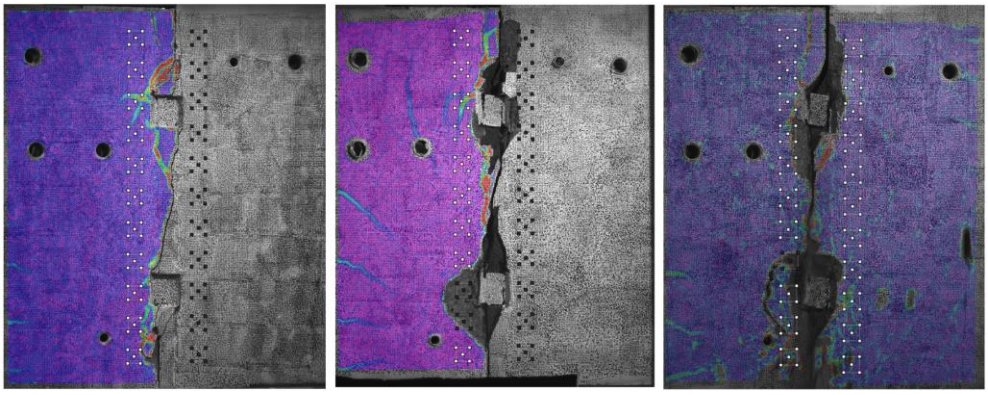

Figure 3-8 Observed specimen failure mechanisms after the peak load (from left to right) SA1T1: 1081kN; SA1T2: 1306kN; SA1T3: 1191kN;

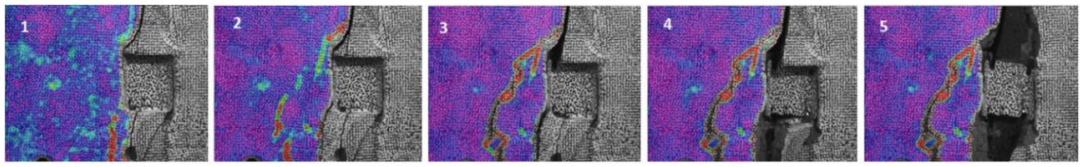

Figure 3-9 Post-failure behavior of the connection around the welded plate (SA1T1)

For the three tests a stiffness average value of $1.6 \cdot 10^7$ *kN/m/m* was determined for the initial stage, typical for monolithic connections. After the cracking load is reached, a great shear slip takes place. The post-crack stiffness was determined as having an average value of $6.6 \cdot 10^5$ *kN/m/m*. This value presents a 95.5% decrease compared to the initial stiffness and it was calculated as a secant slope between the average cracking and failure load. The individual results are summarized in Table 3.2.4.

Due to technical issues the first test had to be stopped at 951 kN and it was repeated afterwards. This way the behavior of a pre-cracked connection was captured and the stiffness (secant slope) has been determined at a value of $1.5 \cdot 10^6$ *kN/m/m*.

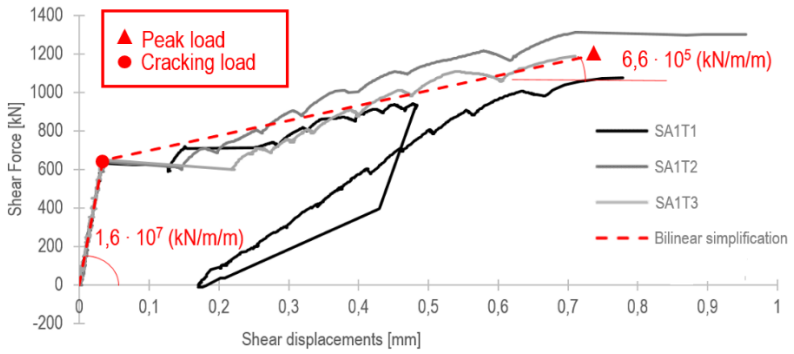

Figure 3-10 Shear force vs average shear slip along the joint height

After the peak load, DIC failed to correlate images due to the large discontinuities (also shown in Figure 3-8). As seen there, the damage after the peak load was very severe and there was almost no residual capacity.

Figure 3-11 presents the shear displacements and joint dilation along the joint height, at different force levels. The plots are shown only for the 2nd test, since the values are quite similar.

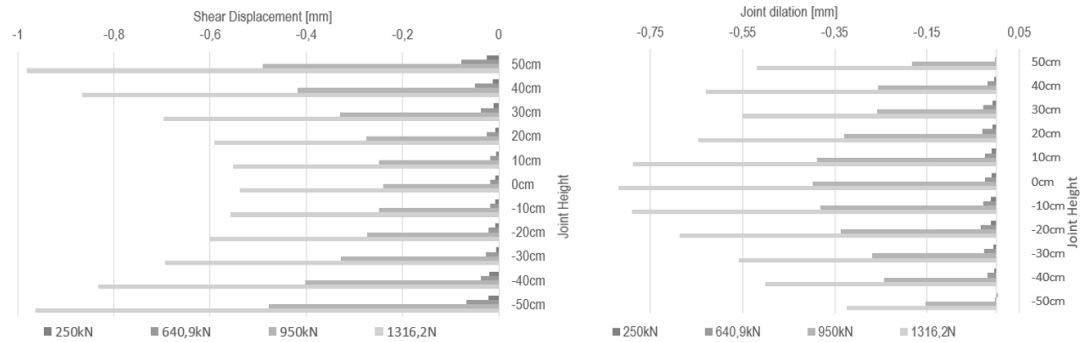

Figure 3-11 Shear displacements and joint dilation distribution along the joint height (for SA1T2)

Table 3.2.4 - SA1 test results (individual result and average result)

	F_{crack} [kN]		F_{peak} [kN]		$K_{initial}$ [kN/m/m]		K_{final} [kN/m/m]	
SA1T1	646		1081		1,6E+07		4.8E+05	
SA1T2	641	646	1306	1193	1,5E+07	1,6E+07	8,3E+05	6.6E+05
SA1T3	650		1191		1,6E+07		6,6E+05	

3.3 Welded plates and shear keys (SA2)

3.3.1 Specimens' presentation

These test specimens were designed in a similar way as the previous test series (SA1, see chapter 3.2.1), with two parameters variation: different joint grout and a smaller width of the shear keys. These specimens' particularities are described below:

- the inserts were fixed before concreting with constructive welding at the anchors free ends;
- the welded plates width was increased to accommodate the inserts position for some specimens (from 60mm to 65mm);
- the shear keys dimensions (including the width) are according to the standard Strangbetong detail, yet the recess edges were omitted. This is due to grouting difficulties using thixotropic mortar (the gap between the wall edges was increased from 2cm, as presented in Figure 3-1, to 4.4cm, as presented in Figure 3-12);
- joint casting was done with a dry mix non-sagging mortar widely used in Finland: Weber ESL C30/37 [14]. The joint was cast in vertical position using a manual method. One side of the joint was fully molded from the beginning, while the mold on the other side was installed progressively during the casting. Material test results are presented in Table 3.3.1, 3.3.2 and 3.2.3.

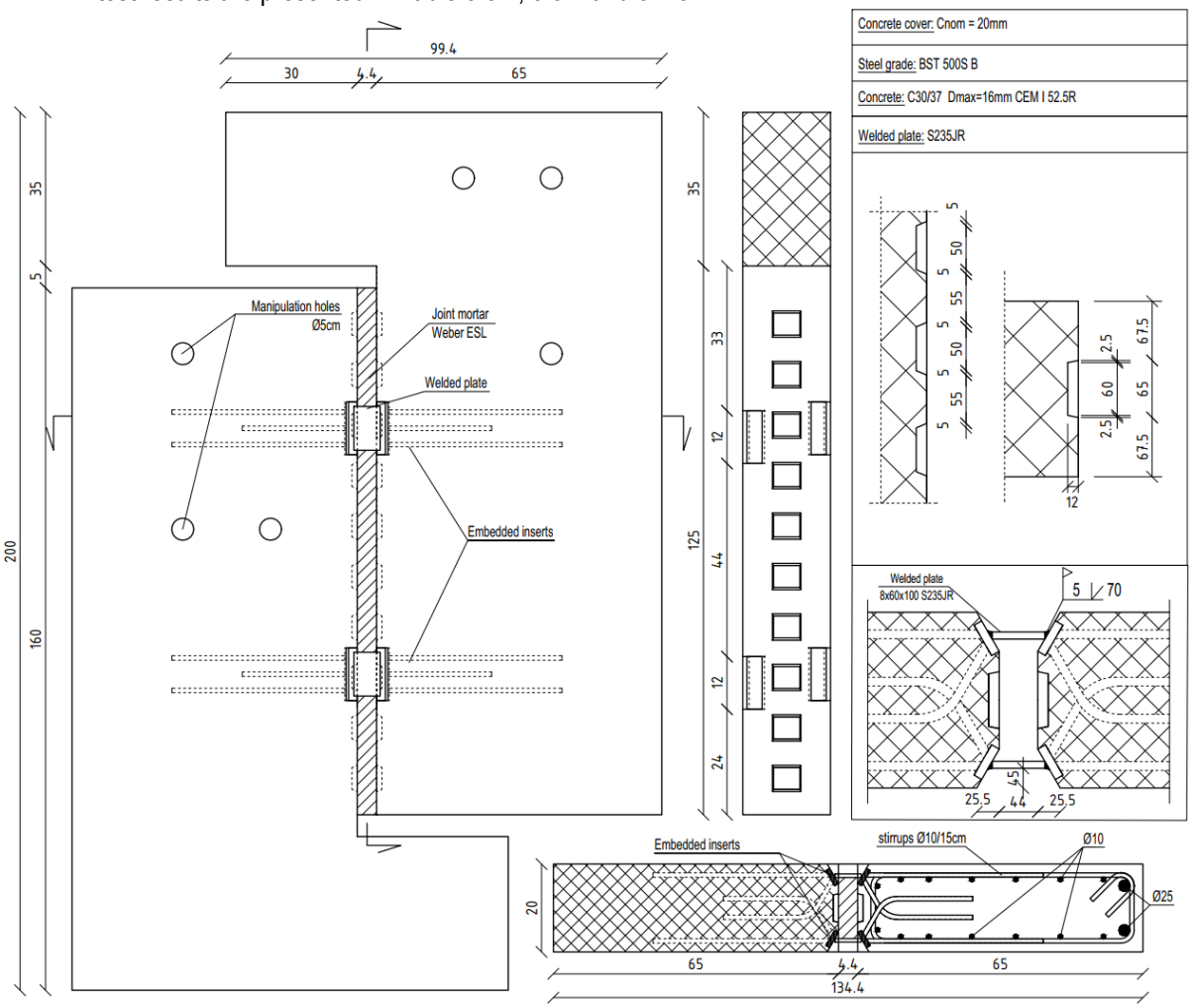

Figure 3-12 Configuration of SA2 specimens (dimensions in cm)

Figure 3-13 Specimens from SA2 (from left to right 1st, 2nd and 3rd test specimen)

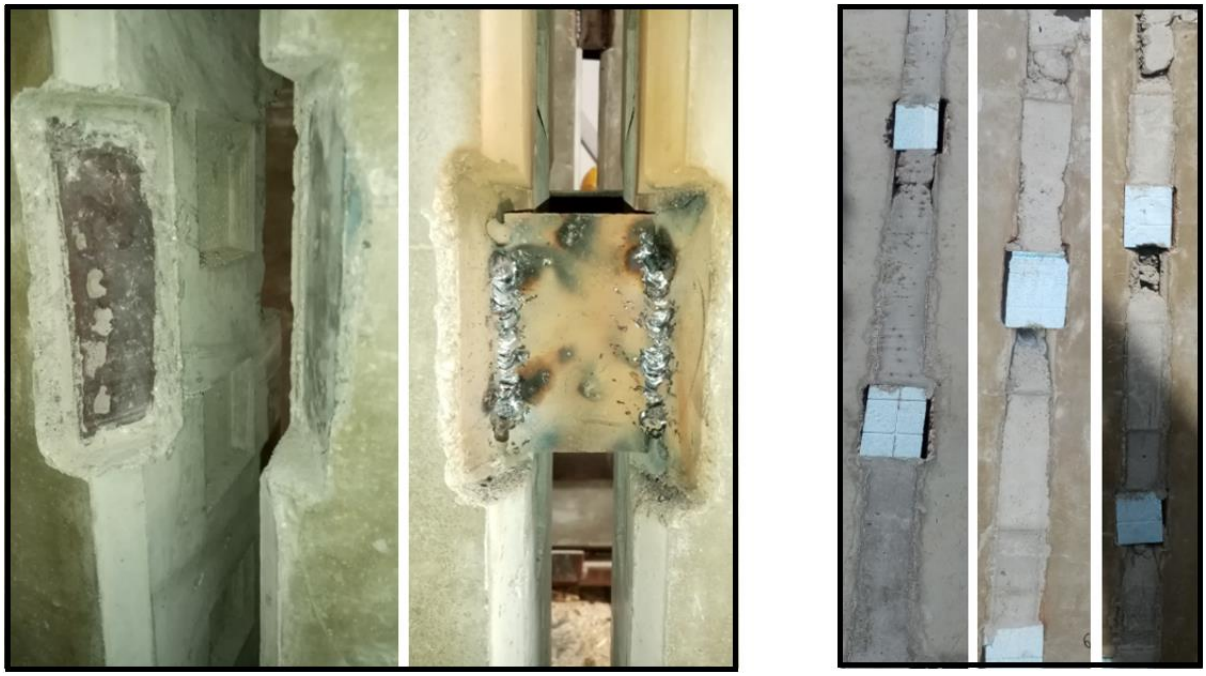

Figure 3-14 Joint casting (left image: 1st test before grouting; right image: 1st, 2nd and 3rd test specimen after grouting)

Table 3.3.1 - Concrete mechanical properties

$f_{cm.cube}$[1] [MPa]	f_{ctm}[2] [MPa]	E_{cm}[3] [GPa]	$f_{cm.prism}$[4] [MPa]
81,76	3,96	38,64	57,65
CoV: 0,05	CoV: 0,17	CoV: 0,01	CoV: 0,07

1 - average of 4 compressive tests according to SR EN 12390-3 on 150mm cubes; specimens age 74 days

2 - average of 8 tensile splitting tests using SR EN 12390-6 multiplied with a factor of 0,9 [7]; specimens age 74 days

3 - average of 3 elasticity modulus tests using SR EN 12390-13 on 100x100x300mm prisms; specimens age 75 days

4 - average of 3 prisms compressive strength according to SR EN 12390-13; specimens age 75 days

The concrete strength class requested was C30/37.

Table 3.3.2 - Joint mortar mechanical properties

$f_{cm.cube}$[1] [MPa]	$f_{cm.cube.40mm}$[2] [MPa]	f_{ctm}[3] [MPa]	$f_{ctm.40mm}$[4] [MPa]	E_{cm}[5] [GPa]	$f_{cm.prism}$[6] [MPa]
55,18 CoV: 0,05	51,33 CoV: 0,12	-	5,46 CoV: 0,07	29,73 CoV: 0,05	48,33 CoV: 0,03

1 - average of 4 compressive tests according to SR EN 12390-3 on 150mm cubes; specimens age 69 days

2 - average of 6 compressive tests on 40mm cubes according to SR EN 196-1 ; specimens age 77 days

3 - tests not performed

4 - average of 3 flexural tensile tests on 40x40x160mm prisms according to SR EN 196-1 and converted according to 3.23 relationship from EN 1992-1-1; specimens age 77 days

5 - average of 3 elasticity modules tests using SR EN 12390-13 on 100x100x300mm prisms; specimens age 75 days

6 - average of 3 prisms compressive strength according to SR EN 12390-13; specimens age 75 days

Weber ESL is a non-sagging mortar especially designed for vertical and horizontal joints of concrete elements according to EN 1504-4. The declared Strength class is C30/37-4 according to SFS-EN 206-1 with >40MPa according to EN 12390-3 and approximately 50MPa according to EN 12190

Table 3.2.3 - Steel mechanical properties

	f_y[1] [MPa]	f_u[2] [MPa]	E_s[3] [MPa]	ε_u[4] [%]
Insert anchors BST 500S	560,3	669,0	202.141	11,5
Steel insert S355	362,9	505,0	225.305	15,1
Welded plate S235	326,0	463,5		

1 - Lower yielding strength

2 - Stress at the maximum force

3 - Young modulus (determined using digital extensometer and/or DIC)

4 - Strain at the maximum force (determined using digital extensometer and/or DIC)

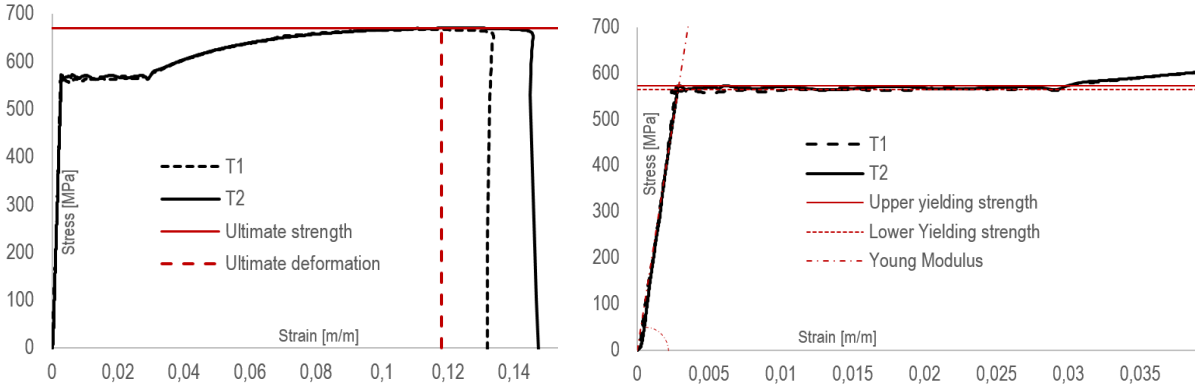

Figure 3-15 Experimental stress strain curve for 10mm diameter insert anchors

3.3.2 Experimental results

The tests were carried out after the grouting material reached 50, 63, 78 days of maturity. During all three tests, a similar behavior has been observed. The results are considered consistent. The initial stiffness was high (close to monolithic emulative connections). In the pre-cracking stage, low indications of interface de-bonding were observed only through DIC analysis. The moment of cracking is marked by the progressive change of the slope of the force – shear slip graph and by the strains that started to increase at a higher rate in the welded plates. This behavior is similar with the previous series with welded plates and shear keys (SA1). Yet, the more inferior mechanical properties of Weber ESL grout and the decrease of the width of the shear keys has led to a more ductile behavior.

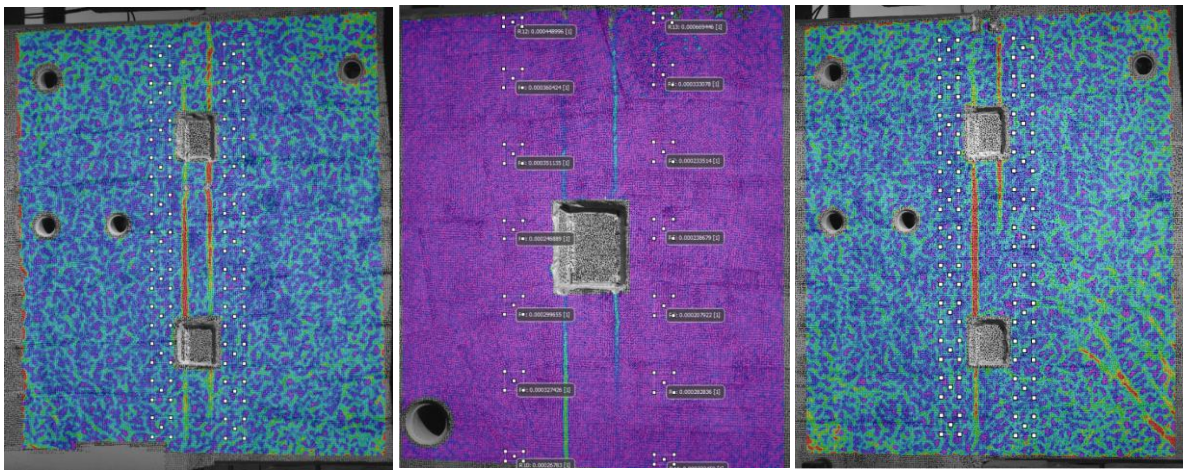

Figure 3-16 Crack pattern visualization after cracking load (from left to right) SA2T1: 308.9kN, SA2T2: 300.6kN, SA2T3: 300.8kN, (using DIC, major strains)

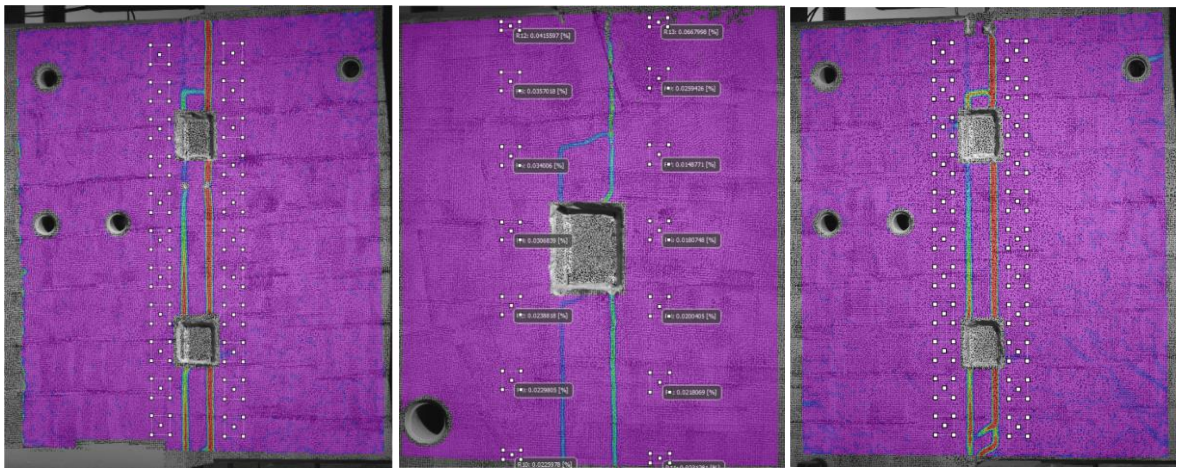

Figure 3-17 Crack pattern visualization at the reaching of the peak load (from left to right) SA2T1: 689.3kN, SA2T2: 616.4kN, SA2T3: 572.6kN, (using DIC, major strains)

After the peak load, no significant yielding plateau was present; the post-peak behavior might be associated to a softening behavior, until the welding rupture occurred. One interface presented complete key shear-off, observed after test (Figure 3-19) and indicated by the vertical cracks showed in Figure 3-17 and Figure 3-18.

Close observations after the tests showed yielding of the anchor bars too. Each specimen had two out of four embedded inserts slightly pulled out (Figure 3-19 and Figure 3-20). Yet the concrete surrounding the inserts did not burst, as observed in the previous series with welded plates and shear keys (SA1 series). Note that for the SA2T3 specimen, the welding of the anchor bar ruptured (Figure 3-20 right image).

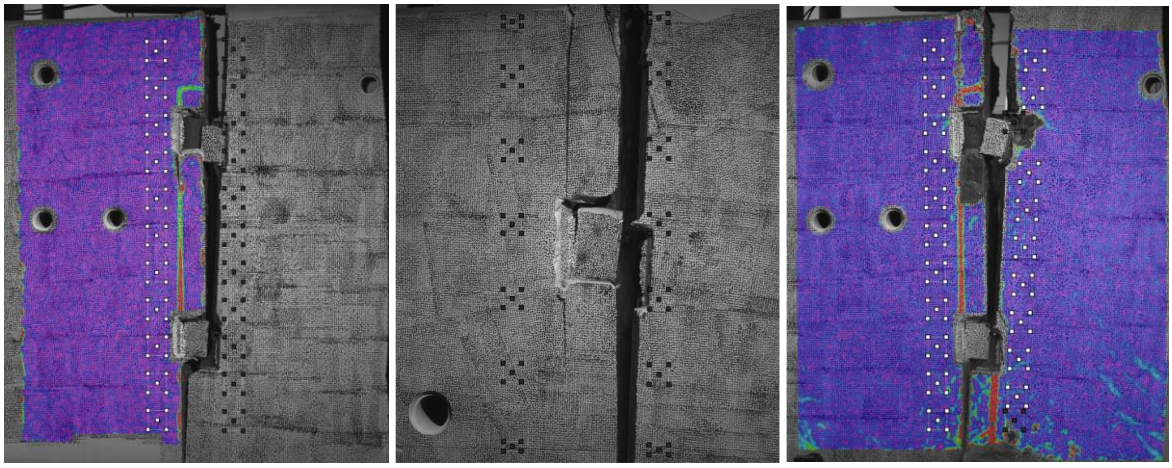

Figure 3-18 Test specimens after failure (from left to right) SA2T1, SA2T2, SA2T3

Figure 3-19 Test specimens interfaces after dismantling (from left to right) SA2T1, SA2T2, SA2T3

Figure 3-20 Indications of embedded insert pullout (from left to right) SA2T1, SA2T2, SA2T3 (anchor welds failure)

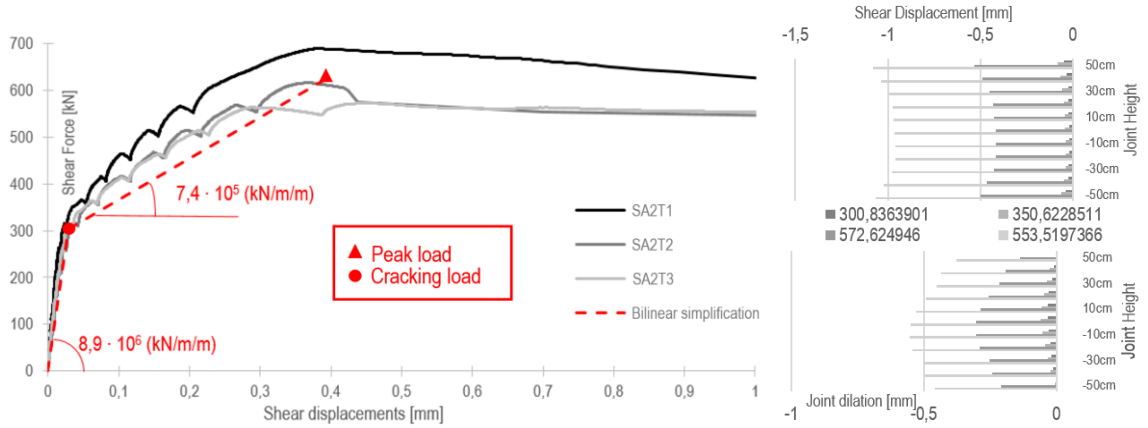

Figure 3-21 Left image: shear force vs average shear slip along the joint height (initial behavior zoomed in); right image: shear displacements and joint dilation distribution along the joint height (for SA2T2)

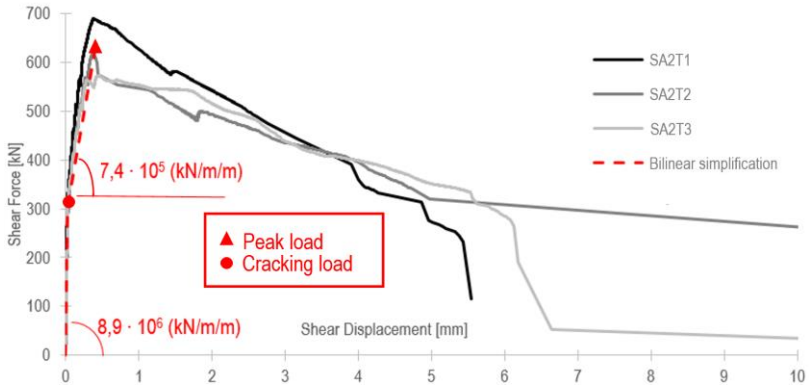

Figure 3-22 Shear force vs shear slip overall behavior (including post-peak behavior)

Table 3.3.4 – SA2 test results (individual result and average result)

	F_{crack} [kN]		F_{peak} [kN]		$K_{initial}$ [kN/m/m]		K_{final} [kN/m/m]	
SA2T1	309		689		9,7E+06		9,0E+05	
SA2T2	301	303	616	626	8,0E+06	8,9E+06	7,8E+05	7,4E+05
SA2T3	301		573		9,1E+06		5,3E+05	

3.4 Grouted connection with shear keys and bolts - CLock connection (SA3)

3.4.1 Specimens' presentation

This connection detail is a new proposal coming from the Connection Group of Consolis Design Standardization Project. This proposal aims to bring a more balanced connection layout, having high and reliable shear resistance (comparable to the welded plates and shear keys connections) and in the same time, allowing a practical, fast and economical casting process (comparable to the wire loop connections).

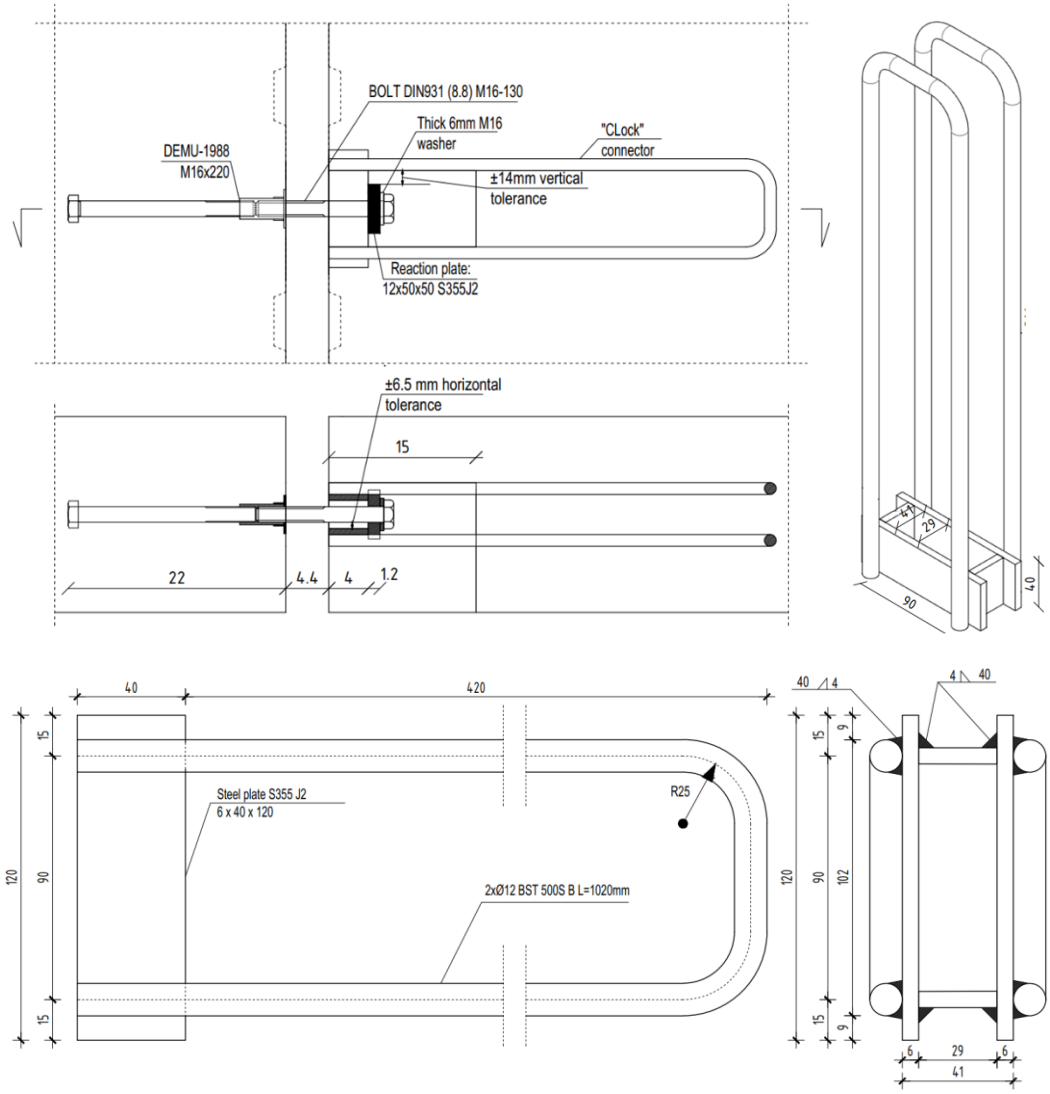

Figure 3-23 CLock connection detail

These test specimens were designed in a similar way as the previous welded plates test series. The welded plate assembly is replaced with the detail presented in Figure 3-23. The specimens particularities are described below:

- the casting process was simplified, the bolts went through holes into the mold, from one panel through the other (Figure 3-26). The bolt de-tightening and re-tightening was successfully verified before joint casting;
- the bolt net section area was reduced (in the attempt to reduce the gross area to the net area) for strain gauges application from 157mm^2 to 115mm^2 (Figure 3-26, left);
- the bolts adhesion to the grout was interrupted by the strain gauges protection material;
- bolt tightening torque was not measured;

- the wall recess designed for the bolt tightening was casted with an increased length (20cm instead of 15cm). This means a reduction of the bonding length for the CLock connector reinforcement. However, no damage was observed as a cause of reinforcement slippage;
- joint casting was done with the same dry mix non-sagging mortar widely used in Finland: Weber ESL C30/37 [14]. Material test results are presented in Table 3.4.1 and 3.4.2, with the Coefficient of Variation (CoV) with log normal distribution. To be noted that the temperature was above 25ºC and the material had a much poorer workability. This probably led to higher air content into the joint. The joint surface needed aesthetical repairment (Figure 3-27 right).

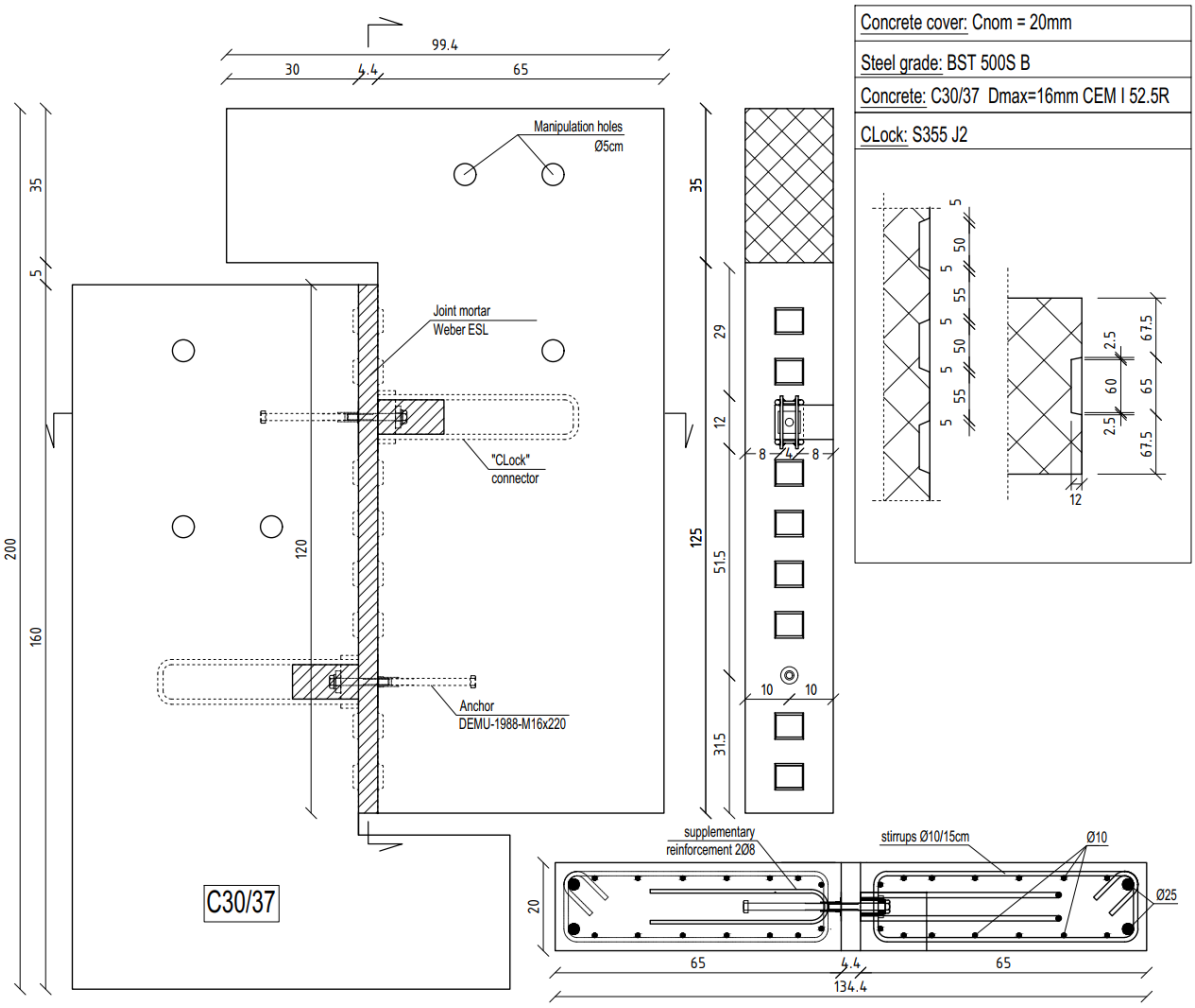

Figure 3-24 Configuration of SA3 specimens (dimensions in cm)

Figure 3-25 Test specimens SA3 (from left to right 1st, 2nd and 3rd test specimen)

Figure 3-26 CLock connection before panels casting (left); Strain gauges on bolts (right)

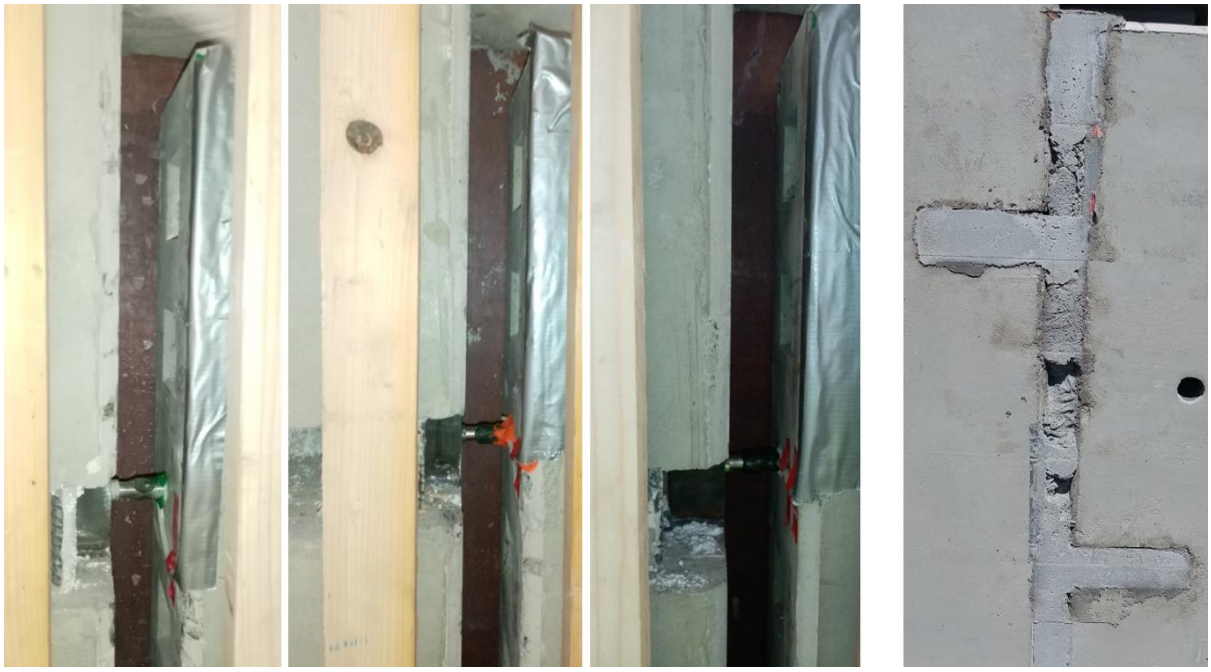

Figure 3-27 Joint casting (left image: test specimens before joint casting; right image: 1st test specimen before joint surface repairmen)

Table 3.4.1 - Concrete mechanical properties

$f_{cm.cube}$[1] [MPa]	f_{ctm}[2] [MPa]	E_{cm}[3] [GPa]	$f_{cm.prism}$[4] [MPa]
71,87	3,53	37,51	50,33
CoV: 0,03	CoV: 0,1	CoV: 0,04	CoV: 0,1

1 - average of 4 compressive tests according to SR EN 12390-3 on 150mm cubes; specimens age 36 days

2 - average of 10 tensile splitting tests using SR EN 12390-6 multiplied with a factor of 0,9 [7]; specimens age 39 days

3 - average of 3 elasticity modulus tests using SR EN 12390-13 on 100x100x300mm prisms; specimens age 41 days

4 - average of 3 prisms compressive strength according to SR EN 12390-13; specimens age 41 days

The concrete strength class requested was C30/37

Due to the early age of the specimens at testing, additional material tests were performed. Material test results showed that the age of the material test specimens influenced the compressive strength, but did not influenced the tensile strength.

Table 3.4.2 - Joint mortar mechanical properties

$f_{cm.cube}$[1] [MPa]	$f_{cm.cube.40mm}$[2] [MPa]	f_{ctm}[3] [MPa]	$f_{ctm.40mm}$[4] [MPa]	E_{cm}[5] [GPa]	$f_{cm.prism}$[6] [MPa]
43,99	36,99		4,76	26,15	39,50
CoV: 0,03	CoV: 0,02		CoV: 0,13	CoV: 0,02	CoV: 0,05
49,66	43,10		4,51		
	CoV: 0,07		CoV: 0,11		
	43,69		4,63		
	CoV: 0,03		CoV: 0,05		

1 - average of 4 and respectively 2 compressive tests according to SR EN 12390-3 on 150mm cubes; specimens age 29 and respectively 39 days

2 - average of 6 compressive tests on 40mm cubes according to SR EN 196-1; specimens age 27, 34, and respectively 41 days

4 - average of 4 flexural tensile tests on 40x40x160mm prisms according to SR EN 196-1 and converted according to 3.23 relationship from EN 1992-1-1; specimens age 27, 34 and respectively 41 days

5 - average of 3 elasticity modulus tests using SR EN 12390-13 on 100x100x300mm prisms; specimens age 39 days

6 - average of 5 prisms compressive strength according to SR EN 12390-13; specimens age 39 days

Weber ESL is a non-sagging mortar especially designed for vertical and horizontal joints of concrete elements according to EN 1504-4. The declared Strength class is C30/37-4 according to SFS-EN 206-1 with >40MPa according to EN 12390-3 and approximately 50MPa according to EN 12190

Table 3.4.3 - Steel mechanical properties

	f_y[1] [MPa]	f_u[2] [MPa]	E_s[3] [MPa]	ε_u[4] [%]
Insert anchors BST 500S	530,6	682,9	202.949	11,1
Steel insert S355	420,9	495,4	222.265	15,2

1 - Lower yielding strength

2 - Stress at the maximum force

3 - Young modulus (determined using digital extensometer and/or DIC)

4 - Strain at the maximum force (determined using digital extensometer and/or DIC)

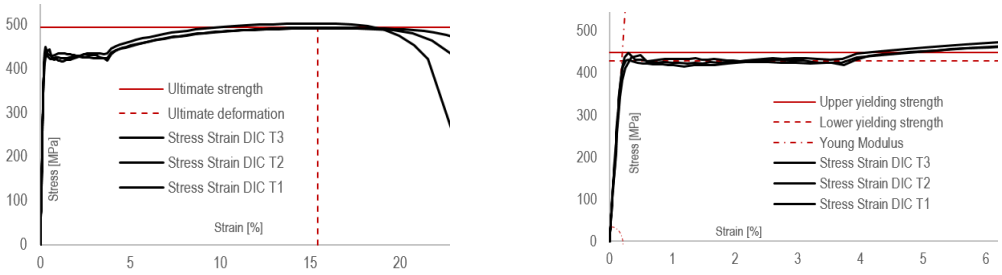

Figure 3-28 Experimental stress strain curve for the CLock material test specimen

Table 3.4.5 - Demu anchor - Bolt assembly, uniaxial tensile test

	F_{max}[1] [kN]	f_u[2] [MPa]	Δ_i[3] [mm]
Demu anchor - bolt assembly - T1	102,9	708,6	1,14
Demu anchor - bolt assembly (section reduced to 12.1mm diameter) - T2	102,2	703,8	-

1 - Maximum recorded force

2 - Stress at the maximum force calculated for the sleeve section (21mm outer diameter; 16mm inner diameter)

3 - Elongation measured at the maximum force, using a digital extensometer with a gauge length of 100 mm

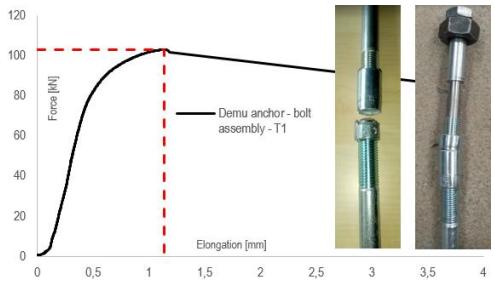

3.4.2 Experimental results

The test were carried out when the grouting material reached 28, 35, 41 days of maturity. Tests exhibited similar behavior up to the cracking load (indicated in Figure 3-36): linear behavior with slightly lower stiffness values compared to the previous tests (SA1 and SA2). DIC strain analysis showed low de-bonding of the interface prior to these values (Figure 3-29). After the crack progressive occurrence, the stiffness progressively decreased to a considerably low value, until the reaching of a peak load associated to very high shear displacements (as seen in Figure 3-37). The very low stiffness and the surface strains indicated severe damage of the shear keys (Figure 3-30), probably complete cut-off. The peak load can be associated to a friction mechanism combined with a dowel effect of the bolts (catenary effect). The dowel mechanism can be observed after tests too (Figure 3-33).

Note that the 2nd specimen bolts were poorly tightened. That caused de-bonding to start much faster, reducing the stiffness compared to the other two tests (Figure 3-36). It is proposed to provide a tightening torque to ensure that all the CLock pieces are in good contact, preventing premature sliding.

The 1st specimen was loaded faster than recommended, only 6 load steps were carried out until the reaching of the cracking load.

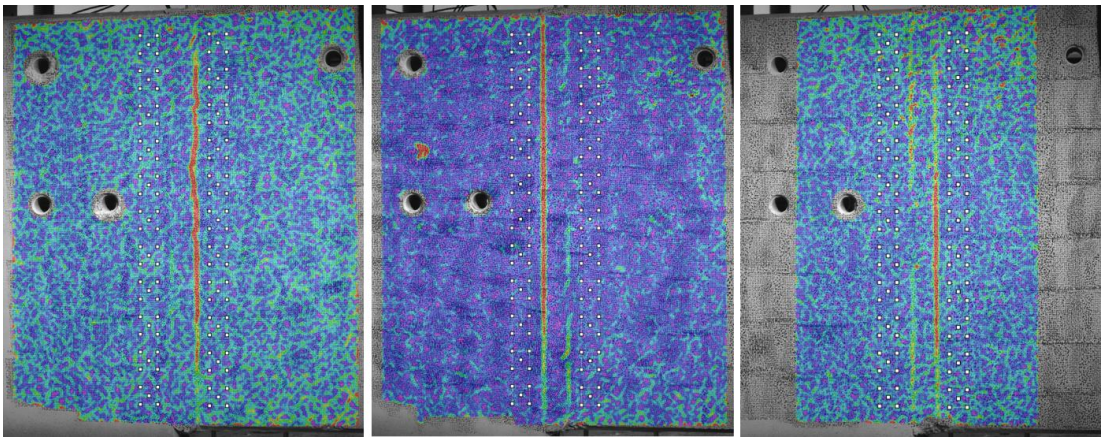

Figure 3-29 Crack pattern visualization at the cracking load (from left to right) SA3T1: 161.1kN, SA3T2: 127kN, SA3T3: 131.4kN, (using DIC, major strains)

Figure 3-29 shows cracking on right hand side of the joint for 1st and the 3rd test, while for the 2nd, the crack is on the left side. In a push-off configuration, both sides of the joint are loaded equally. The keys cut-off or the interface de-bonding usually appear on one of the two sides. This is due to non-homogeneity inherent of the concrete; one face will be weaker and crack.

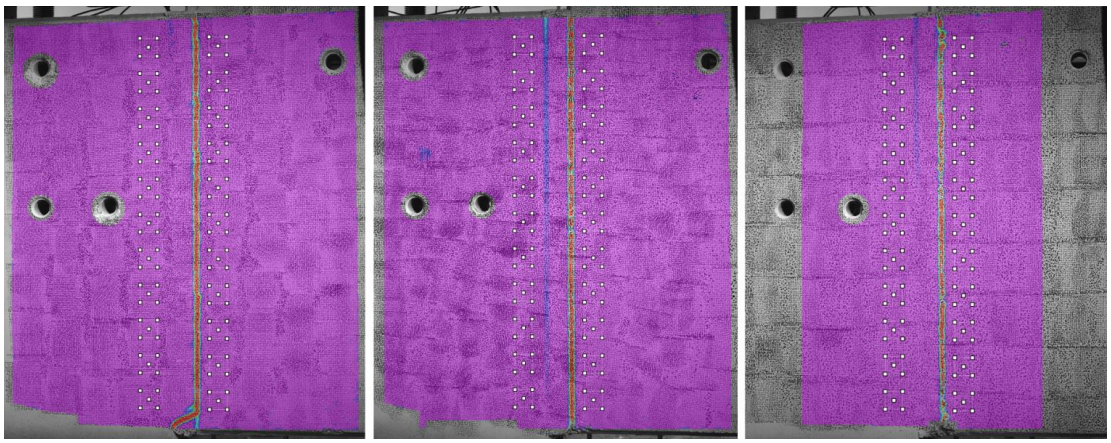

Figure 3-30 Crack pattern visualization during force stabilization, after cracking (from left to right) SA3T1, SA3T2, SA3T3

After the cracking load, the two panels started to lose their planarity. The joint dilation measured on the front face was 1mm higher than the one on the rear face, at the peak load. The bolts placed on the center of the wall represent a “hinged connection” in out of plane direction. The opening used for bolt tightening creates an eccentric shear key and so, the relative rotation of the two panels occurred in the same direction for all three specimens.

The rupture of the anchor nut caused the connection failure. Figure 3-33 shows that the whole bolt is bended due to the dowel effect, yet the anchor nut was the lowest link in the chain for all three specimens.

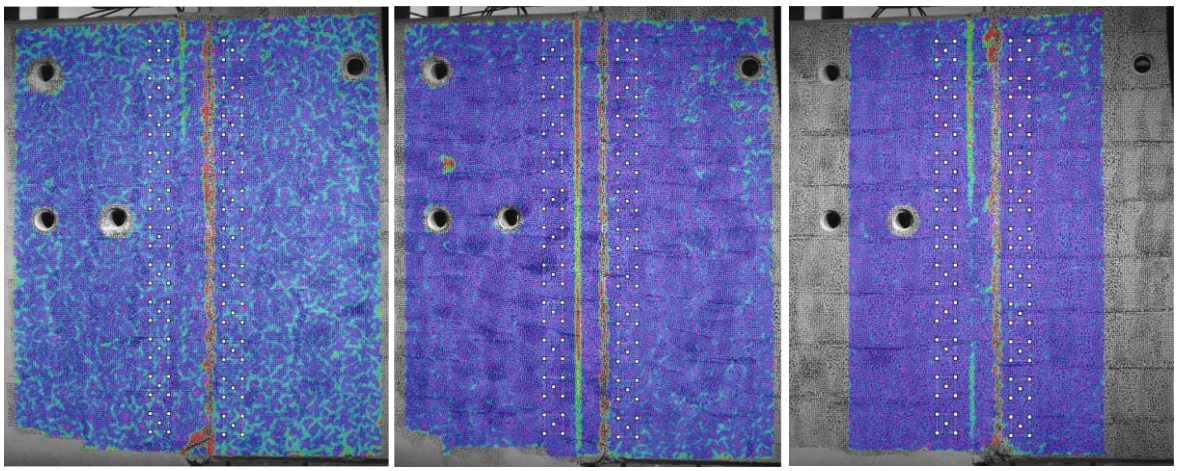

Figure 3-31 Crack pattern visualization at the reaching of the peak load (from left to right) SA3T1: 213.2kN, SA3T2: 224.2kN, SA3T3: 219.7kN, (using DIC, major strains)

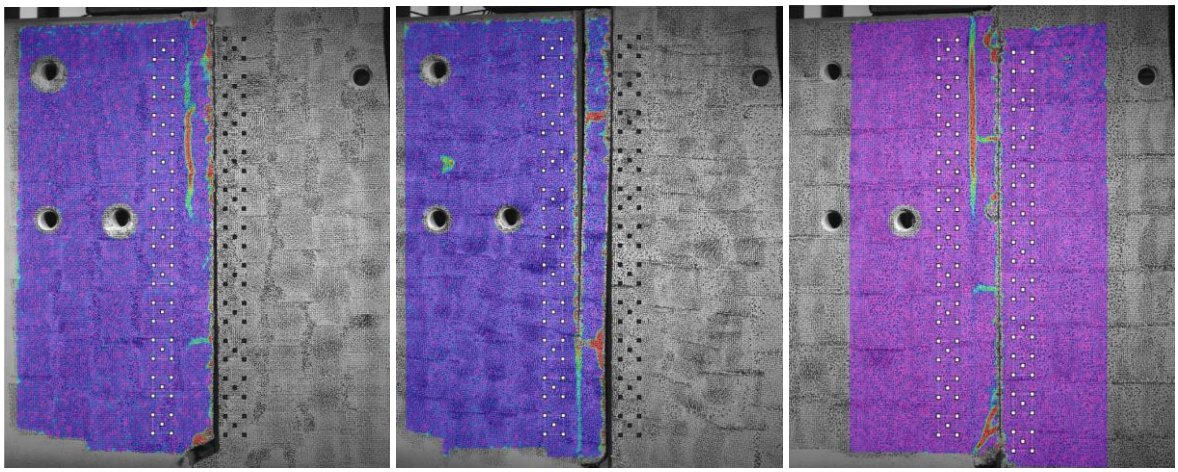

Figure 3-32 Test specimens after failure (from left to right) SA3T1, SA3T2, SA3T3

Figure 3-33 Part of the bolted steel assembly in the grouted area

Figure 3-34 Test specimens interfaces after dismantling (from left to right) SA3T1, SA3T2, SA3T3

Figure 3-35 Observed grout quality after testing (SA3T3)

The anchor nut failure could be expected since the net area of a M16 bolt is 157mm^2 and the nut sectional area is 145.2mm^2. According to the technical manual, the nut exterior diameter is 21mm, the bolt nominal diameter is 16mm, meaning that the net area of the nut would be the area of the ring section with the thickness of 5mm. However, the strength of the nut should be higher, to compensate for the smaller area and steer the failure into the bolt. Yet, it seems that the nut strength is actually lower, inasmuch as the area of the bolt was reduced to 113mm^2.

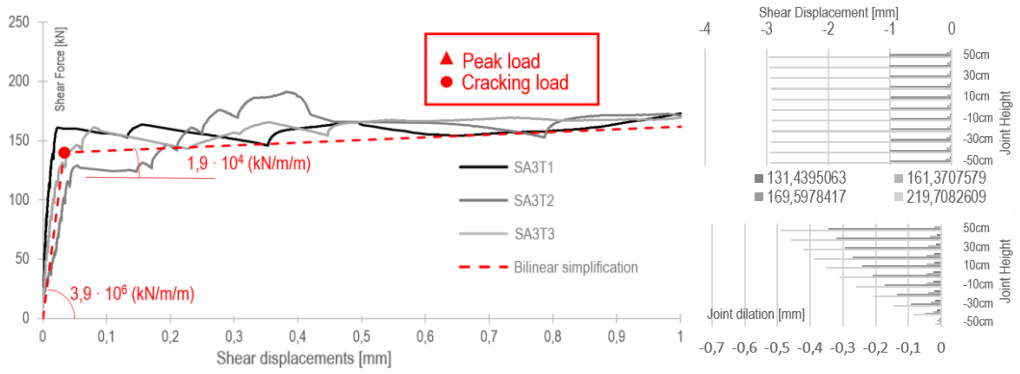

Figure 3-36 Left image: shear force vs average shear slip along the joint height (initial behavior zoomed in); right image: shear displacements and joint dilation distribution along the joint height (for SA3T2)

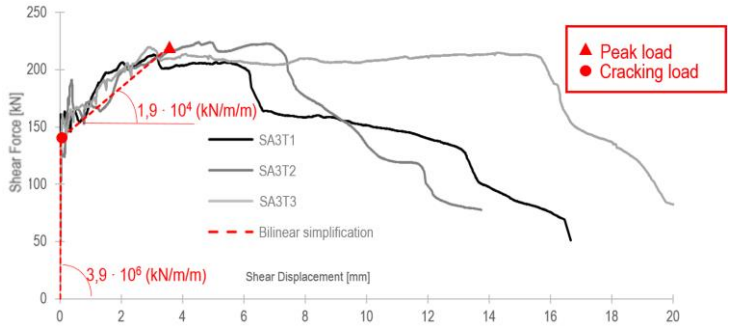

Figure 3-37 Shear force vs shear slip overall behavior (including post-peak behavior)

CLock connection exhibited an unstable and not very consistent post-cracking behavior, so only the initial stage must be taken into consideration for now. It is difficult to predict how choosing the peaks of the bilinear simplification (from Figure 3-37) will influence the shear wall assembly behavior.

Some things might be improved for this connection prototype. The anchor bolt nut should have a better strength, to be able to utilize the full strength of the bolt. Wall recess could be formed by a pre-installed EPS, which should be cut by an automatic machine. The wall reinforcement detailing should consider the wall recess that is needed to install the bolt. The quality control should ensure that the bolt is properly tighten in the assembly stage (a tightening torque should be provided). The Clock detail might use a rectangular open section to simplify the manufacturing process and the amount of welding required.

Table 3.4.4 – SA3 test results (individual result and average result)

	F_{crack} [kN]		F_{peak} [kN]		$K_{initial}$ [kN/m/m]		K_{final} [kN/m/m]	
SA3T1	161		213		5,9E+06		1,4E+04	
SA3T2	127	140	224	219	2,2E+06	3,9E+06	1,8E+04	1,9E+04
SA3T3	131		220		3,6E+06		2,5E+04	

3.5 Summary of the results. Comparisons with calculations

The experimental results presented in this chapter are summarized in table 3.5.1. All test specimens have a joint height of 1.2m, a wall thickness of 200mm and a joint width of 44mm. The mortar material properties summarized here are determined according to SR EN 196-1, on small material test specimens. This approach is considered relevant for the considered connection layout since the width of the joint is small.

Table 3.5.1 Summary of test results from connections with grouted shear keys and steel assemblies

Test index		[1]f_c [MPa]	[2]f_t [MPa]	[3]b_{key} [cm]	[4]h_{key} [cm]	[5]n_{key}	[6]f_y [MPa]	[7]A_s [mm^2]	[8]F_{crack} [kN]	[9]F_{peak} [kN]	[10]$K_{initial}$ [kN/m/m]	[11]K_{final} [kN/m/m]
SA1	SA1T1	81,2	10,60	20	6	6	560,3	785	646	1081	1,6E+07	6,4E+05
	SA1T2					7			641	1306	1,5E+07	8,3E+05
	SA1T3					6,5			650	1191	1,6E+07	6,6E+05
SA2	SA2T1	51,3	5,46	6,5	6	10	560,3	785	308,9	689,3	9,7E+06	9,0E+05
	SA2T2								300,6	616,4	8,0E+06	7,8E+05
	SA2T3								300,8	572,6	9,1E+06	5,3E+05
SA3	SA3T1	37,0	4,76	6,5	6	8	-	226	161,1	213,2	5,9E+06	1,4E+04
	SA3T2	43,1	4,51						127	224,2	2,2E+06	1,8E+04
	SA3T3	43,7	4,63						131,4	219,7	3,6E+06	2,5E+04

1 - average compressive strength on 40mm mortar cubes according to SR EN 196-1

2 - average tensile strength for mortar according to SR EN 196-1 flexural tensile tests on 40x40x160mm prisms converted according to 3.23 relationship from EN 1992-1-1

3 - width of the shear keys
4 - height of the shear keys
5 - number of shear keys
6 - yielding strength of tying steel assemblies (determined from the literature)
7 - area of the reinforcement of the weakest link from the tying steel assemblies
8 - test cracking load
9 - highest load reached in each experiment (ultimate load)
10 - secant slope of the shear load - shear displacement graph from 0 to the cracking load
11 - secant slope of the shear load - shear displacement graph from the cracking load to the ultimate load

Table 3.5.2 and Table 3.5.3 shows the mean values of the three tests of each series (designed to be identical) and the spread (in percentages) from the mean value. Here we can see that for the welded plates specimens (SA1 and SA2) the cracking load have a small spread of values (up to 1.8%). The peak loads have a larger spread of values (up to 10.1%). For the bolted connection, the spread was opposite (the cracking loads, up to 15.21%; the peak loads, up to 2.66%). Large spread of values (± 20%) is usually encountered in shear tests, e.g. [5] [9].

Table 3.5.2 - Loads: mean results and differences from the mean values

	Specimen	F_{crack} [kN]	mean	difference	F_{peak} [kN]	mean	difference
SA1	SA1T1	646	646	0,05%	1081	1193	-9,36%
	SA1T2	641		-0,72%	1306		9,50%
	SA1T3	650		0,67%	1191		-0,14%
SA2	SA2T1	309	303	1,80%	689	626	10,09%
	SA2T2	301		-0,93%	616		-1,55%
	SA2T3	301		-0,87%	573		-8,54%
SA3	SA3T1	161	140	15,21%	213	219	-2,66%
	SA3T2	127		-9,18%	224		2,36%
	SA3T3	131		-6,03%	220		0,30%

Table 3.5.3 – Stiffness: mean results and differences from the mean values

	Specimen	$K_{initial}$ [kN/m/m	mean	difference	K_{final} [kN/m/m]	mean	difference
SA1	SA1T1	1,6E+07	1,6E+07	4,43%	4,8E+05	6,6E+05	-26,86%
	SA1T2	1,5E+07		-4,57%	8,3E+05		26,12%
	SA1T3	1,6E+07		0,13%	6,6E+05		-6,84%
SA2	SA2T1	9,7E+06	8,9E+06	8,62%	9,0E+05	7,4E+05	22,21%
	SA2T2	8,0E+06		-10,82%	7,8E+05		5,25%
	SA2T3	9,1E+06		2,20%	5,3E+05		-27,46%
SA3	SA3T1	5,9E+06	3,9E+06	50,51%	1,4E+04	1,9E+04	-25,69%
	SA3T2	2,2E+06		-42,97%	1,8E+04		-5,97%
	SA3T3	3,6E+06		-7,55%	2,5E+04		31,66%

The spread of values is even higher in terms of stiffnesses (Table 3.5.3). We can see for the welded plate specimens that the initial stiffness deviated up to 10.8% from the mean value of three specimens designed to be identical. For the second stage, deviation was 27.5%. The CLock specimens (SA3) had differences in terms of stiffness up to 50.51%.

When discussing the applicability of Linear Elastic Finite Element method for estimating the internal forces in precast constructions, two major facts should be clarified:

- the first is how to interpret the statistical spread? Should the values be statistically decreased, so the overall shear wall behavior will be on the safe side? If the stiffness is considered lower than in reality, the vertical connections will be designed for a lower load and their capacity will be on the unsafe side;
- the second: Linear Elastic Finite Element Analyses are using linear elastic springs for connections. The cracking load is the moment where the uncertainty starts. Here, deeper investigations with a Non Linear Finite Elements Analysis (e.g. Diana FEA), might be able to provide insights and lead to recommendations for safe stiffness values proposals to be used for simplified Linear Elastic Finite Element global analysis.

For estimating the shear capacity of the vertical joints, EN 1992-1-1 states that the longitudinal shear resistance of grouted joints between slab or wall elements may be calculated according to chapter 6.2.5 [7]: the interface shear resistance between concrete layers cast at different times. This is a very general approach and its range of applicability and references are not clearly stated. The multitude of novel connection layouts, more and more economical from the casting and labor time perspective, rises debates whether such a general approach is universally applicable or not. The 6.25 equation from EN 1992-1-1 [7] is presented below.

$$V_{Rd} = (c\, f_{ctd} + \sigma_n\, \mu + \rho\, f_{yd}\, (\mu\, sin\, \alpha + cos\alpha))\, A_i = c\, f_{ctd}\ A_i + A_s\, f_{yd}\, \mu \qquad (1)$$

$$V_{Rd} \leq 0.5\, \vartheta\, f_{cd}\, A_i$$

The design relationships (1) consists of three terms that consider the cohesion between the two materials, external normal pressure across the interface and the contribution of tying reinforcement, respectively. No external force was applied during experiments, so $\sigma_n = 0$.

The first term from eq. (1) considers the bonding of the interface, dependent on the tensile strength (f_{ctd}) and a factor "c" for considering the interface roughness (c equals to 0.25 for very smooth interface, 0.5 for indented interface). Paragraph (4) from chapter 6.2.5 of EN 1992-1-1 states that in cases when the joint can be significantly cracked, factor "c" should be taken as 0 for smooth and rough joints and 0.5 for indented joints (also discussed in section 10.9.3 (12) of [7]). As seen in the specimens' descriptions the interface area is not fully indented, so the interface area should be chosen according to Figure 3-38. Material test specimens showed that the tensile strength

of the concrete was lower than the tensile strength of the grout. Yet, the failure crack crossed the grout in all experiments, so the tensile strength of grout will be used further in calculations.

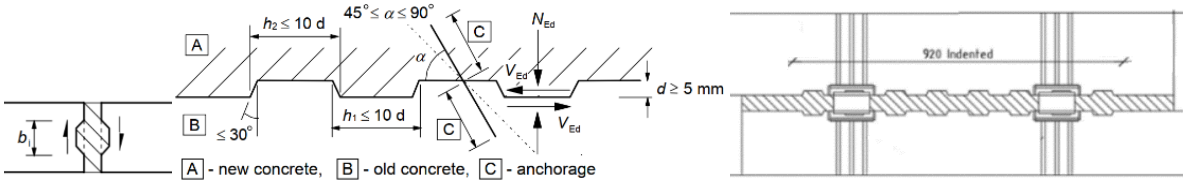

Figure 3-38 Example of indented interfaces from EN 1992-1-1 [7]; example of interface length [in mm] from SA1;

Air bubbles were observed in the joints casted with thixotropic mortar. Weber ESL technical manual [14], declares an air content of 8-12%. This might also impact the calculations. Consequently, the interfaces area for the specimens casted with thixotropic mortar (SA2 and SA3) was reduced by a factor of 0.88.

The third term of eq. (1) considers the contribution of the reinforcement area (A_s) to the shear resistance, by multiplying the reinforcement ratio ($\rho = A_s / A_i$) with the interface roughness factor. It considers the relative angle of the reinforcement to the interface (α). This term is backed by the shear-friction hypothesis: the shear resistance is given by the clamping force provided by the reinforcement up to its yielding load, multiplied with a friction coefficient [1]. The classical reinforcement is replaced with the welded steel assembly. The contribution of the welded steel assembly is difficult to assess. The steel plate welded to the embedded insert might fail in tension under different mechanisms: yielding of the anchor bars, welding failure, yielding of the welded plate.

During experiments, the tensile yielding of the anchor bars seemed to cause the failure of the shear-friction/shear-lock mechanism. The calculation method for the tie force obtained from the 10 mm diameter anchor bars is presented in Figure 3-39. The tying force (clamping force, F_{tie}) is presented in Table 3.5.4 for the SA1 and SA2 series.

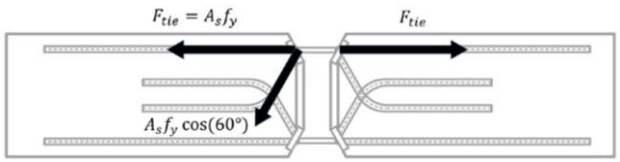

Figure 3-39 Calculation scheme for reinforcement contribution

As regards SA2, the CLock prototype was designed to direct the failure through the bolt: the CLock anchor section, anchorage and steel plates were easy to design for the capacity of the bolt. On the other side, the embedded bolt (anchor) needs verifications according EN 1992-4 that are difficult to satisfy for a C30/37 and a 200mm wall edge. Even if all concrete failure verification according to EN 1992-4 are satisfied, the safety factors for bolts embedded in concrete are higher than the ones for steel structures (from EN 1993). Axial tensile tests on the embedded anchor-to-bolt assembly showed that the weakest link is the anchor sleeve (Table 3.4.5). For the code design calculation – experimental comparison (Table 3.5.4), the CLock tensile capacity was taken directly from the axial tensile tests.

Based on the descriptions presented above, the experimental peak loads are compared to the formula 6.25 from EC2 using mean material properties.

Table 3.5.4 Eurocode 2 (6.25) – experimental comparison, using mean material properties

	f_{ct} [MPa]	b_i [m]	L_i [m]	F_{tie} [kN]	F_{calc} [kN]	F_{test} [kN]	F_{test} / F_{calc}	$F_{test.mean}$ / F_{calc}
SA1T1	10,63	0,200	0,92	439,84	1373,8	1081,0	0,79	
SA1T2	10,63	0,200	0,92	439,84	1373,8	1306,0	0,95	0,87
SA1T3	10,63	0,200	0,92	439,84	1373,8	1191,0	0,87	
SA2T1	5,46	0,065	1,20	439,84	583,2	689,30	1,18	
SA2T2	5,46	0,065	1,20	439,84	583,2	616,40	1,06	1,07
SA2T3	5,46	0,065	1,20	439,84	583,2	572,60	0,98	
SA3T1	4,76	0,065	1,20	205,2	348	213,20	0,61	
SA3T2	4,51	0,065	1,20	205,2	339,5	224,20	0,66	0,64
SA3T3	4,63	0,065	1,20	205,2	343,6	219,70	0,64	

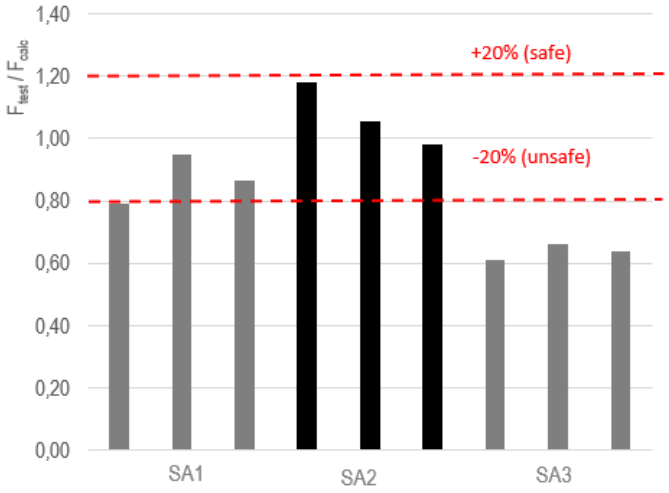

Figure 3-40 Test and calculation comparison chart

Table 3.5.4 and Figure 3-40 shows the comparison between the EN1992-1-1 calculations and the test results. A ±20% deviation is usually encountered in concrete shear behavior and it is generally an acceptable spread of values (e.g. [4]). The average ratio between the experimental load and model resistances is 0,86. However, should be emphasized that eq. (1) does not explicitly take into account the dowel effect, that was observed after the experiments (discussed in chapter 3.4.2). Unlike the welded plates series (SA1 and SA2), the Clock connection (SA3) reached the peak load at relatively high shear displacements. The shear displacements of the vertical connections should be lower than a certain limit. That limit should be chosen to make sure their bearing capacity is utilized before the complete failure of the horizontal connections (crushing of the mortar and/or the tensile rupture of the vertical ties).

4 CONNECTION WITH HIGH STRENGTH WIRE LOOPS

4.1 Introduction

High strength wire loops pre-installed in wire boxes [15], facilitate the on-site assembly process, by replacing the classic connections with overlapped U-bars and shear keys. This topic was previously discussed at the 14th fib Symposium, Rome, 2022 [16]. Scientific literature provides good insight for this connection type [4], [5]. A rigid-plastic upper bound model, calibrated with experimental results [4] is provided to estimate the ultimate shear strength. The current design practice in Europe is dictated by EN 1992-1-1, chapter 6.2.5 [7], yet it does not provide methods to estimate the clamping force provided by the wire loops. The clamping force might be estimated using the rigid-plastic model; however, this approach should not be carried out if rupture of the wire ropes is decisive [4]. The failure of the wire loop was shown to be brittle, not complying with the requirements of EN 1992-1-1, Annex C [7]. Therefore, for this connection type, it is proposed that the wire rope should be the strongest link in the connection. Then the crushing of the mortar and the yielding of the lacer bar should provide ductility and allow stress redistribution [4].

The stiffness topic has been addressed by several researchers (e.g. [5]), although, when compared, the results obtained by Jørgensen [4] and Biswal [5] show disagreement in terms of post-elastic shear behavior.

This section will present the results of three test series containing three different commercial connection layouts. First two are comparing Peikko PVL80 [15] wire boxes with the much larger boxes, Pintos Okaria 80 [17], provided with a thinner wire. The last series uses a Phillip [18] constructive rail provided with 5 pairs of wires (mainly used to transfer small loads).

4.2 Wire loops series 1: Peikko PVL 80 (WL1)

4.2.1 Specimens' presentation

The tested connection detail was designed according to the technical specifications provided by Peikko [15] and the description presented in chapter 3.2.1. The particularities of this series are presented below:

- the lacer bar was provided with end plates (secured by screwing) in order to compensate for the lack of anchorage length at the joint extremities;
- joint casting was done with a dry mix non-sagging mortar widely used in Finland and the Baltic Countries: Weber ESL C30/37 [14]. The joint was casted manually, in a vertical position. One side of the joint was fully molded from the beginning, while the mold on the other side was installed progressively during the casting. Mean material properties and their coefficient of variation with normal distribution (CoV) are presented in Table 4.2.1 and 4.2.2;
- existing horizontal cracks were observed on the joint surface before testing (≤0.1mm crack width). The existing cracks did not grow during tests and did not show a significant depth;
- the wire loops are not perfectly fixed in the boxes, having the possibility of sliding in and out the box. In case of several wire loops it was noticed that the wire overlapping was around 50mm instead of 60mm (as described in the technical specifications [15]).

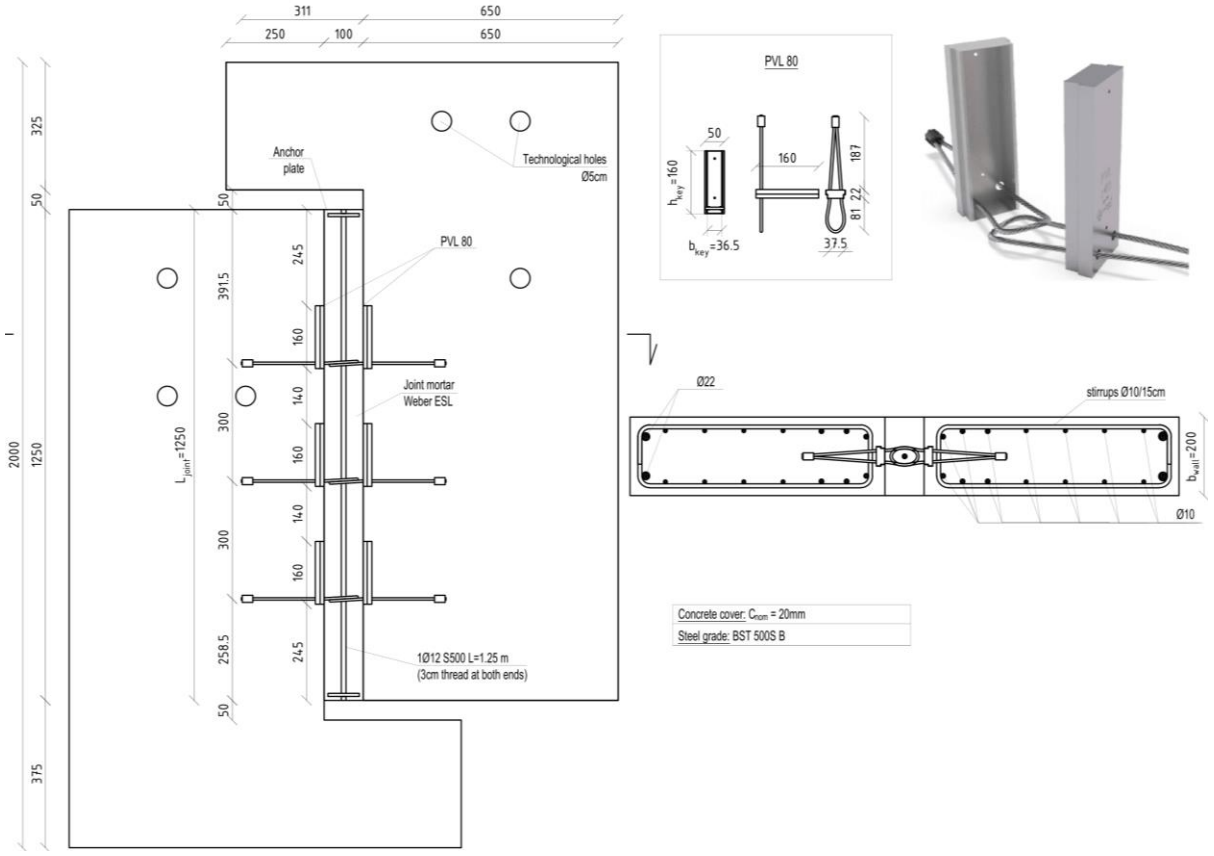

Figure 4-1 Configuration of WL1 specimens (dimensions in mm)

Figure 4-2 Test specimens from WL1 (from left to right 1st, 2nd and 3rd test specimen)

Figure 4-3 Wire boxes before panels casting

Figure 4-4 Test specimens before (left images) and after (right images) joint casting

Table 4.2.1 - Concrete mechanical properties

$f_{cm.cube}$[1] [MPa]	f_{ctm}[2] [MPa]	E_{cm}[3] [GPa]	$f_{cm.prism}$[4] [MPa]
76,20	3,74	39,46	53,23
CoV: 0,02	CoV: 0,12	CoV: 0,04	CoV: 0,15

1 - average of 3 compressive tests according to SR EN 12390-3 on 150mm cubes; specimens age 123 days

2 - average of 7 tensile splitting tests using SR EN 12390-6 multiplied with a factor of 0,9 [7]; specimens age 130 days

3 - average of 3 elasticity modulus tests using SR EN 12390-13 on 100x100x300mm prisms; specimens age 124 days

4 - average of 3 prisms compressive strength according to SR EN 12390-13; specimens age 124 days
The concrete strength class requested was C30/37.

Table 4.2.2 - Joint mortar mechanical properties

$f_{cm.cube}$[1] [MPa]	$f_{cm.cube.40mm}$[2] [MPa]	f_{ctm}[3] [MPa]	$f_{ctm.40mm}$[4] [MPa]	E_{cm}[5] [GPa]	$f_{cm.prism}$[6] [MPa]
56,73	58,86	2,34	5,09	28,86	51,78
CoV: 0,08	CoV: 0,07	CoV: 0,08	CoV: 0,08	CoV: 0,01	CoV: 0,09

1 - average of 6 compressive tests according to SR EN 12390-3 on 150mm cubes; specimens age 68 days

2 - average of 12 compressive tests on 40mm cubes according to SR EN 196-1 ; specimens age 65 days

3 - average of 6 tensile splitting tests using SR EN 12390-6 multiplied with a factor of 0,9 [7]; specimens age 92 days

4 - average of 6 flexural tensile tests on 40x40x160mm prisms according to SR EN 196-1 and converted according to 3.23 relationship from EN 1992-1-1; specimens age 65 days

5 - average of 3 elasticity modulus tests using SR EN 12390-13 on 100x100x300mm prisms; specimens age 85 days

6 - average of 3 prisms compressive strength according to SR EN 12390-13; specimens age 85 days
Weber ESL is a non-sagging mortar especially designed for vertical and horizontal joints of concrete elements according to EN 1504-4. The declared Strength class is C30/37-4 according to SFS-EN 206-1 with >40MPa according to EN 12390-3 and approximately 50MPa according to EN 12190

Table 4.2.3 - Steel mechanical properties

	F_{max}[0] [kN]	f_y[1] [MPa]	f_u[2] [MPa]	E_s[3] [MPa]	ε_u[4] [%]
Lacer bar BST 500S		530,6	682,9	202.949	11,1
Peikko - PVL 80 *	46,0	814,4	814,4	37.626	2,55%

0 - Maximum recorded force
1 - Lower yielding strength
2 - Stress at the maximum force
3 - Secant Young modulus (determined using digital extensometer and/or DIC)
4 - Strain at the maximum force (determined using digital extensometer and/or DIC)
* Stresses in wires are determined according to the node equilibrium presented below along with the test set-up.

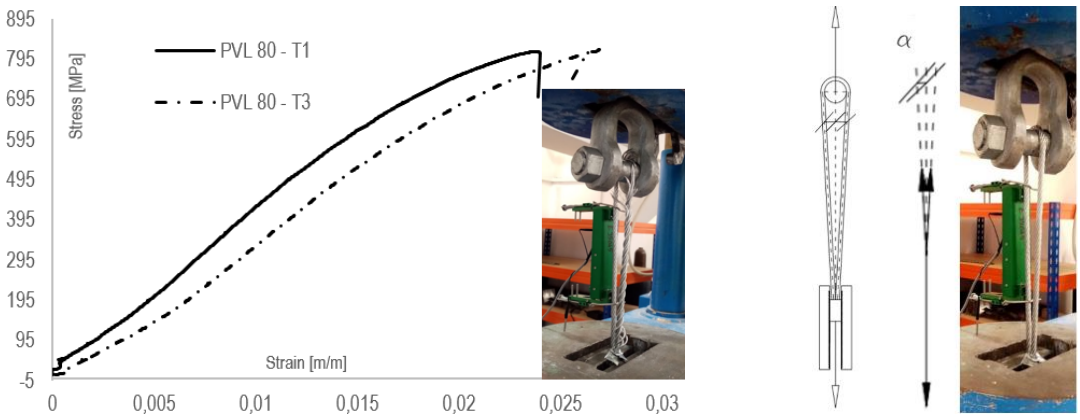

Figure 4-5 Experimental stress-strain curve for two PVL 80 wire loops and test set-up (preloaded by ≈ 0.5kN to straighten the wires)

4.2.2 Experimental results

At the time of testing, the grouting material age ranged between 63 and 85 days. Although the three testing specimens had identical joint set-ups and were casted in similar conditions, significant differences were measured in terms of force - shear slip behavior, cracking load and peak load. The results are considered very inconsistent. The force - shear slip behavior can be divided in two stages: a pre-cracking stage followed by a post-cracking stage.

In the pre-cracking stage, very small shear-slip displacements were measured: ≈0.15mm for the 1st and the 3rd test and 0.04mm for the 2nd test. This stage is completed by reaching the cracking load, which was also equal to the peak load for the 1st and the 2nd test. After the end of this stage, LVDTs measured shear slips around 12mm for the 1st test, 5mm for the 2nd and 2mm for the 3rd test (at the starting of the post-cracking stage). Figure 4-6 show the test specimens at the end of the pre-cracking stage.

In all three tests, a descending branch in the curve can be identified, followed by a hardening branch. Only for the 3rd test, the hardening branch reached a peak load (of 161,7kN) higher than the cracking load (increased by 135%). The relative shear displacement associated to the peak load was 16.6mm. The completion of this stage is marked by the wires rupture for the 2nd and the 3rd specimen (shown in Figure 4-7). The failure crack went through the grout shear keys (complete key shear-off; see Figure 4-8). In the 1st test, only one wire broke and the others remained bonded in the grout (see Figure 4-8). Air gaps surrounding the wires were observed after the test (Figure 4-8), that probably increased their elongations. This might explain why there was no increase in capacity at higher shear displacements. The 1st test was stopped due to shear displacement limitations imposed by the configuration of the test set-up.

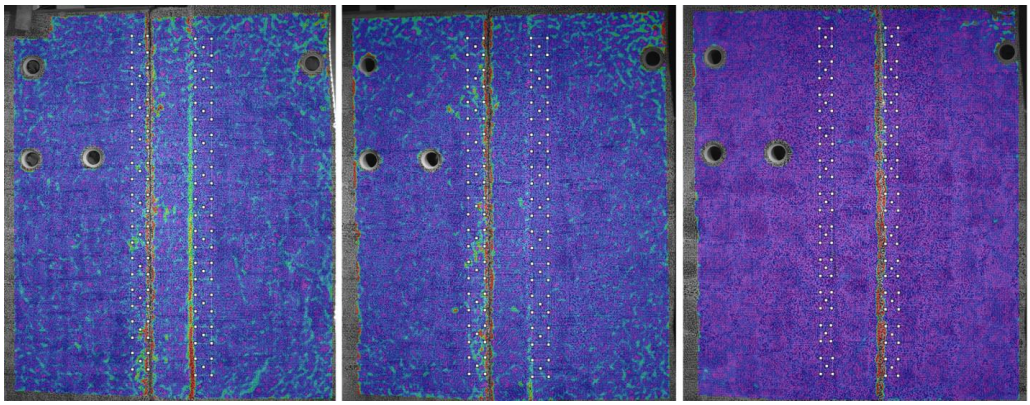

Figure 4-6 Crack pattern visualization just after the cracking load (from left to right). Cracking loads for Test 1: 102.5kN, Test 2: 147.2kN, Test 3: 68.9kN (major strains, using DIC)

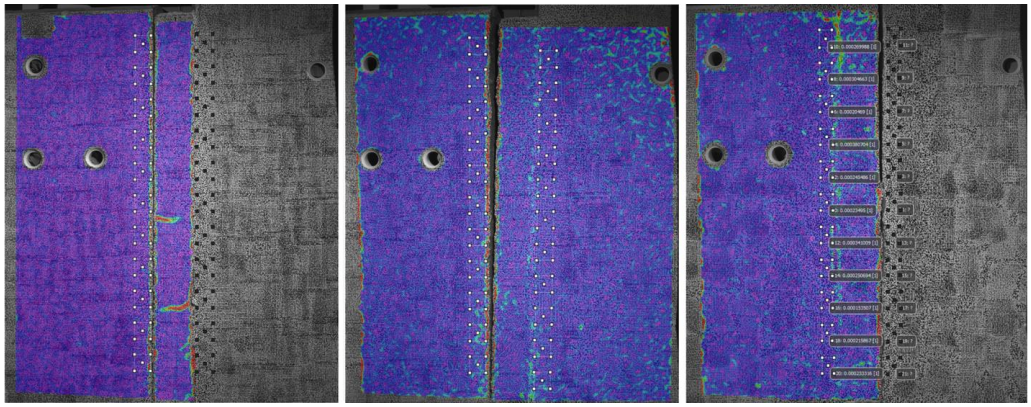

Figure 4-7 Observed failure mechanisms after failure (from left to right). Peak loads for Test 1: 102.5kN, Test 2: 147.2kN, Test 3: 161.7kN

Figure 4-6 and Figure 4-7 shows cracking and failure of the left hand side interface of the joint for 1st and the 2nd test. While for the 3rd test, the crack is on the right side. The same explanation is given here, as in chapter 3.4.2. The non-homogeneity inherent of the concrete will cause one interface to be weaker and crack.

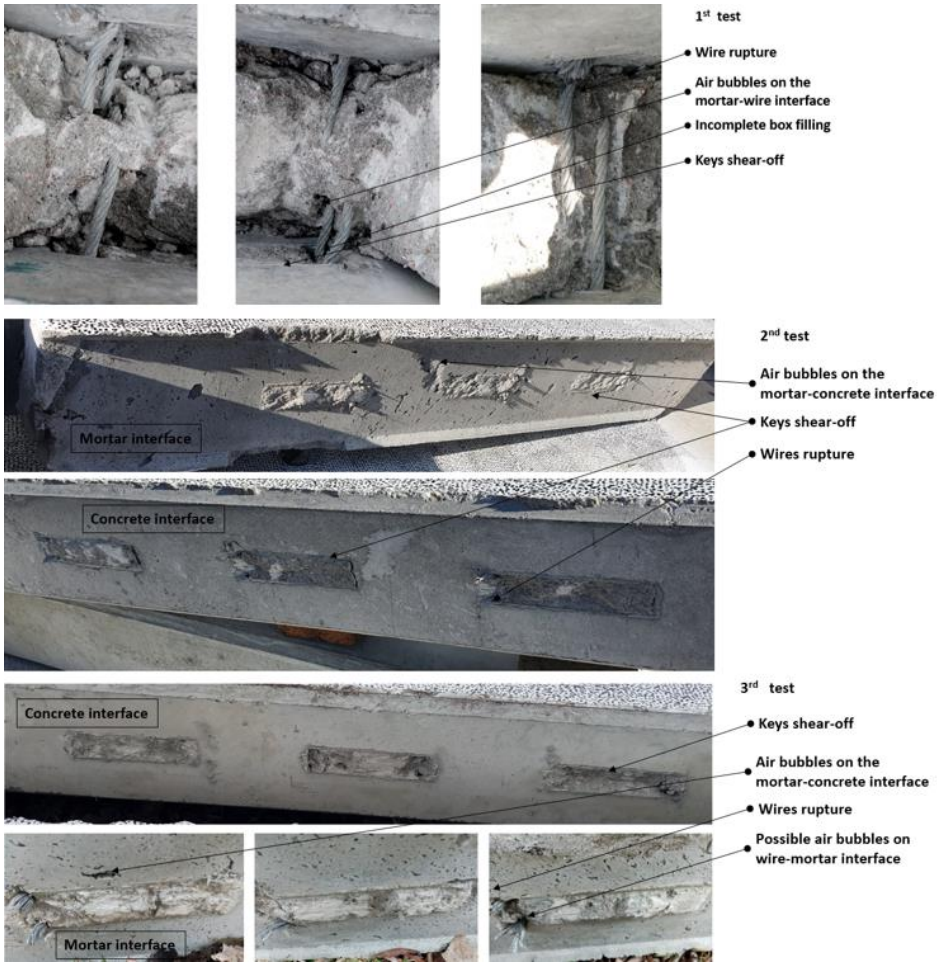

Figure 4-8 Analysis of the failed connections

In the pre-cracking stage, for the 1st and the 3rd test, the stiffness can be approximated by two secant slopes: first one with $1.5 \cdot 10^6$ kN/m/m stiffness value and the following slope is decreased by 87.8% to a value of $3 \cdot 10^5$ kN/m/m. For the 2nd specimen, the stiffness had an increase of 381.5% (to an average value of $1.3 \cdot 10^7$ kN/m/m) compared with the other two specimens. The stiffness remained constant up to 82% of the cracking (and peak) load.

The post-cracking stage is presented in Figure 4-10. Here it can be observed that the 1st and the 2nd test do not reach a higher load than the cracking load. This behavior might be associated with the results presented by Biswal [5], shown in Figure 4-11 (right side graph). The 3rd test reached a higher peak load in the post-cracking stage (as discussed in previous chapter) having a stiffness decrease of 98.93% from the pre-cracking stage (post-cracked stiffness: $4.5 \cdot 10^3$ kN/m/m). This behavior might be associated with the test results presented by Jørgensen [4], shown in Figure 4-11 (left side graph).

There is a major difference between Jørgensen and Biswal in joint casting procedure. The test specimens presented by Jørgensen were casted with a greased joint interface. The test specimens presented by Biswal were casted with an artificially roughened interface. For the test specimens presented in this report, the interface did not received any treatment before joint grouting (left as cast interface). Due to the small area of the shear keys, the cohesion of the very smooth surface has a big influence on the peak loads. This topic will be debated in chapter 4.7.

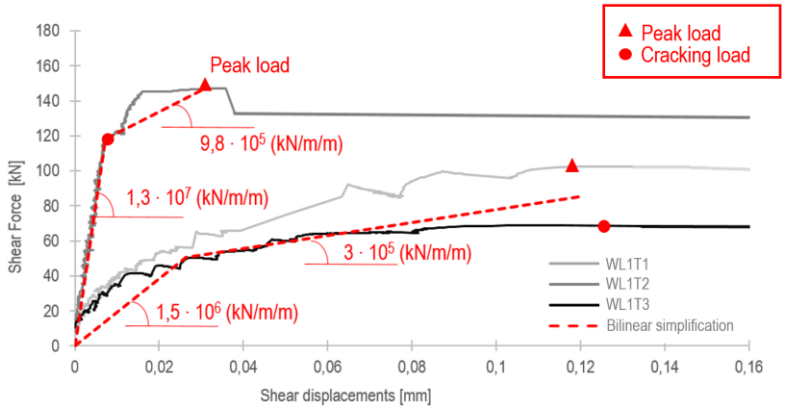

Figure 4-9 Shear force vs average shear slip along the joint height (initial behavior zoomed in)

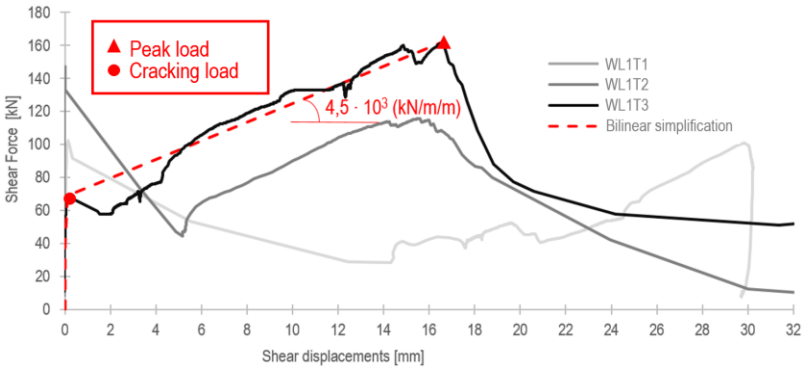

Figure 4-10 Shear force vs shear slip overall behavior (including post-peak behavior)

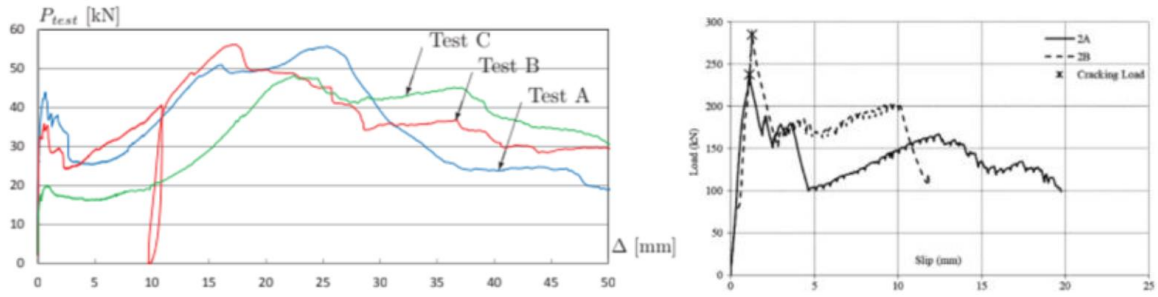

Figure 4-11 Load vs shear slip presented by Jørgensen [4] **tests on PVL60 (left image) and Biswal** [5] **on PVL 100 (right image)**

The results presented here and in the past are raising great concerns regarding the structural use of this type of wire loops connections. It is safer to be avoided for structural systems that require strong interaction between the wall elements, for achieving stability or satisfying other ULS verifications (e.g. horizontal connections, wall panels strength).

Table 4.2.4 – Load and stiffness: mean results

		F_{crack} [kN]	F_{peak} [kN]	$K_{initial}$ [kN/m/m]	K_{final} [kN/m/m]
WL1	WL1T1	103	103	1,4E+06 and 3,5E+05	-
	WL1T2	147	147	1,3E+07	-
	WL1T3	68,9	162	1,8E+06 and 2,7E+05	4,5E+03

4.3 Wire loops series 2: Pintos Okaria WI 80 (WL2)

4.3.1 Specimens' presentation

The tested connection was designed and casted according to the technical specifications provided by Okaria [17]. The description of the test specimens is identical to the specimens from WL1 series, presented in chapter 4.2.1. In this case, the wires could not be completely straightened, and the overlapping has various dimensions: from 37 to 50mm. The wires before joint casting are presented in Figure 4-14.

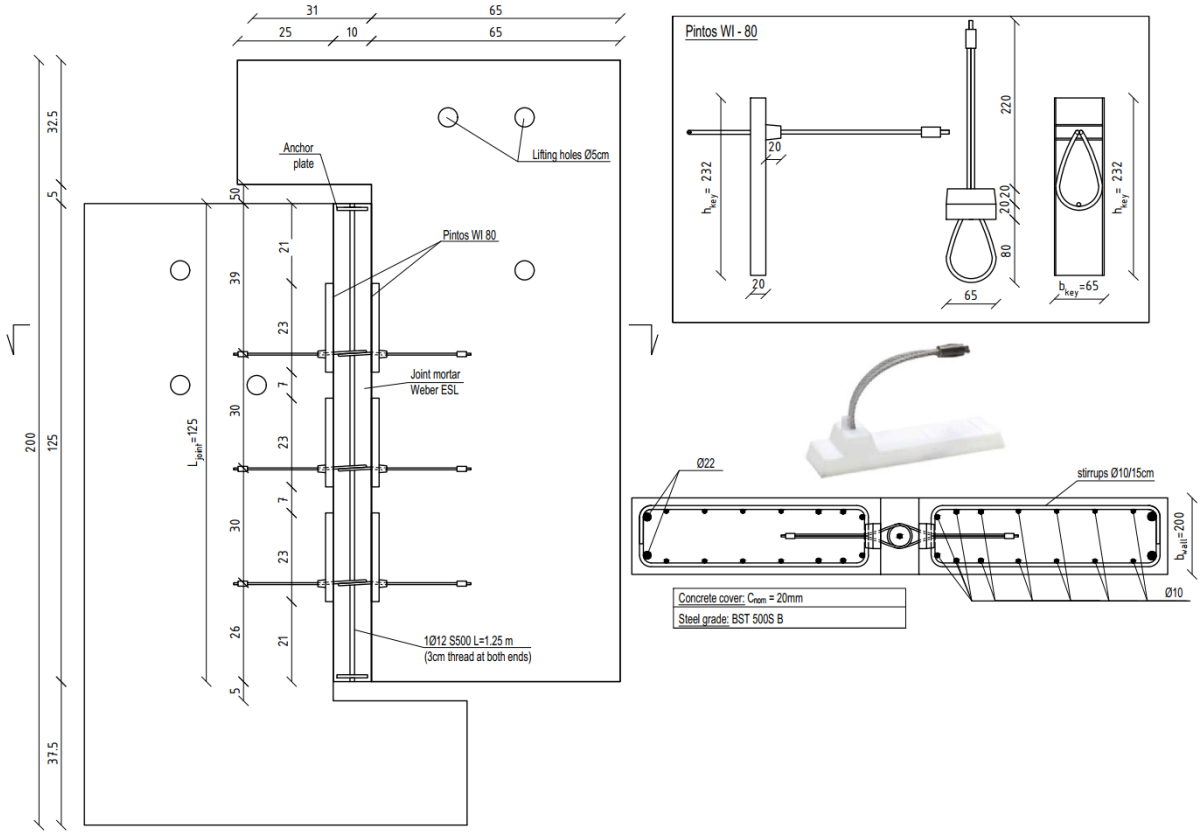

Figure 4-12 Configuration of WL2 specimens (dimensions in cm)

Figure 4-13 Test specimens (from left to right 1st, 2nd and 3rd test specimen)

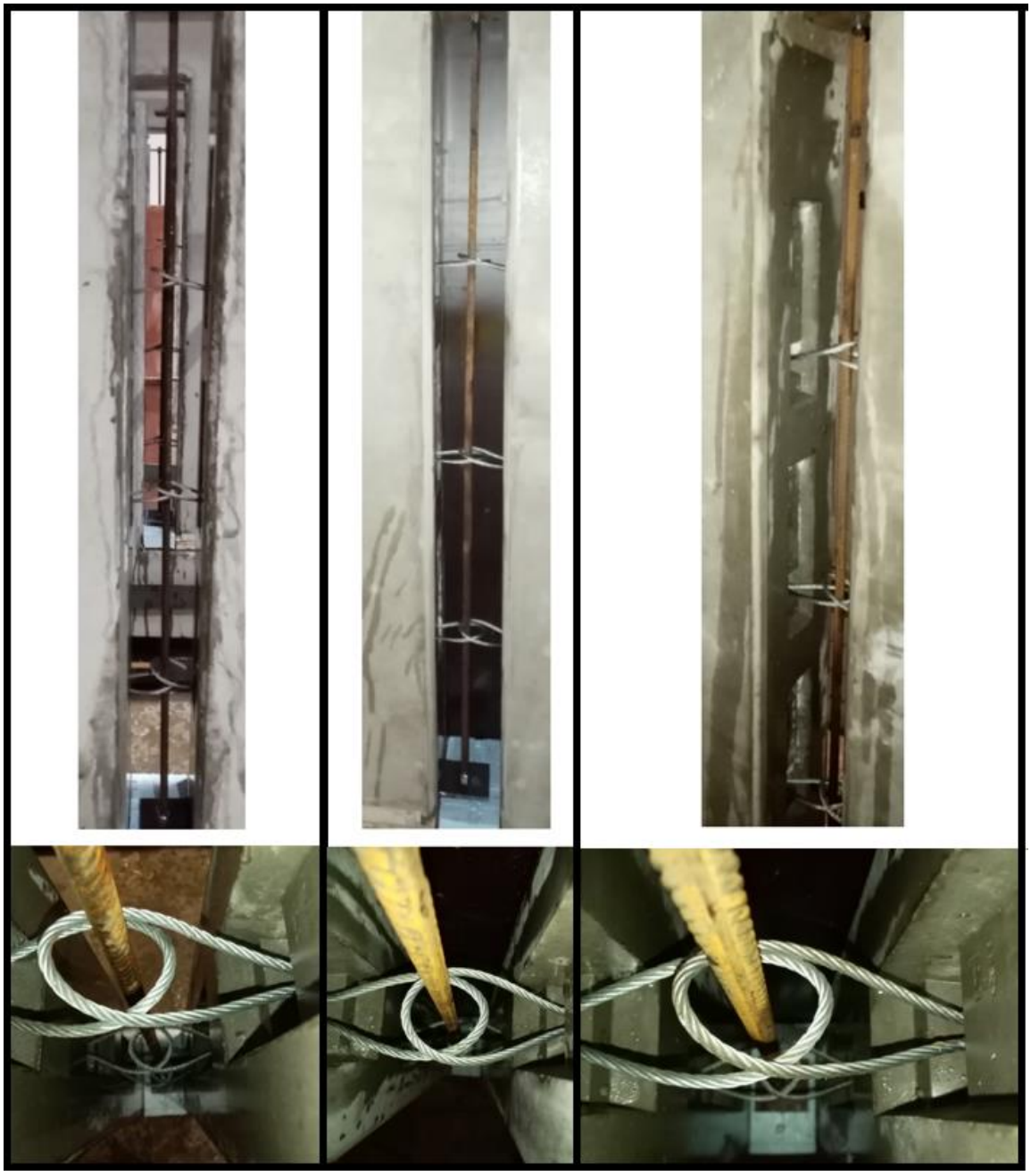

Figure 4-14 Test specimens before joint casting (from left to right 1st, 2nd and 3rd test specimen)

Table 4.3.1 - Concrete mechanical properties

$f_{cm.cube}$[1] [MPa]	f_{ctm}[2] [MPa]	E_{cm}[3] [GPa]	$f_{cm.prism}$[4] [MPa]
74,85	3,52	36,86	55,14
CoV: 0,05	CoV: 0,12	CoV: 0,02	CoV: 0,06

1 - average of 3 compressive tests according to SR EN 12390-3 on 150mm cubes; specimens age 73 days

2 - average of 3 tensile splitting tests using SR EN 12390-6 multiplied with a factor of 0,9 [7]; specimens age 85 days

3 - average of 3 elasticity modulus tests using SR EN 12390-13 on 100x100x300mm prisms; specimens age 87 days

4 - average of 3 prisms compressive strength according to SR EN 12390-13; specimens age 87 days

The concrete strength class requested was C30/37.

Table 4.3.2 - Joint mortar mechanical properties

$f_{cm.cube}$[1] [MPa]	$f_{cm.cube.40mm}$[2] [MPa]	f_{ctm}[3] [MPa]	$f_{ctm.40mm}$[4] [MPa]	E_{cm}[5] [GPa]	$f_{cm.prism}$[6] [MPa]
49,24	54,73	2,36	5,48	27,36	44,03
CoV: 0,03	CoV: 0,08	CoV: 0,1	CoV: 0,11	CoV: 0,02	

1 - average of 3 compressive tests according to SR EN 12390-3 on 150mm cubes; specimens age 57 days

2 - average of 6 compressive tests on 40mm cubes according to SR EN 196-1 ; specimens age 75 days

3 - average of 5 tensile splitting tests using SR EN 12390-6 multiplied with a factor of 0,9 [7]; specimens age 57 days

4 - average of 6 flexural tensile tests on 40x40x160mm prisms according to SR EN 196-1 and converted according to 3.23 relationship from EN 1992-1-1; specimens age 75 days

5 - average of 3 elasticity modulus tests using SR EN 12390-13 on 100x100x300mm prisms; specimens age 71 days

6 - average of 2 prisms compressive strength according to SR EN 12390-13; specimens age 71 days

Weber ESL is a non-sagging mortar especially designed for vertical and horizontal joints of concrete elements according to EN 1504-4. The declared Strength class is C30/37-4 according to SFS-EN 206-1 with >40MPa according to EN 12390-3 and approximately 50MPa according to EN 12190

Table 4.3.3 - Steel mechanical properties

	F_{max}[0] [kN]	f_y[1] [MPa]	f_u[2] [MPa]	E_s[3] [MPa]	ε_u[4] [%]
Lacer bar BST 500S		530,6	682,9	202.949	11,1
Pintos Okaria WI 80 *	37,8	963,6	963,6	61.020	1,76%

0 - Maximum recorded force

1 - Lower yielding strength

2 - Stress at the maximum force

3 - Secant Young modulus (determined using digital extensometer and/or DIC)

4 - Strain at the maximum force (determined using digital extensometer and/or DIC)

* Stresses in wires are determined according to the node equilibrium presented below along with the test set-up.

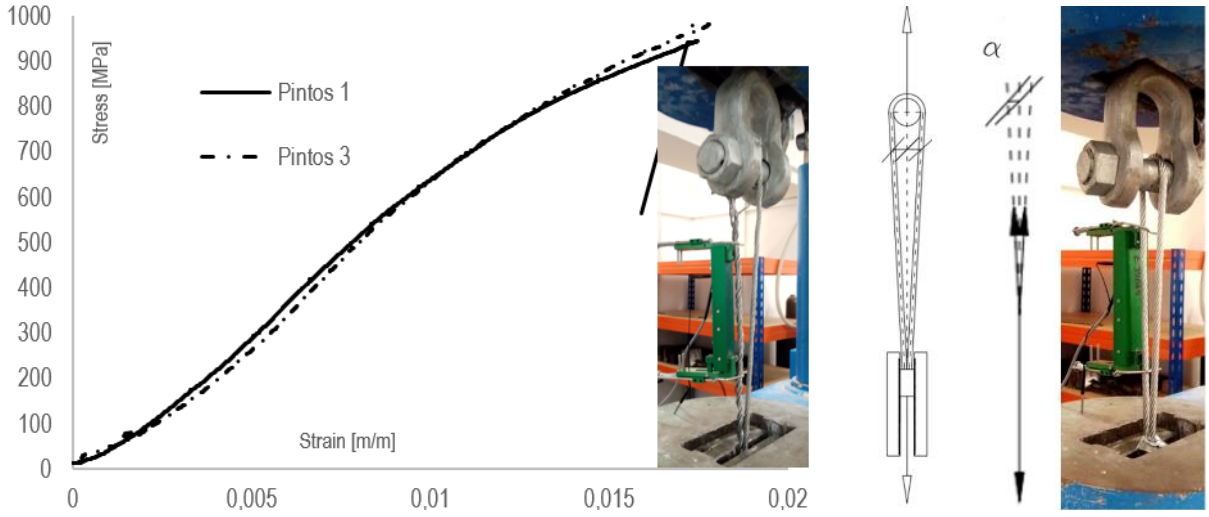

Figure 4-15 Experimental stress-strain curve for two Pintos wire loops and test set-up (preloaded by ≈ 0.5kN to straighten the wires)

4.3.2 Experimental results

At the time of testing, the grouting material age ranged between 56 and 84 days. The force - shear slip behavior can be divided in two stages: a pre-cracking stage followed by a post-cracking stage. 1st & 3rd test show a very similar pre-cracking behavior: similar cracking load and similar stiffness. 2nd test from this series displays a much lower cracking value (40% lower) and stiffness (80% lower). The peak loads have similar values for the 1st and the 3rd test, but the shear displacements associated to the peak loads are: 8.5mm for the 1st and 0.4mm for the 3rd. The 2nd specimen presents a poorer post-cracking behavior compared to the other two.

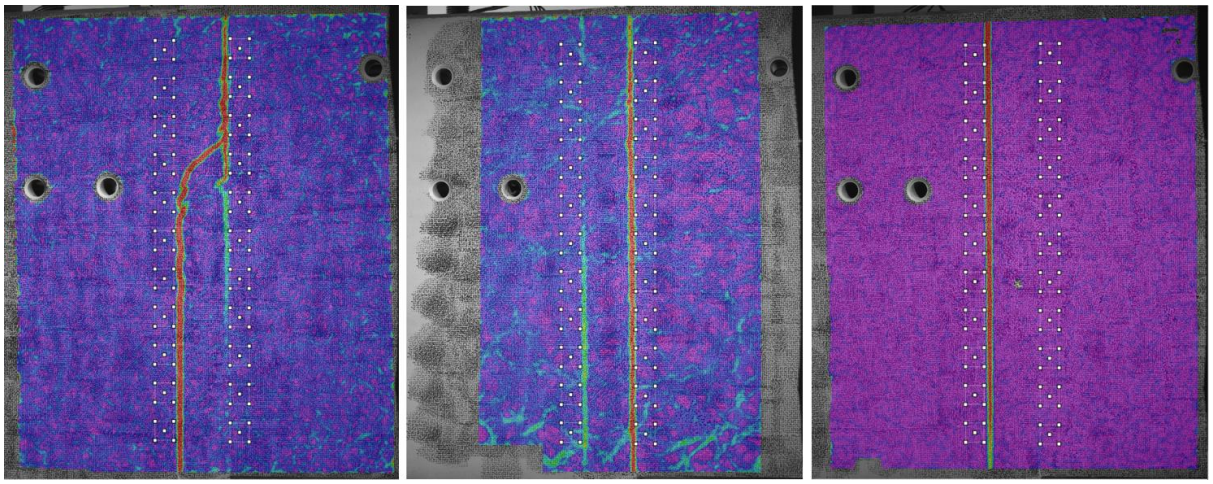

Figure 4-16 Crack pattern visualization just after the cracking load (from left to right). Cracking loads for WL2T1: 182.9kN, WL2T2: 109.1kN, WL2T3: 181.4kN (major strains, using DIC)

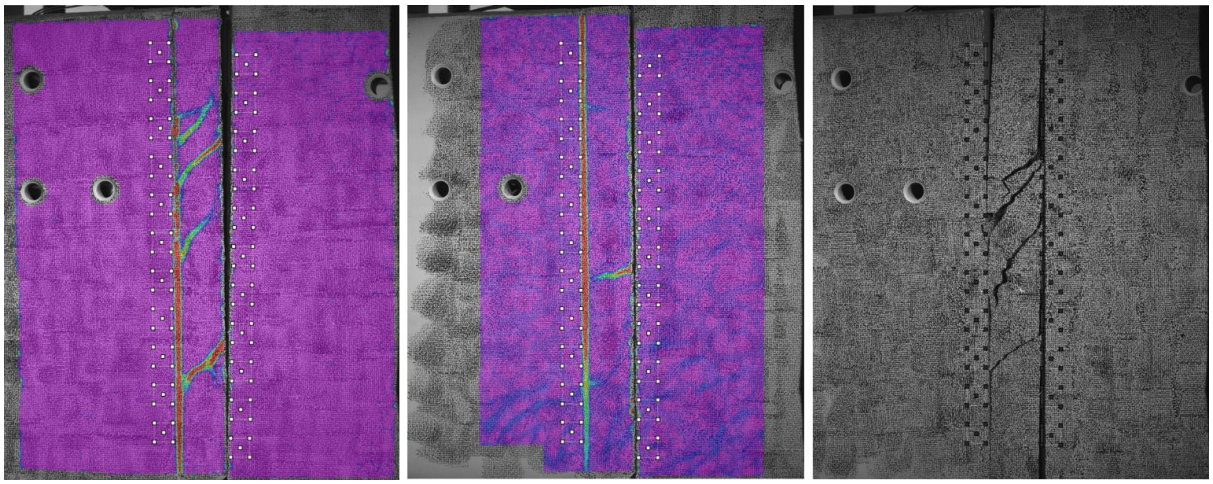

Figure 4-17 Observed failure mechanisms after failure (from left to right). Peak loads for Test 1: 227.7kN, Test 2: 168.2kN, Test 3: 243kN

Major dissimilarities can be observed between the three identical specimens, in terms of failure mechanisms. Figure 4-18 shows corner crushing of the keys and wires rupture for the 1st and the 2nd specimen. The 3rd specimen was the only one that exhibited the wire anchorage failure. After closer look to the 2nd specimen (Figure 4-18 in the middle), significant air bubbles were observed in the shear keys. This might explain why the stiffness and shear capacity were lower for this specimen.

Figure 4-18 WL2 specimens after testing (from left to right: 1st test, 2nd test, 3rd test)

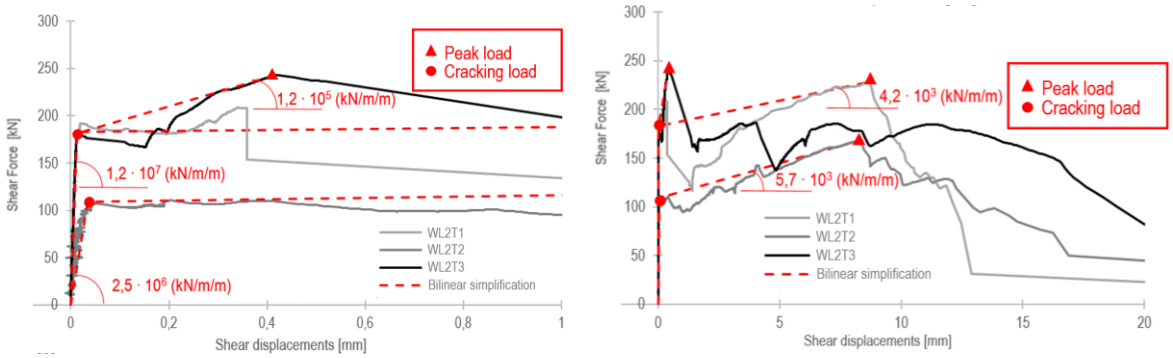

Figure 4-19 Shear force vs average shear slip along the joint height (left image: initial behavior zoomed in; right image: including post-peak behavior)

Table 4.3.4 – WL2 test results (individual and average results)

	F_{crack} [kN]		F_{peak} [kN]		$K_{initial}$ [kN/m/m]		K_{final} [kN/m/m]	
WL2T1	183		228		1,2E+07		4,2E+03	
WL2T2	109	158	168	213	2,5E+06	8,8E+06	5,7E+03	-
WL2T3	181		243		1,2E+07		1,2E+05	

4.4 Wire loops series 3: Phillip constructive rails (WL3)

4.4.1 Specimens' presentation

The tested connection was designed and casted according to the technical specifications provided by Philipp [18]. The test specimens are presented in Figure 4-20 and the reinforcement layout is shown in Figure 4-21. The description of the test specimens is identical to the specimens from WL1 series, presented in chapter 4.2.1. For this type of connector, the wires are provided with a fixing system that prevents wires from sliding and ensures a constant overlapping length into the joint. It was not possible to straighten the wires to obtain a perfect overlapping in the horizontal plane (see Figure 4-22). In other words, the angle between the wires and the joint surface was not 90º.

The producer declares this connection layout as a constructive connection, not a structural one. The rail surface is profiled, with small grooves (Figure 4-23) that are not complying to EN1992-1-1, chapter 6.2.5, conditions for rough interfaces.

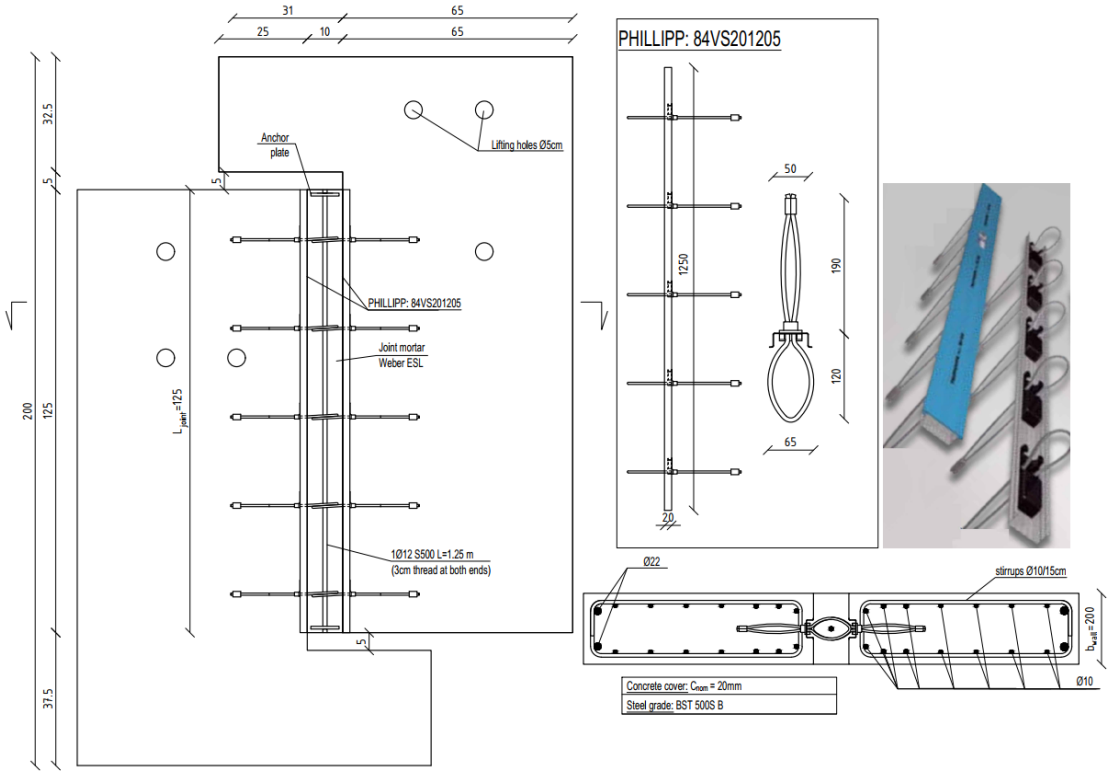

Figure 4-20 Configuration of WL3 specimens (dimensions in cm)

Figure 4-21 Test specimens from WL3 (from left to right 1st, 2nd and 3rd test specimen)

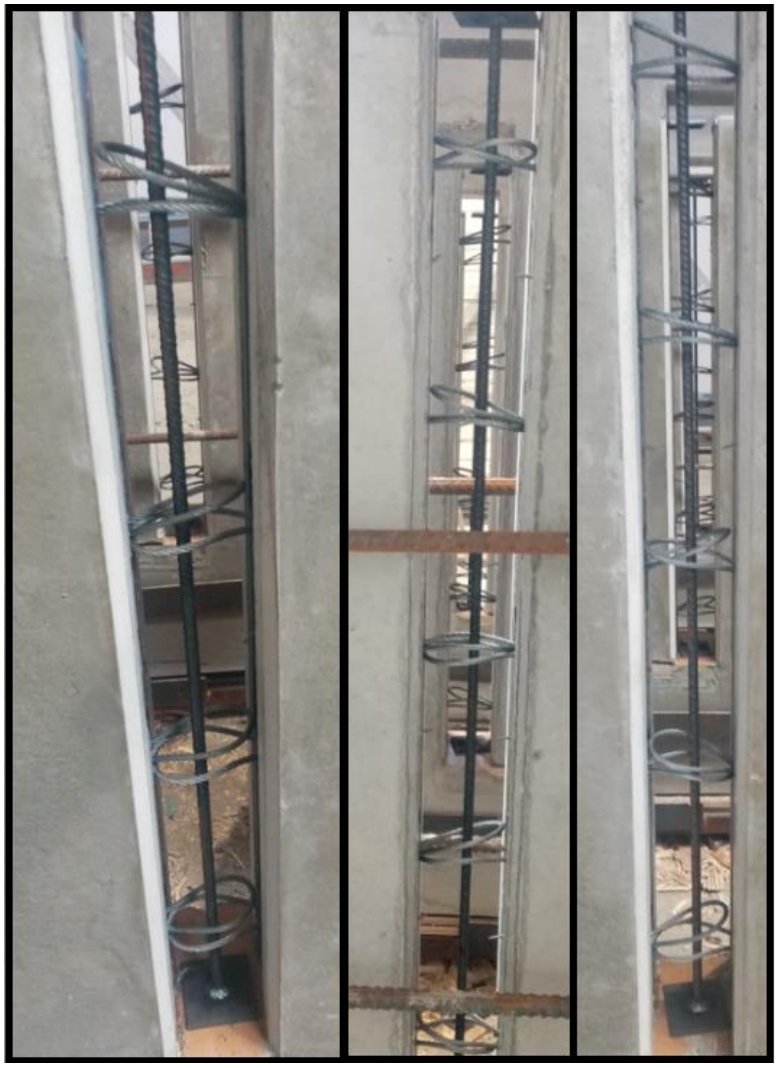

Figure 4-22 Test specimens before joint casting WL3 (from left to right 1st, 2nd and 3rd test specimen)

Figure 4-23 Profiled surface

Table 4.4.1 - Concrete mechanical properties

$f_{cm.cube}$[1] [MPa]	f_{ctm}[2] [MPa]	E_{cm}[3] [GPa]	$f_{cm.prism}$[4] [MPa]
77,52	4,17	40,11	58,92
CoV: 0,01	CoV: 0,12		

1 - average of 4 compressive tests according to SR EN 12390-3 on 150mm cubes; specimens age 75 days

2 - average of 8 tensile splitting tests using SR EN 12390-6 multiplied with a factor of 0,9 [7]; specimens age 75 days

3 - average of 2 elasticity modulus tests using SR EN 12390-13 on 100x100x300mm prisms; specimens age 80 days

4 - average of 2 prisms compressive strength according to SR EN 12390-13; specimens age 80 days

The concrete strength class requested was C30/37.

Table 4.4.2 - Joint mortar mechanical properties

$f_{cm.cube}$[1] [MPa]	$f_{cm.cube.40mm}$[2] [MPa]	f_{ctm}[3] [MPa]	$f_{ctm.40mm}$[4] [MPa]	E_{cm}[5] [GPa]	$f_{cm.prism}$[6] [MPa]
54,61	53,52	2,25	4,13	31,14	47,84
CoV: 0,05	CoV: 0,09	CoV: 0,08	CoV: 0,07	CoV: 0,08	CoV: 0,03

1 - average of 3 compressive tests according to SR EN 12390-3 on 150mm cubes; specimens age 72 days

2 - average of 6 compressive tests on 40mm cubes according to SR EN 196-1 ; specimens age 86 days

3 - average of 6 tensile splitting tests using SR EN 12390-6 multiplied with a factor of 0,9 [7]; specimens age 72 days

4 - average of 3 flexural tensile tests on 40x40x160mm prisms according to SR EN 196-1 and converted according to 3.23 relationship from EN 1992-1-1; specimens age 86 days

5 - average of 3 elasticity modulus tests using SR EN 12390-13 on 100x100x300mm prisms; specimens age 77 days

6 - average of 3 prisms compressive strength according to SR EN 12390-13; specimens age 77 days

Weber ESL is a non-sagging mortar especially designed for vertical and horizontal joints of concrete elements according to EN 1504-4. The declared Strength class is C30/37-4 according to SFS-EN 206-1 with >40MPa according to EN 12390-3 and approximately 50MPa according to EN 12190

Table 4.4.3 - Steel mechanical properties

	F_{max}[0] [kN]	f_y[1] [MPa]	f_u[2] [MPa]	E_s[3] [MPa]	ε_u[4] [%]
Lacer bar BST 500S		530,6	682,9	202.949	11,1
Phillip constructive rails *	39,5	Rupture of the anchor			

0 - Maximum recorded force

1 - Lower yielding strength

2 - Stress at the maximum force

3 - Secant Young modulus (determined using digital extensometer and/or DIC)

4 - Strain at the maximum force (determined using digital extensometer and/or DIC)

* Stresses in wires are determined according to the node equilibrium presented below along with the test set-up.

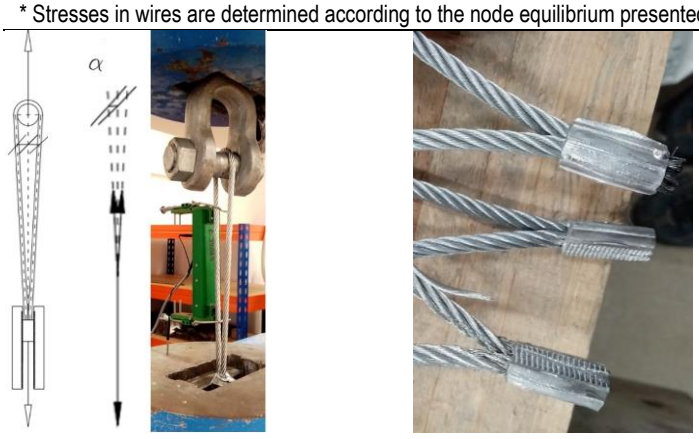

Figure 4-24 Test set-up for wire loops and failure mode for Phillip constructive rails (preloaded by ≈ 0.5kN to straighten the wires)

4.4.2 Experimental results

At the time of testing, the grouting material age ranged between 52 and 84 days. During all three tests, a similar behavior has been observed. The results are considered consistent. The force - shear slip behavior can be divided in three stages: a pre-cracking stage (Figure 4-25) followed by a post-cracking stage and a yielding plateau. This stage delimitation was chosen as the cracking moment is marked by the progressive change of the slope of the force – shear slip graph. The pre-cracking stage presented a pseudo-elastic behavior.

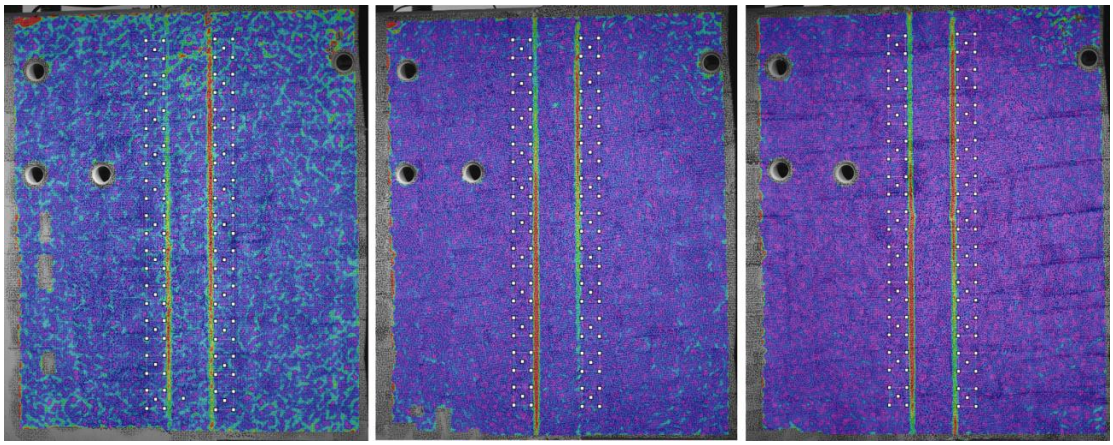

Figure 4-25 Crack pattern visualization cracking load (from left to right). Cracking loads for WL3T1: 166.4kN, WL3T2: 170.1kN, WL3T3: 171.3kN (major strains, using DIC)

The post-cracking stage displays a lower stiffness up to a first peak load (crack pattern shown in Figure 4-26). At this point, inclined cracks are showing up at the bottom and there are indications of a horizontal crack at the top. These are indications that the wires are becoming active. Following the first peak load, the yielding plateau shows a softening behavior, followed by a hardening branch up to the ultimate load (shown in Figure 4-27). The ultimate load was associated to very high displacements. In the authors' opinion, the ultimate load is not representing an Ultimate Limit State for this connection. The ultimate load for the connections was associated to very high shear displacements that are most likely to occur only in the situation of a global collapse.

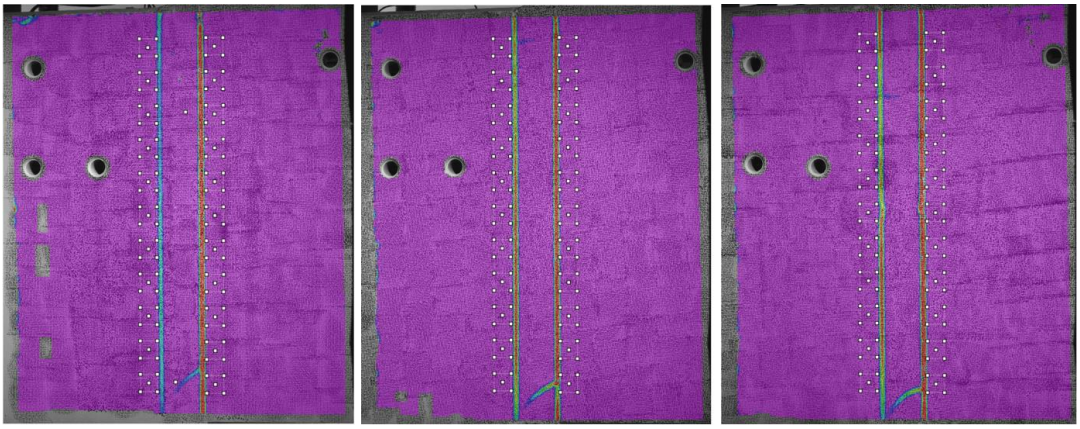

Figure 4-26 Crack pattern visualization at the first peak load (from left to right). First peak loads for WL3T1: 287.9kN, WL3T2: 292.5kN, WL3T3: 239.8kN (major strains, using DIC)

The third stage completion is not marked by rupture. The deformability of the connections exceeded the test set-up allowance (Figure 4-28) and the specimens had to be unloaded. This connection displayed a very good behavior, due to the consistency of the results, the high capacity (compared to wire loop connections) and very good ductility. An additional test series was planned for the Philipp Power Duo rail system. The producers present this system as a load bearing one.

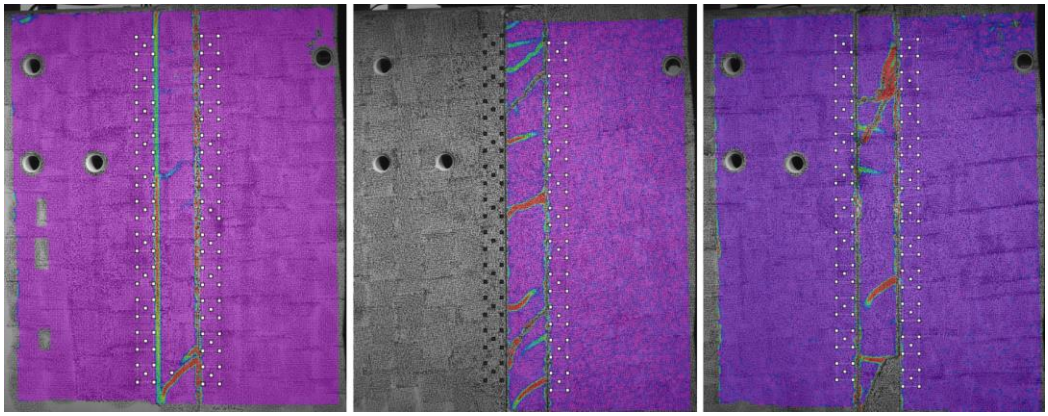

Figure 4-27 Crack pattern visualization at the reaching of the ultimate load (from left to right) WL3T1: 300.1kN WL3T2: 312.3kN, WL3T3: 326.3kN, (using DIC, major strains)

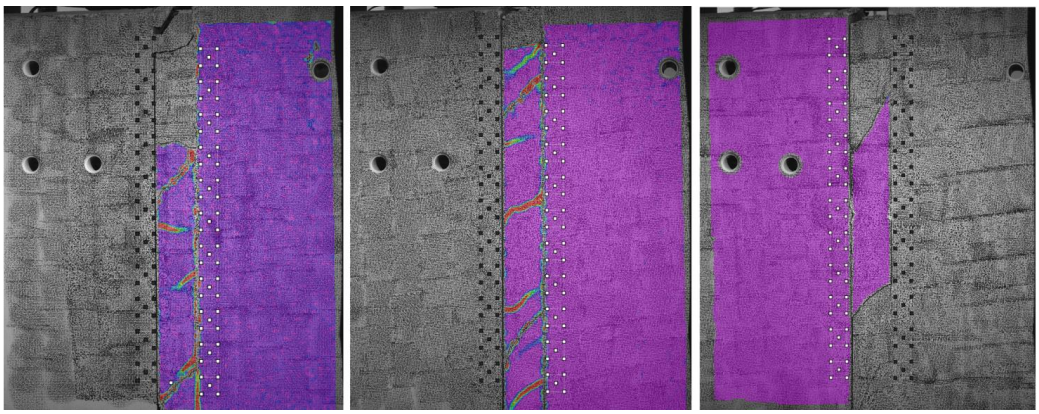

Figure 4-28 Observed failure mechanisms after failure (exceeding the deformability limit of the test set-up)

The failure mechanisms were much more difficult to assess for this connection, since the walls remained connected to each other. The attempts to disconnect the walls led to more damage, obscuring the damage caused by the test. Surface observations indicate that it was a shear slip of one of the two interfaces. It is hard to assume whether if the slip occurred inside the rail, or if the mortar remained bonded into the rail and a shear cut occurred in the plane of the interface.

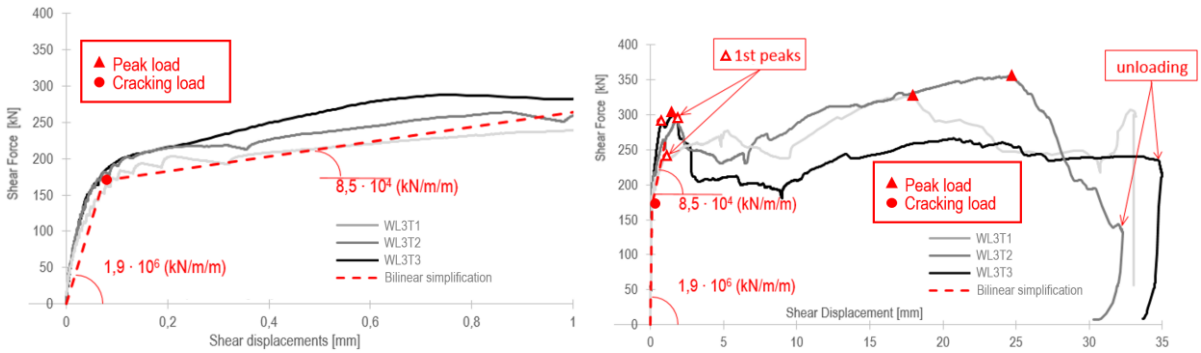

Figure 4-29 Shear force vs average shear slip along the joint height (left image: initial behavior zoomed in; right image: including post-peak behavior)

Table 4.4.4 – WL3 test results (individual result and average result)

	F_{crack} [kN]		F_{peak} [kN]		$K_{initial}$ [kN/m/m]		K_{final} [kN/m/m]	
WL3T1	166		300		2,3E+06		1,4E+05	
WL3T2	170	169	312	313	2,0E+06	1,9E+06	5,6E+04	8,5E+04
WL3T3	171		326		1,4E+06		5,8E+04	

4.5 Wire loops series 4: RSteel R3L-WIDE 100 (WL4)

Based on the experimental procedure described in this paper, two additional test series (WL4 and WL5) have been conducted.

4.5.1 Specimens' presentation

The tested connection was designed and casted according to the technical specifications provided by RSteel [19]. The wires before joint casting are presented in Figure 4-33, left. The description of the test specimens is identical to the specimens from WL1 series, presented in chapter 4.2.1. The filling material had a poor workability. The joint surface needed aesthetical repairment (Figure 4-33, right).

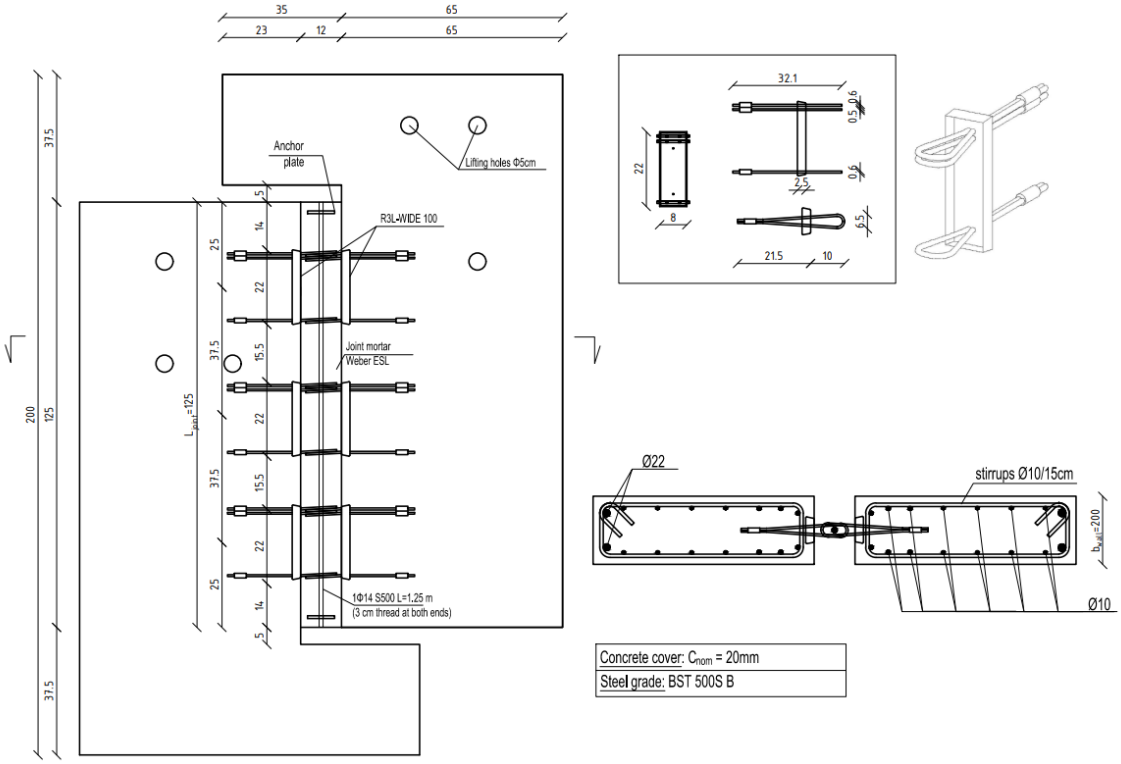

Figure 4-30 Configuration of WL4 specimens (dimension in cm)

Figure 4-31 Test specimens (from left to right 1st, 2nd and 3rd test specimen)

Figure 4-32 Wire boxes before panels casting

Figure 4-33 Test specimens before (left images) and after (right images) joint castings

Table 4.5.1 - Concrete mechanical properties

$f_{cm.cube}$[1] [MPa]	f_{ctm}[2] [MPa]	E_{cm}[3] [GPa]	$f_{cm.prism}$[4] [MPa]
76,86	4,03	38,85	56,82
CoV: 0,05	CoV: 0,1	CoV: 0,02	CoV: 0,08

1 - average of 3 compressive tests according to SR EN 12390-3 on 150mm cubes; specimens age 50 days

2 - average of 3 tensile splitting tests using SR EN 12390-6 multiplied with a factor of 0,9 [7]; specimens age 53 days

3 - average of 3 elasticity modulus tests using SR EN 12390-13 on 100x100x300mm prisms; specimens age 60 days

4 - average of 3 prisms compressive strength according to SR EN 12390-13; specimens age 60 days

Table 4.5.2 - Joint mortar mechanical properties

$f_{cm.cube}$[1] [MPa]	$f_{cm.cube.40mm}$[2] [MPa]	f_{ctm}[3] [MPa]	$f_{ctm.40mm}$[4] [MPa]	E_{cm}[5] [GPa]	$f_{cm.prism}$[6] [MPa]
53,01	-	2,29	-	31,02	48,69
CoV: 0,07	CoV: -	CoV: 0,14	CoV: -	CoV: 0,05	CoV: 0,07

1 - average of 3 compressive tests according to SR EN 12390-3 on 150mm cubes; specimens age 52 days

2 - test results are unavailable

3 - average of 5 tensile splitting tests using SR EN 12390-6 multiplied with a factor of 0,9 [7]; specimens age 52 days

4 - test results are unavailable

5 - average of 3 elasticity modulus tests using SR EN 12390-13 on 100x100x300mm prisms; specimens age 60 days

6 - average of 2 prisms compressive strength according to SR EN 12390-13; specimens age 60 days

Table 4.5.3 - Steel mechanical properties

	F_{max}[0] [kN]	f_y[1] [MPa]	f_u[2] [MPa]	E_s[3] [MPa]	ε_u[4] [%]
Lacer bar BST 500S		530,6	682,9	202.949	11,1
RSteel R3L-WIDE 100 *	41,0	725,7	725,7	49.109	1,51%

0 - Maximum recorded force

1 - Lower yielding strength

2 - Stress at the maximum force

3 - Secant Young modulus (determined using digital extensometer and/or DIC)

4 - Strain at the maximum force (determined using digital extensometer and/or DIC)

* Stresses in wires are determined according to the node equilibrium presented below along with the test set-up.

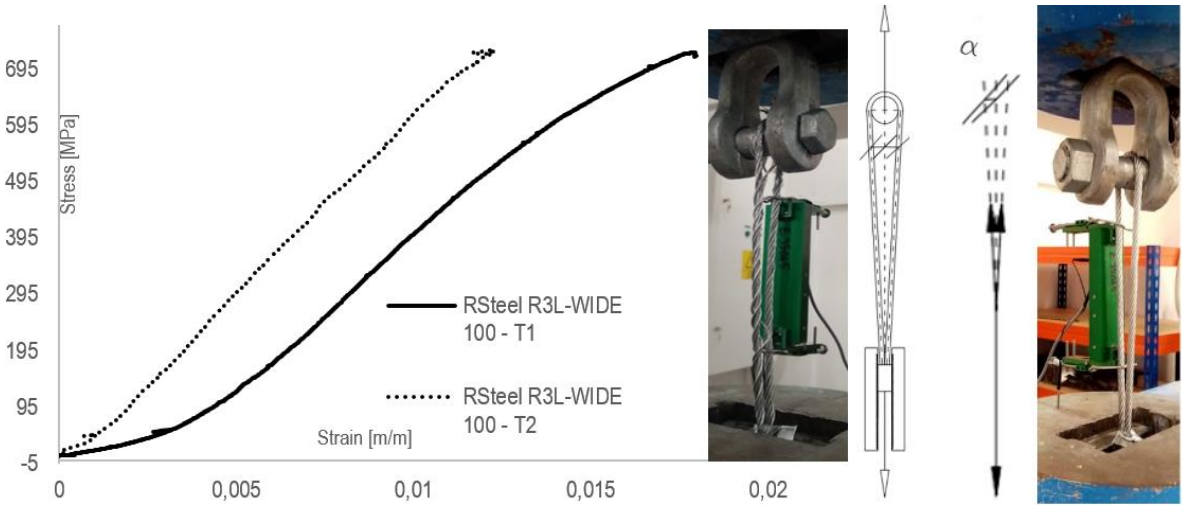

Figure 4-34 Experimental stress-strain curve for two RSteel wire loops and test set-up (preloaded by ≈ 0.5kN to straighten the wires)

4.5.2 Experimental results

At the time of testing, the grouting material age ranged between 52 and 60 days. The force - shear slip behavior can be divided in two stages: a pre-cracking stage followed by a post-cracking stage. Two tests show a very similar pre-cracking behavior and similar stiffness. 1st test from this series displays a higher cracking value (around 20%). The peak loads have similar values for the 2nd and the 3rd test; the shear displacements associated to the peak loads are: 6.5 mm for the 1st; 6.80 mm for the 2nd and 5.5 mm for the 3rd test.

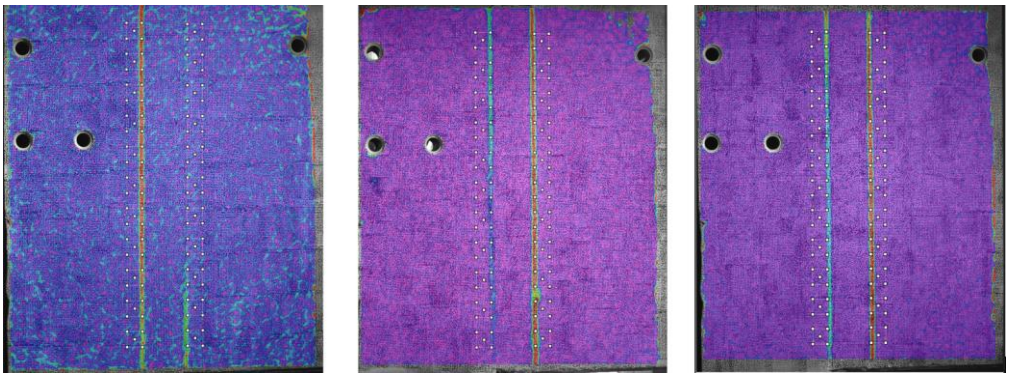

Figure 4-35 Crack pattern visualization just after the cracking load (from left to right).

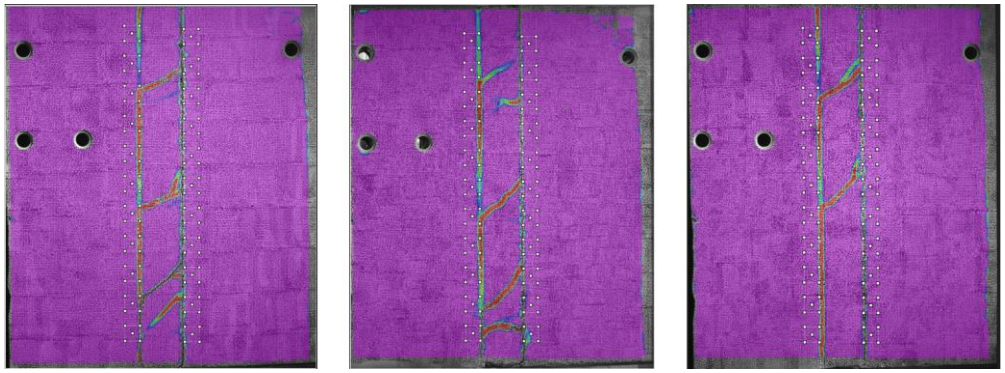

Figure 4-36 Observed failure mechanisms after failure (from left to right).

The three specimens showed the same failure mechanism, diagonal cracks were observed for each specimen. The walls remained connected to each other; the joint deformability exceeded the test set-up allowance.

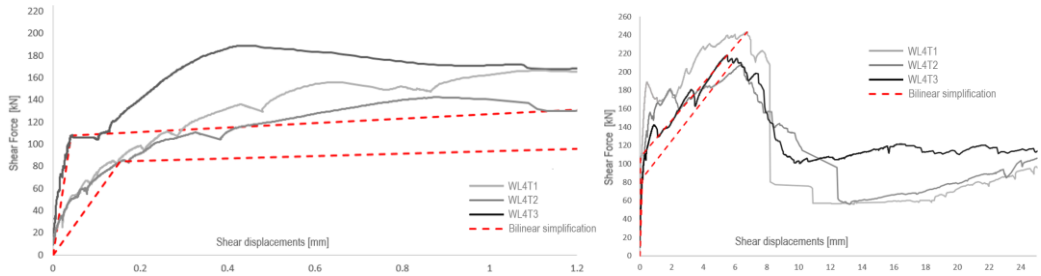

Figure 4-37 hear force vs average shear slip along the joint height (initial behavior zoomed in, left; overall behavior, right

Table 4.5.4 – WL4 test results (individual result and average result)

	F_{crack} [kN]		F_{peak} [kN]		$K_{initial}$ [kN/m/m]		K_{final} [kN/m/m]	
WL4T1	108		243		2,0E+06		1,6E+04	
WL4T2	83,9	92	208	223	4,7E+05	9,7E+05	1,6E+04	1,7E+04
WL4T3	85,2		218		4,1E+05		2,0E+04	

4.6 Wire loops series 4: Philipp Power Duo Rails (WL5)

4.6.1 Specimens' presentation

This connection layout was chosen for testing due to the very promising results presented in chapter 4.4, provided by the non-structural rail (WL3 test series).

The tested connection was designed and casted according to the technical specifications provided by Philipp Group [20]. The wires before joint casting are presented in Figure 4-40. For this type of connector, the wires are provided with a fixing system that prevents wires sliding and ensures a constant overlapping length into the joint. The description of the test specimens is identical to the specimens from WL1 series, presented in chapter 4.2.1. The filling material had a poor workability. The joint surface needed aesthetical repairment.

The structural rail can be described as a recessed joint with shear keys. Until now, all the test specimens were designed as plain joints with shear keys. A recessed joint was previously avoided due to the grouting difficulties posed by using the thixotropic mortar and non-mechanized joint casting. Yet, for WL5 the recess edges could not be omitted, since the recess is inherent to the Phillip structural rail manufacturer' design.

The distance between the concrete wall elements prescribed by the technical manual is between 15-40mm. The test specimens were designed with the maximum of 40mm. Yet, due to the configuration of the test specimens (no access from above), the 12mm lacer bar could not be introduced. A pre-stressing tendon with ≈12mm diameter (6 intertwined wires of 4.1mm diameter) replaced the lacer bar.

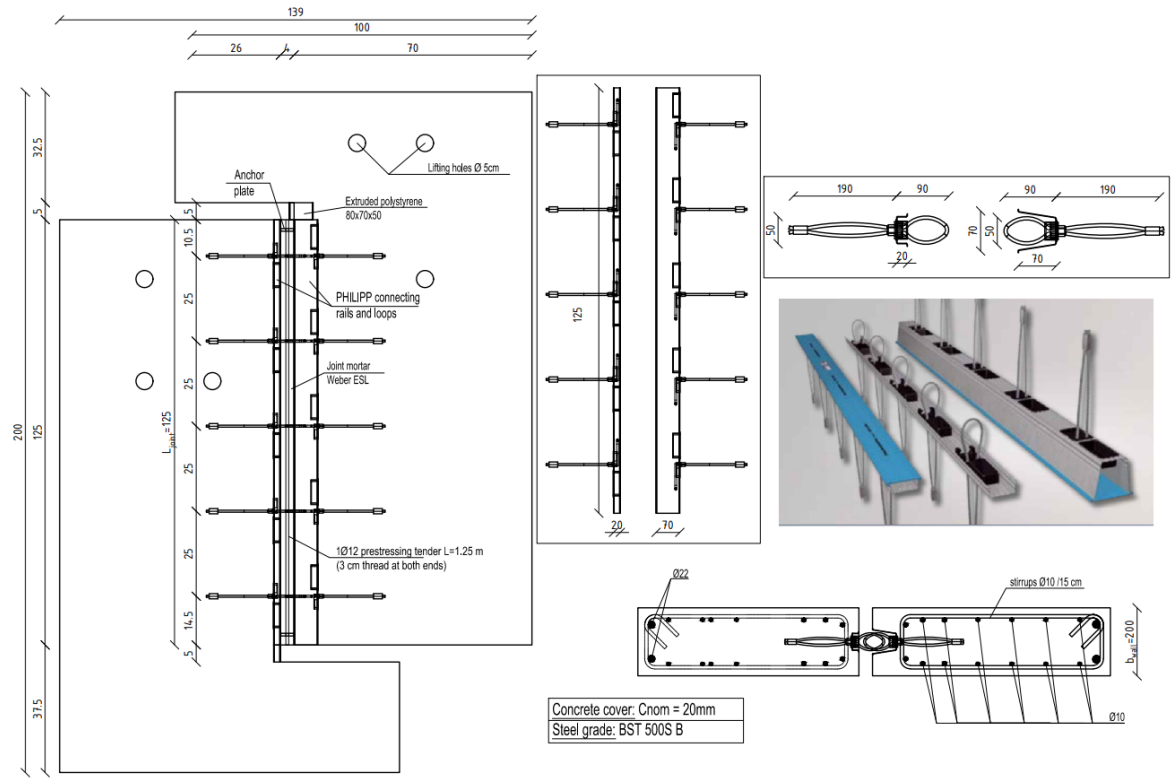

Figure 4-38 Configuration of WL5 specimens (dimensions in cm)

Figure 4-39 Test specimens from WL5 (from left to right 1st, 2nd and 3rd test specimen)

Figure 4-40 Test specimens before joint casting

Table 4.6.1 - Concrete mechanical properties

$f_{cm.cube}$[1] [MPa]	f_{ctm}[2] [MPa]	E_{cm}[3] [GPa]	$f_{cm.prism}$[4] [MPa]
74,90	3,55	37,09	54,20
CoV: 0,02	CoV: 0,12	CoV: 0,03	CoV: 0,04

1 - average of 5 compressive tests according to SR EN 12390-3 on 150mm cubes; specimens age 53 days

2 - average of 10 tensile splitting tests using SR EN 12390-6 multiplied with a factor of 0,9 [7]; specimens age 61 days

3 - average of 3 elasticity modulus tests using SR EN 12390-13 on 100x100x300mm prisms; specimens age 50 days

4 - average of 3 prisms compressive strength according to SR EN 12390-13; specimens age 50 days

Table 4.6.2 - Joint mortar mechanical properties

$f_{cm.cube}$[1] [MPa]	$f_{cm.cube.40mm}$[2] [MPa]	f_{ctm}[3] [MPa]	$f_{ctm.40mm}$[4] [MPa]	E_{cm}[5] [GPa]	$f_{cm.prism}$[6] [MPa]
55,44	-	2,16	-	30,55	44,22
CoV: 0,05	CoV: -	CoV: 0,12	CoV: -	CoV: 0,02	CoV: 0,08

1 - average of 5 compressive tests according to SR EN 12390-3 on 150mm cubes; specimens age 52 days

2 - test results are unavailable

3 - average of 6 tensile splitting tests using SR EN 12390-6 multiplied with a factor of 0,9 [7]; specimens age 60 days

4 – test results are unavailable

5 - average of 3 elasticity modulus tests using SR EN 12390-13 on 100x100x300mm prisms; specimens age 49 days

6 - average of 3 prisms compressive strength according to SR EN 12390-13; specimens age 49 days

Table 4.6.3 - Steel mechanical properties

	F_{max}[0] [kN]	f_y[1] [MPa]	f_u[2] [MPa]	E_s[3] [MPa]	ε_u[4] [%]
Lacer bar BST 500S		530,6	682,9	202.949	11,1
Philip Power Duo System	55,7				

0 - Maximum recorded force

1 - Lower yielding strength

2 - Stress at the maximum force

3 - Secant Young modulus (determined using digital extensometer and/or DIC)

4 - Strain at the maximum force (determined using digital extensometer and/or DIC)

Figure 4-41 Wire loops after testing (preloaded by ≈ 0.5kN to straighten the wires)

4.6.2 Experimental results

The tests were carried out after the grouting material reached 48, 55, 61 days of maturity. The test results showed inconsistencies between the three tests designed to be identical. The 1st specimen had a significantly higher stiffness and cracking load. The cracking load was equal to the peak load. A residual strength was provided and the deformability of the connections exceeded the test set-up allowance.

Figure 4-42 Crack pattern visualization at the reaching of the peak load (from left to right).

Figure 4-43 Observed failure mechanisms after failure (from left to right). Peak loads for Test 1: 178.8 kN; Test 2: 124.7 kN; Test 3: 102.2 kN

Although the non-structural Philipp rail proved very good load capacity and ductility during testing, the Philip Power Duo System was quite the opposite: the cracking loads were inconsistent and no post-cracking capacity was provided (only a residual). Yet, it should be taken into account that this test specimen had significant casting deviations from the technical manual and from the previous wire loop series:

- The lacer bar was replaced with a pre-stressing strand;
- Due to the small gap between the walls, the mortar poorly filled the deep recess provided by the Phillip Power Duo System, so the shear keys from one side of the connection were barely active. During all three tests slippage occurred into the deep recess (also observed through DIC in Figure 4-43).

Both deviations are caused by the small space between the walls. In site normal conditions, the lacer bar can be easily introduced from above. The joint filling on site is usually done with a mechanical pump. However, if not carefully used, the mechanical pump might provide similar filling quality as the one manually obtained in this test series.

Table 4.6.4 – WL5 test results (individual result and average result)

	F_{crack} [kN]		F_{peak} [kN]		$K_{initial}$ [kN/m/m]		K_{final} [kN/m/m]	
WL5T1	179		179		2,1E+06		-	
WL5T2	125	135	125	135	3,8E+05	1,2E+06	-	-
WL5T3	102		102		1,2E+06		-	

Due to the above-mentioned reasons, the test results obtained from this series will not be taken into account in further analysis and they are not considered conclusive.

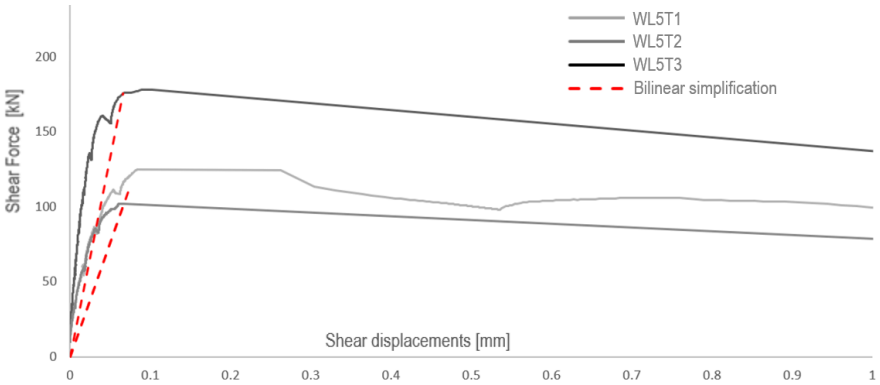

Figure 4-44 Shear force vs average shear slip along the joint height (initial behavior zoomed in

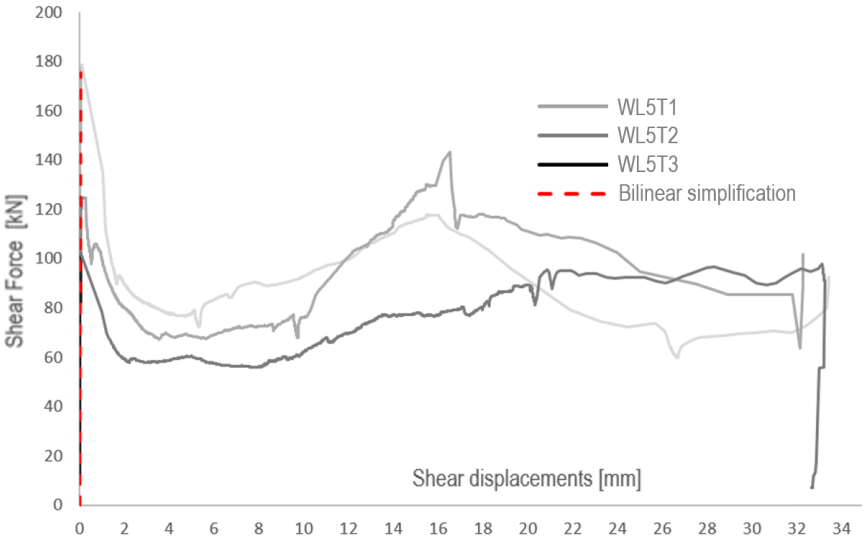

Figure 4-45 Shear force vs shear slip overall behavior (including post-peak behavior)

4.7 Summarized wire loops test results (with the supplementary test series)

All test specimens have a joint height of 1.25m, a wall thickness of 200mm. The mortar material properties summarized here are determined according to SR EN 12390, on large material test specimens. This method is specified for concrete material properties determination, yet it is considered to provide relevant results for this connection layout since the width of the joint is equal to the material test specimens.

Table 4.7.1 Summary of test results from connections with grouted shear keys and steel assemblies

Test index		[1] f_c [MPa]	[2] f_t [MPa]	[3] b_{key} [cm]	[4] h_{key} [cm]	[5] n_{key}	[6] F_{wire} [kN]	[7] A_s [mm^2]
WL1	WL1T1 WL1T2 WL1T3	56,70	2,34	3,65	16	3	46	3 x 6mm wires
WL2	WL2T1 WL2T2 WL2T3	49,20	2,36	6,5	23,2	3	37,8	3 x 5mm wires
WL3	WL3T1 WL3T2 WL3T3	54,61	2,25	5	125	1	39,5	5 x 6mm wires
WL4	WL4T1 WL4T2 WL4T3	53,01	2,29	8	22	3	41	2 x 6mm + 1 x 5 mm wires
WL5	WL5T1 WL5T2 WL5T3	55,44	2,16	4,8	125	1	55,7	5 x 6 mm wires

1 - average compressive strength on 150mm cubes according to SR EN 12390-3
2 - average tensile strength according to SR EN 12390-6 splitting tests
3 - width of the shear keys
4 - height of the shear keys
5 - number of shear keys
6 - Maximum recorded force during wire tensile testing
7 - Reinforcement area

* Due to the reasons presented in chapter 4.6.2, the test results obtained from WL5 are not considered conclusive.

Table 4.7.2 and Table 4.7.3 shows the mean values of the three tests of each series (designed to be identical) and the spread (in percentages) from the mean value. The wire loop tests batch needs to be discussed in terms of which connection layout provides the most consistent results. It is clear that the Phillip constructive Rail system (WL3) had the most consistent results. The Pintos wire boxes (WL2) series consisted in two test specimens that provided similar results. Unfortunately, the 2nd test of Pintos series (WL2T2) provided with much lower values in terms of cracking load, peak load and stiffness. It was observed in 4.3.2 that significant air bubbles were present in the shear keys of the 2nd specimen, having a dramatic impact on its behavior. This underlines the sensitivity at casting of the wire loop connection. The Peikko PVL 80 series (WL1) showed the most inconsistent results, in all the phenomena analyzed: cracking load, peak load and stiffnesses.

Table 4.7.2- Loads: mean results and differences from the mean values

	Specimen	F_{crack} [kN]	mean	difference	F_{peak} [kN]	mean	difference
WL1	WL1T1	103		-3,48%	103		-25,26%
	WL1T2	147	106	38,61%	147	137	7,34%
	WL1T3	68,9		-35,12%	162		17,91%
WL2	WL2T1	183		15,92%	228		6,92%
	WL2T2	109	158	-30,89%	168	213	-21,02%
	WL2T3	181		14,97%	243		14,10%
WL3	WL3T1	166		-1,69%	300		-4,09%
	WL3T2	170	169	0,49%	312	313	-0,19%
	WL3T3	171		1,20%	326		4,28%
WL4	WL4T1	108		16,61%	243		9,08%
	WL4T2	83,9	92	-9,02%	208	223	-6,85%
	WL4T3	85,2		-7,60%	218		-2,23%

If we are to compare WL1 with WL2 (Peikko PVL 80 vs Pintos Okaria 80), all the parameters of the connection layout are similar with the exception of the wire diameter and the boxes dimensions (6mm for Peikko and 5mm for Pintos and respectively, Pintos shear keys have a 2.55 higher area than Peikko). Pintos specimens (WL2) had a 1.49 times higher average cracking load. Philipp rails (WL3) have no shear keys, only the channel surface, provided with small grooves (not complying with EN1992-1-1, chapter 6.2.5, as a rough interface). The exact failure mechanism was not assessed (whether the slip occurred inside the rail, or the shear cut occurred in the plane of the interface, as discussed In 4.4.2), yet, it seems that the rail channel might be assimilated with a large shear key (with 1.38 times bigger area than the shear keys of WL2). The average cracking load obtained for WL3 was only 1.07 times higher than Pintos'. Philipp rail had more wires (5 pieces); however, it is considered that the wires become fully active only after the 1st peak load, following the descending branch, observed in Figure 4-29. The wires contribution might be observed comparing the peak loads (Philipp rail, SA3 average peak load was 1.47 times higher than Pintos', WL2). However, it is not clear why the peak load of Peikko PVL 80 was not higher than Pintos', since Peikko' wires had 6mm in diameter instead of Pintos' 5mm (WL2 had an average peak load 1.55 times higher than WL1, Peikko'). RSteel R3L-WIDE (WL4) had a similar indented area compared to Pintos, WL2, only 0.89 times lower. However, the average cracking load of WL4 was 0.58 times smaller than WL2. The cracking loads measured in WL4 series are comparable only with the test results obtained in WL2T2 test.

Table 4.7.3- Stiffness: mean results and differences from the mean values

	Specimen	$K_{initial}$ [kN/m/m]	mean	difference	K_{final} [kN/m/m]	mean	difference
WL1	WL1T1	1,4E+06 and 3,5E+05		-	-		-
	WL1T2	1,3E+07	-	-	-	-	-
	WL1T3	1,8E+06 and 2,7E+05		-	4,5E+03		-
WL2	WL2T1	1,2E+07		34,46%	4,2E+03		-90,45%
	WL2T2	2,5E+06	8,8E+06	-71,36%	5,7E+03	4,4E+04	-86,95%
	WL2T3	1,2E+07		36,90%	1,2E+05		177,40%
WL3	WL3T1	2,3E+06		21,52%	1,4E+05		64,79%
	WL3T2	2,0E+06	1,9E+06	5,63%	5,6E+04	8,5E+04	-33,47%
	WL3T3	1,4E+06		-27,16%	5,8E+04		-31,31%
WL4	WL4T1	2,0E+06		108,61%	1,6E+04		-7,34%
	WL4T2	4,7E+05	9,7E+05	-51,05%	1,6E+04	1,7E+04	-9,07%
	WL4T3	4,1E+05		-57,56%	2,0E+04		16,41%

When discussing the applicability of Linear Elastic Finite Element Analysis for estimating the internal forces in precast constructions, an additional fact should be clarified (on top of the discussions in chapter 3.5). Have the

peak loads associated to very high shear displacements any use for the overall structural system resistance? Can shear walls accommodate so high deformations so the vertical connections would reach their peak loads? Either way, even smaller shear slips that are associated to the post-cracking behavior observed in tests (observed in reference [4] too), will jeopardize the functionality of the building.

Wire loops connections test results are compared with the same calculation approach as described in chapter 3.5. Yet, there are some particularities to be discussed for these connections' layouts.

The approach given by EN 1992-1-1 (shown in chapter 3.5, eq. (1)) is highly dependent on the tensile strength of the mortar. Usually, the mechanical properties of the mortar are determined using SR EN 196-1, on small probes: 40x40x160mm prisms, tested in three-point bending configuration. In this research, the mortar was additionally tested according to SR EN 12390 (part 5 and 6), on larger probes: 100x100x550mm prisms subjected to four-point bending test. The remaining undamaged ends of the same specimen were subjected to tensile splitting tests. The results were converted to uniaxial tensile strength (f_{ctm}) according to EN 1992-1-1. It was noticed that the results obtained from the larger prisms were much lower than the results obtained on the small prisms. Further, it was presumed that the tests on larger prisms provide more realistic results, since the joint width is 100mm. Air bubbles were observed in the joints casted with thixotropic mortar. As previously discussed, the Weber ESL technical manual [13], declares an air content of 8-12%. Consequently, the interfaces area for the specimens casted with thixotropic mortar was reduced by a factor of 0.88.

Note that the Philipp rail surface is not indented, nor rough. In calculations the bonding factor will be taken as smooth, c = 0.35.

F_{tie}, the clamping force provided by the wire loops, can be calculated with the model proposed by Jørgensen, which imposes a failure mechanism of concrete crushing between the wire loops [4]. As seen in chapter 4.2 and 4.3 (wire boxes tests), four out of six test specimens failed through wire rupture. One specimen (WL1T1) had excessive deformations and only one specimen (WL2T3) had a failure mechanism of concrete crushing between the wire loops. Therefore, the rigid plastic modeling proposed by Jørgensen will not be carried out. The tensile tests performed on wire loops (presented in table 4.2.3, 4.3.3, 4.5.3) showed a very low elasticity modulus and a brittle failure. The present test results are in agreement with the wire tests results presented by Jørgensen (Figure 4-46). If elasticity modulus is low, then the forces in the wires at small displacements are consequently low. The failure of the wire is brittle, not complying with the requirements of EN 1992-1-1, Annex C [7]. Consequently, the clamping force contribution should be completely neglected (F_{tie} = 0), when calculating the shear resistance according to EN 1992-1-1, chapter 6.2.5. Therefore, the calculation results are compared with the cracking loads.

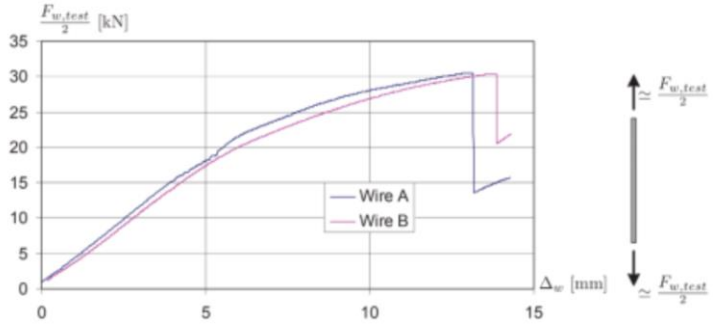

Figure 4-46 Wire tests presented by Jørgensen [4]

Based on the descriptions presented above and in chapter 3.5, the experimental cracking loads are compared to the formula 6.25 from EC2 using mean material properties.

Table 4.7.4 Peak loads after Eurocode 2 (6.25), using mean material properties, compared with experimental peak loads

Specimens	f_{ct} [MPa]	b_{key} [m]	L_i [m]	F_{calc} [kN]	F_{test} [kN]	F_{test} / F_{calc}	$F_{test.mean}$ / F_{calc}
WL1T1	2,35	0,037	1,25	47,2	102,50	2,17	2,25
WL1T2	2,35	0,037	1,25	47,2	147,20	3,12	
WL1T3	2,35	0,037	1,25	47,2	68,90	1,46	
WL2T1	2,36	0,065	1,25	84,4	182,90	2,17	
WL2T2	2,36	0,065	1,25	84,4	109,05	1,29	1,87
WL2T3	2,36	0,065	1,25	84,4	181,40	2,15	
WL3T1	2,25	0,050	1,25	43,3	166,40	3,84	
WL3T2	2,25	0,050	1,25	43,3	170,10	3,93	3,91
WL3T3	2,25	0,050	1,25	43,3	171,30	3,95	
WL4T1	2,29	0,061	1,25	76,8	107,52	1,40	
WL4T2	2,29	0,061	1,25	76,8	83,89	1,09	1,20
WL4T3	2,29	0,061	1,25	76,8	85,20	1,11	

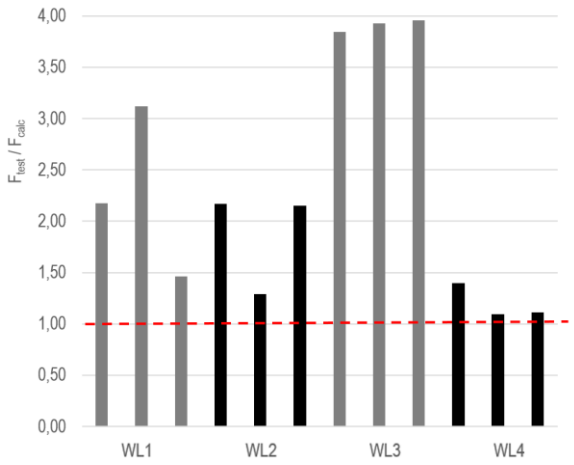

Figure 4-47 Experimental – Eurocode 2 calculation model resistance ratio

We can see that the resistance provided by calculations according to Eurocode 2 is very conservatory compared with test results, using the mean material properties from tests. The average ratio of model resistance and experimental resistance is 2.31. Only WL4 test results were close to the calculated values, and eventually the individual test results of WL2T2 or WL1T3 specimens. Using this approach, only the width of the shear keys is taken into account (previously discussed in chapter 3.5, reference to Figure 3-38). If the smooth area is considered, much higher results are provided. The following relationship is assuming the possibility of superimposing the effects of the very smooth interface resistance and the indented interface resistance:

$$V_{R.test} = c_{ind}\, f_{ctm}\, A_{ind} + c_{vs}\, f_{ctm}\, A_{vs} + F_{tie}\, \mu_{ind}\, A_{ind}/A_i + F_{tie}\, \mu_{vs}\, A_{vs}/A_i \qquad (2)$$

where:

- c and μ are factors which depend on the roughness of the interface; c_{ind} = 0.5 (for indented interface); c_{vs} = 0.25 (for very smooth interface); μ_{ind} = 0.9 (for indented interface); μ_{vs} = 0.5 (for very smooth interface);
- f_{ctm} – mean tensile strength from determined from material testing;
- F_{tie} – the clamping force estimated with different methods for various connectors;

- A_{ind} – area of the shear keys, complying to Figure 6.9 from [7], calculated as follows: $A_{ind} = n \cdot h_{key} \cdot b_{key}$;
- A_{vs} – surface casted against specially prepared wooden molds: $A_{vs} = A_i - A_{ind}$;
- A_i - is the total area of the joint: $A_i = b_{wall} \cdot L_{joint}$.
- F_{tie} - is the axial tensile capacity of the connection reinforcement (for SA series is calculated according to discussions surrounding Figure 3-39 and for WL series is neglected).

All the tests are compared with the adapted relationship (2) and presented below.

Table 4.7.5 Relationship deviated from Eurocode 2, using mean material properties, compared with experimental results

Specimen	f_{ct} [MPa]	b_{joint} [m]	b_{key} [m]	h_{key} [m]	n_{key}	L_{joint} [m]	F_{tie} [kN]	F_{calc} [kN]	F_{test} [kN]	F_{test} / F_{calc}	$F_{test.mean}$ / F_{calc}
SA1T1	10,63	0,20	0,200	0,060	6,00	1,20	439,8	1101,8	1081,0	0,98	
SA1T2	10,63	0,20	0,200	0,060	7,00	1,20	439,8	1142,5	1306,0	1,14	1,06
SA1T3	10,63	0,20	0,200	0,060	6,50	1,20	439,8	1122,2	1191,0	1,06	
SA2T1	5,46	0,20	0,065	0,060	10,00	1,20	439,8	583,6	689,3	1,18	
SA2T2	5,46	0,20	0,065	0,060	10,00	1,20	439,8	583,6	616,4	1,06	1,07
SA2T3	5,46	0,20	0,065	0,060	10,00	1,20	439,8	583,6	572,6	0,98	
SA3T1	4,76	0,20	0,065	0,060	8,00	1,20	205,2	397,3	213,2	0,54	
SA3T2	4,51	0,20	0,065	0,060	8,00	1,20	205,2	382,4	224,2	0,59	0,56
SA3T3	4,63	0,20	0,065	0,060	8,00	1,20	205,2	389,5	219,7	0,58	
WL1T1	2,35	0,20	0,037	0,160	3,00	1,25	0,0	138,3	102,5	0,74	
WL1T2	2,35	0,20	0,037	0,160	3,00	1,25	0,0	138,3	147,2	1,06	0,77
WL1T3	2,35	0,20	0,037	0,160	3,00	1,25	0,0	138,3	68,9	0,50	
WL2T1	2,36	0,20	0,065	0,232	3,00	1,25	0,0	153,3	182,9	1,19	
WL2T2	2,36	0,20	0,065	0,232	3,00	1,25	0,0	153,3	109,1	0,71	1,03
WL2T3	2,36	0,20	0,065	0,232	3,00	1,25	0,0	153,3	181,4	1,18	
WL3T1	2,25	0,20	0,050	1,250	1,00	1,25	0,0	136,1	166,4	1,22	
WL3T2	2,25	0,20	0,050	1,250	1,00	1,25	0,0	136,1	170,1	1,25	1,24
WL3T3	2,25	0,20	0,050	1,250	1,00	1,25	0,0	136,1	171,3	1,26	
WL4T1	2,29	0,20	0,061	0,220	3,00	1,25	0,0	146,2	107,5	0,74	
WL4T2	2,29	0,20	0,061	0,220	3,00	1,25	0,0	146,2	83,9	0,57	0,63
WL4T3	2,29	0,20	0,061	0,220	3,00	1,25	0,0	146,2	85,2	0,58	

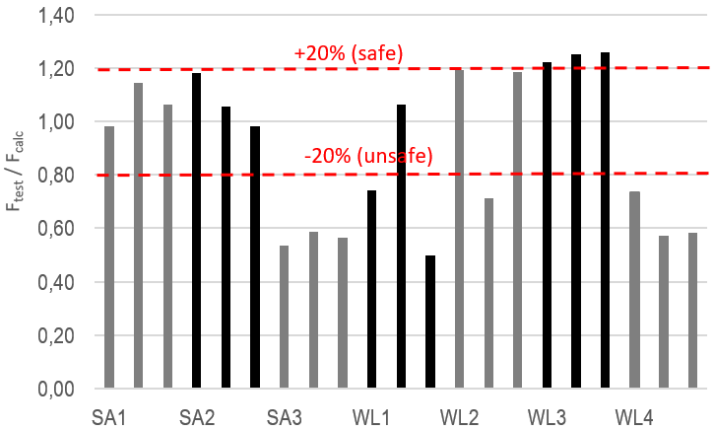

Figure 4-48 Experimental – calculation model resistance ratio

Table 4.7.5 and Figure 4-48 shows the comparison between eq. (2) and the test results. A ±20% deviation is usually encountered in concrete shear behavior and it is generally an acceptable spread of values (e.g. [4]). The welded plates specimens (SA1 and SA2) as well as the wire rails (WL3) are in a good agreement with this equation. Wire boxes series (WL1 and WL2) had a very wide spread of results, so they are very problematic in comparison with numerical models. The bolted connection (SA3) showed a very low ratio of test results per calculation results. This is an indication that the calculations are not capturing with good accuracy the phenomena that is taking place in the bolted connection during shear loading. The additional test series (WL4) had a poor comparison with this calculation interpretation.

FIB Model Code 2010 [21] proposes a different approach in calculating the shear at the interface between concrete cast at different times. Based on the same principles as the equation (1) from EN 1992-1-1 chapter 6.2.5, two calculation approaches are presented: one for interface without reinforcement and another for interfaces intersected by dowels or reinforcement.

In the comments section it is stated that if special measurements are taken to ensure that the surface is clean and degreased, the adhesive bond might be taken into account as shear resistance, without superimposing the effects of the reinforcement crossing the interface (eq. (3)). It is easy to observe that this equation is identical with eq. (1), removing the term that takes into account the reinforcement. This is a major difference from EN 1992-1-1 and it seems to be in a better agreement with the physical phenomenon. At the peak load, most of the specimens were cracked and the contribution of the grout was brought by the shear-lock/shear-friction mechanism; not the adhesion. Moreover, it is stated that the adhesion coefficients (c_a) can depend on a variety of influencing parameters (testing method/test set-up, surface treatment, etc.). Consequently, in Model Code 2010, a very conservative value is given for the adhesion coefficient for very smooth areas (c_a=0.025, ten times lower than in EN 1992-1-1). For the indented areas, the same values are given (c_a=0.5) as in EN 1992-1-1.

$$V_{Rd} = (c_a\, f_{ctd} + \sigma_n\, \mu)\, A_i = c_a\, f_{ctd}\, A_i \qquad (3)$$

$$V_{Rd} \leq 0.5\, \vartheta\, f_{cd}\, A_i$$

For the interfaces intersected by dowels or reinforcement, Model Code 2010 recommends a different equation:

$$V_{Rd} = \left(c_r\, f_{ck}^{\frac{1}{3}} + \sigma_n\, \mu + k_1\, \rho\, f_{yd}\, (\mu\, sin\, \alpha + cos\alpha) + k_2\, \rho \sqrt{f_{yd}\, f_{cd}}\right) A_i$$
$$= c_r\, f_{ck}^{\frac{1}{3}}\, A_i + k_1 A_s\, f_{yd}\, \mu + k_2\, A_S \sqrt{f_{yd}\, f_{cd}} \qquad (4)$$

$$V_{Rd} \leq \beta_c\, \vartheta\, f_{cd}\, A_i$$

The 1st term of the equation (4) uses a factor (c_r = 0.2 for very rough/indented interfaces) that takes in account aggregate interlock effects at rough interfaces. For very smooth and smooth interfaces, this factor is 0. The tensile strength of the concrete or grout is now replaced with $f_{ck}^{1/3}$. This is another difference, since the tensile strength can be expressed as a function of the compressive strength as 0.3 $f_{ck}^{2/3}$ [7].

The second term of eq. (4) takes into account the contribution of the shear friction mechanism. In addition to eq. (1) and (2), in this formulation, the reinforcement is subjected to tensile and shear forces combined (dowel action). Consequently, the axial strength is reduced by an interaction coefficient for tensile force that is activated in the reinforcement or the dowels (k_1 = 0.5, for rough/indented interfaces).

The dowel resistance is taken into account in the 3rd term and is reduced by an interaction coefficient for flexural resistance (k_2 = 0.9, for rough/indented interfaces).

Finally, shear stress is limited not to exceed a certain fraction of the compressive strength, with a coefficient taking into account the strength of the compression strut (β_c = 0.5, for rough/indented interfaces).

Equation (3) from Model Code 2010 could be used for the wire loops connections, since the wire loop does not have any bending stiffness and the axial stiffness is too low. Model Code 2010 does not state whether the resistance of the very smooth surfaces and the resistance of the indented surface can be superimposed. Anyway, even though the cleanness of the surface is ensured on site, using an adhesion coefficient of 0.025 instead of 0.25 will not provide a significant additional resistance.

Equation (4) from Model Code 2010 compared with test results is showing large underestimation of the peak load. The errors are not uniform. For SA1, the formula underestimates the capacity by a factor of 2.5. For the bolted connections (SA3), the calculations are underestimating only by a factor of 1,11. This is an indication that the method is not capturing with accuracy all the factors on which the resistance is depending.

Table 4.7.6 Relationship from MC2010, using mean material properties, compared with experimental peak loads

Specimens	f_c [MPa]	b_i [m]	L_i [m]	F_{tie} [kN]	F_{calc} [kN]	F_{test} [kN]	F_{test} / F_{calc}	$F_{test.mean}$ / F_{calc}
SA1T1	53,81	0,200	0,92	439,80	482,6	1081,0	2,24	
SA1T2	53,81	0,200	0,92	439,80	482,6	1306,0	2,71	2,47
SA1T3	53,81	0,200	0,92	439,80	482,6	1191,0	2,47	
SA2T1	45,15	0,065	1,20	439,80	388,9	689,30	1,77	
SA2T2	45,15	0,065	1,20	439,80	388,9	616,40	1,59	1,61
SA2T3	45,15	0,065	1,20	439,80	388,9	572,60	1,47	
SA3T1	34,21	0,065	1,20	205,2	193,9	213,20	1,10	
SA3T2	39,73	0,065	1,20	205,2	199,6	224,20	1,12	1,11
SA3T3	39,73	0,065	1,20	205,2	199,6	219,70	1,10	

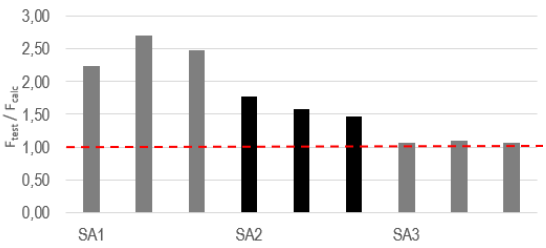

Figure 4-49 Model Code 2010 compared with test results

5 CONCLUSIONS

5.1 Discussions and conclusion

This report presented the output of eighteen push-off shear tests performed on six different connection layouts, widely used for vertical connections between precast wall panels in shear wall assemblies. All connection layouts are using mortar for shear force transfer. Three connections layouts are based on steel assemblies for generating the clamping force. The other three are relying on high strength wire ropes. Three specimens designed to be identical were tested for each connection layout. Six additional push-of tests on two wire loops connection layout were attached to this report.

The welded plates connections showed consistent results. These connections cracked at around 50% of their maximum load capacity. The cracking moment marked a change in behavior, the connections becoming more flexible therefore, there is two-stage behavior: pre-cracking (or initial) stage and post-cracking (or final/plastic) behavior. The failure was very brittle at the reaching of the peak load.

The bolted connection is a prototype meant to be a more balanced connection layout, having high and reliable shear resistance (comparable to the welded plates and shear keys connections) and in the same time, allowing a practical, fast and economical casting process (comparable to the wire loop connections). The shear capacity was lower than expected (overestimated by Eurocode 2). Yet, the results were consistent, showing good ductility, even though the grouting quality was not the best.

Wire loop boxes showed a brittle failure and their capacity showed a very wide spread of values. The wires seemed to become active in transmitting the force, only at high shear displacements. This connection type was proven very sensitive to joint grouting and it seems that is not reliable to be used for complex structural systems. Philipp constructive rail is the only loop connection type that provided consistent results.

In the additional test series, it was observed that a larger number of wire loops increases the connection ductility, providing a more favorable post-cracking behavior. Unfortunately, due to joint casting difficulties caused by the geometry of the Philipp structural rail system, the test results are considered unreliable, and they were neglected.

The tested connections were compared with the design method provided by EN 1992-1-1 and the design proposal presented in Model Code 2010. All the comparisons are performed with mean values for joint material mechanical properties determined through laboratory testing. EN 1992-1-1 calculations compared with test results from specimens using steel assemblies had an average ratio between the experimental load and code resistances of 0,86. For the wire loops specimens the average ratio was 2.31. A deceiving good average ratio of 0,91 (experimental load per model resistance) was obtained with an interpretation of the EN1992-1-1 method. This method assumes that the resistance provided by the very smooth interfaces, the resistance of the shear keys and the resistance of the steel connectors could be superimposed. Yet, test observation showed different stages of degradation and cracking, not a perfect rigid bond-slip behavior. Model Code 2010 recommends different formulation for the interfaces provided with reinforcement for increasing the shear resistance, characterized by a rather non-rigid bond-slip behavior. The pre-normative calculation proposal seems to have more physical meaning than the current approach from EN 1992-1-1, yet the test results compared with this model resistances seem to be over-conservative. An average experimental / model resistance ratio of 1,73 is found. When comparing a specific connection layout with the model resistance, for all the presented calculation models, the errors were not uniform. This means that a general calculation model cannot be applied for all connection layouts. Probably the calculation should be adjusted for the specific connection layout.

The purpose of this experimental program was not to provide a calculation model for the shear resistance. Besides the comparisons with existing resistance models, the aim was to assess the shear stiffness of the joints. The stiffness of all the tested connections has been exceeding by far the initial supposition ($5 \cdot 10^4$ kN/m/m). Secant

stiffness values are provided for all tested connections (individual values and average of three tests). The secant stiffness had one-stage, two-stage and occasionally three intervals. The assessment of stiffness values to be used for design using Linear Elastic Finite Element global analysis is not concluded, due to the non-linearity of the connections' behavior. The spread of stiffness values is another challenging factor in proposing stiffness values for design. If lower stiffness values are used in the global analysis, the overall shear wall behavior should be on the safe side, yet the stiffness of the connections is decisive in predicting how the connections will behave. A misprediction of the shear forces in the vertical connections might lead to their brittle failure and overloading of different structural elements/connections.

5.2 Further research

The test results presented here will be used to calibrate the numerical simulations. As stated by Model Code 2010, this is another way of checking structural performance and is an alternative to physical testing in a laboratory. However, numerical nonlinear models are inherently complex and notoriously difficult to apply with confidence. The best way is to validate the numerical simulations with experiments and sensitivity studies. Model Code 2010 propose a series of safety formats for non-linear analysis applications. Parametric analysis using validated solution strategies should contribute to the identification of the critical parameters.

The final goal of this research project is to improve the design strategies for precast concrete shear walls based on Linear Elastic Finite Element global analysis. To achieve this, the nonlinear numerical simulations on multistory precast shear walls can be used to validate the design strategies.

Bibliography

[1] P. W. Birkeland and H. W. Birkeland, "Connections in Precast Concrete Construction," *ACI Journal,* pp. pp. 345-368, 1966.

[2] A. Cholewicki, "Loadbearing Capacity and Deformability of Vertical Joints in Structural Walls of Large Panel Buildings," *Build. Sci. Vol. 6,* pp. pp. 163-184, 1971.

[3] K. Hansen, M. Kavyrchine, G. Melhorn, S. 0. Olesen, D. Pume and H. Schwing, "Design of vertical keyed shear joints in large panel buildings," *Building Research and Practice,* pp. 202-215, 1974.

[4] H. B. Jørgensen, Strength of Loop Connections between Precast Concrete Elements Part I: U-bar Connections Loaded in Combined Tension and Bending -Part II: Wire Loop Connections Loaded in Shear, University of Southern Denmark, 2014.

[5] A. Biswal, A. Prasad and A. Sengupta, "Study of shear behavior of grouted vertical joints between precast concrete wall panels under direct shear loading," *Structural Concrete,* p. 1–19, 2018.

[6] J. H. Sørensen, Design and Modeling of Structural Joints in Precast Concrete Structures, Technical University of Denmark, Department of Civil Engineering, 2018.

[7] CEN, Eurocode 2: Design of concrete structures - Part 1-1: General rules and rules for buildings, 2004.

[8] CorrelatedSolutions, *Vic-3D 8 Testing Guide.*

[9] J. H. Sørensen, L. C. Hoang, P. N. Poulsen and M. A. Herfelt, "Experimental investigation of keyed shear joints subjected to a combination of compression and shear loads," in *Proceedings of the fib Symposium 2019*, 2019.

[10] Task Group 6.2, "FIB bulletin 43 Structural connections for precast concrete buildings," International Federation for Structural Concrete, Lausanne, Switzerland, 2008.

[11] L. D. Martin and W. J. Korkosz, "CONNECTIONS FOR PRECAST PRESTRESSED CONCRETE BUILDINGS including earthquake resistance," PCI, 1982.

[12] D. Miclăușoiu, G. Á. Sándor, H. Constantinescu, B. Hegheș and M. Nedelcu, "EXPERIMENTAL STUDY OF PRECAST WALL CONNECTION WITH GROUTED SHEAR KEYS AND WELDED PLATES," in *6th fib International Congress*, Oslo, 2022.

[13] Mapei, *Technical Brochure: Mapegrout SV,* 2013.

[14] S.-G. Weber, *Weber ESL: Mortar for concrete element joints C30/37-4,* 15 June 2021.

[15] Peikko, *Technical Manual: PVL Connecting Loop,* 2020.

[16] D. Miclăușoiu, G. Á. Sándor, H. Constantinescu, B. Hegheș and M. Nedelcu, "EXPERIMENTAL STUDY OF PRECAST WALL CONNECTION WITH HIGH STRENGTH WIRE LOOPS," in *14th fib PhD Symposium in Civil Engineering*, Rome, 2022.

[17] T. r. OKARIA, *OKARIA 80/100/120- VAARNALENKKI,* 3.4.2017.

[18] G. PHILIPP, *PHILIPP Connecting rails and loops,* 07.2018.

[19] RSteel, *R3L Wire Rope Loop Box Technical Manual,* 2020.

[20] P. Group, *Connecting rails and loops.*

[21] FIB, *Model Code 2010,* Lausanne, Switzerland: DCC Document Competence Center Siegmar Kästl e.K., Germany, 2012.